Stony Brook University

Thin-film Nanofibrous Composite Membranes by Interfacial Polymerization for Water Purification

A Dissertation Presented

by

Xiao Wang

to

The Graduate School

in Partial Fulfillment of the

Requirements

for the Degree of

Doctor of Philosophy

in

Chemistry

Stony Brook University

December 2013

Stony Brook University

The Graduate School

Xiao Wang

We, the dissertation committee for the above candidate for the

Doctor of Philosophy degree, hereby recommend

acceptance of this dissertation.

Benjamin Chu – Dissertation Advisor
Distinguished Professor of the Chemistry Department

Benjamin S. Hsiao – Dissertation Advisor
Professor of the Chemistry Department

Joseph W. Lauher - Chairperson of Defense
Professor of the Chemistry Department

Peter Khalifah – Third Member
Assistant Professor of the Chemistry Department

Devinder Mahajan – Outside Member
Professor of the Materials Science and Engineering Department

This dissertation is accepted by the Graduate School

Charles Taber
Dean of the Graduate School

Abstract of the Dissertation

Thin-film Nanofibrous Composite Membranes by Interfacial Polymerization for Water Purification

by

Xiao Wang

Doctor of Philosophy

in

Chemistry

Stony Brook University

2013

A thin-film nanofibrous composite (TFNC) membrane system for nanofiltration (NF) with substrates entirely fabricated by fibers was prepared. Water-channel structure was formed at the interface between the polymer barrier layer and the ultrafine cellulose nanofibers (CNs) in the supporting layer, demonstrating the advantages of using a CN substrate over other conventional ones. Both manual coating and slot-die coating were applied for membrane preparations. The resulting membrane performance showed that the slot-die coating method could produce better performance membranes than the manual coating method. With the optimized formulations and coating conditions, TFNC NF membranes coated by the slot-die method had a higher flux, of ~100% more than a reference commercial NF membrane, (NF 270, Filmtec), but with the same salt rejection ratio. This is because of the slot-die coating method could effectively control the barrier layer coating thickness, thus better control the pore size distribution.

Two interfacial polymerization pathways (termed IP and IP-R), regarding the arrangement of the aqueous and organic phases, were investigated on CN and on electrospun scaffolds. It was found that the interfacial polymerization with the aqueous phase above the organic phase (IP-R) yielded better filtration performance, i.e., IP-R based membranes exhibited a higher $MgCl_2$ rejection than IP based membranes, probably because of smaller average pore size in the former.

Finally, preparation of TFNC membranes for reverse osmosis (RO) was formulated by using different inert additives during interfacial polymerization, such as triethylamine (TEA), 1-octyl-3-methylimidazolium chloride (OMIC), camphor-10-sulfonic acid (CSA), isopropyl alcohol (IA) and o-aminobenzoic acid (*o*-ABA) and sodium lauryl sulfate (SLS). Among all the additives, 1-octyl-3-methylimidazolium chloride (OMIC) (an ionic liquid that is soluble in the aqueous phase), was found to be able to achieve the best RO membrane performance. The resulting TFNC RO membranes based on the CN scaffold showed higher A values (water transport coefficient) and lower B values (salt transport coefficient) than those without it.

Table of Contents

List of Figures

List of Tables

Acknowledgments

I would like to thank my advisors Professor Benjamin Chu and Professor Benjamin S. Hsiao for their financial support, invaluable advice and innovative ideas to my Ph.D research projects and for their suggestions, and revision on this dissertation. I am grateful to my committee members, Professor Joseph W. Lauher and Professor Peter Khalifah for their insightful comments, suggestions and encouragements. I would also like to thank Professor Devinder Mahajan for serving on my committee as an outside member. During the completion of this dissertation, I obtained great support form faculty, staff and graduate students around me. In particular, I would like to thank Dr. Jim Quinn and Cheng Pan in the Materials Science and Engineering Department for their help with SEM, AFM and water contact angle tests. I would like to thank Dr. Dufei Fang for design and construction of the slot die coating apparatus, which led to a new direction to my research. I would also like to thank to Dr. Hongyang Ma for his guidance for the preparation of nanofibers and membranes, and Dr. Christian Burger for his wonderful illustrations of several diagrams, that clearly depict the conceptual models in my dissertation. I would like to take this opportunity to thank all my group members, Dr. Yang Liu, Dr. Ran Wang, Dr. Mason Yeh, Dr. Yimin Mao, Dr. Xiao Wei, Dr. Justin Che, Zhe Wang, Yin Su, Rui Yang, Hao Zhou and Zhirui Mo for their inspiring discussions and stimulations. Finally, I would like to thank my parents for their unconditional support, love and understanding for my study in the United States.

Chapter 1 Introduction of Nanofiltration (NF)/Reverse osmosis (RO) Membranes in Water Purification Processes

1.1 Pressure-driven membranes for water purification

According to thermodynamics, substances tend to mix spontaneously when the Gibbs free energy of the final mixture is smaller than the sum of those free energies of each pure substance. Separation or purification is a process opposite to mixing, which changes the net free energy from lower to higher. Hence, energy or driving force is needed to reverse the spontaneous process. In practice, there are many driving forces for purification, such as pressure, electricity, heat, concentration and chemical reactions, and each of them works in its specific process [1]. When it comes to water purification, the pressure-driven membrane process is the most popular one in industrial application for its cost-effective construction and energy-saving operation. In this process, the feed solution is pushed through the membrane by hydraulic force to obtain permeate solution on the other side. Concentration of a certain component in the permeate solution is higher than that in the feed mixture because more of the specific component is being transported in the membrane. Therefore, the separation membrane is the key component of the water purification process to control the quality of permeate solution and work efficiency. In terms of membrane pore size, classification of water purification membranes are as follows[2, 3]:

- Microfiltration (MF) membranes, having pore sizes of 100 nm – 10 μm and operating pressure of 0.1-2.0 bar for removal of large bacteria, yeast and micron sized particles in water
- Ultrafiltration (UF) membranes having pore sizes of 2 nm – 100 nm and operating pressure of 1.0 - 5.0 bar for removal of bacteria, macromolecules, protein and viruses in water
- Nanofiltration (NF) membranes, having pore sizes of ~1nm and operating pressure of 5.0 – 20 bar for removal of multivalent ions, viruses and large organic molecules in water
- Reverse osmosis (RO) membranes, having a "non-porous" structure on top and operating pressure of 10 – 100 bar for removal of salts and small organic molecules in water.

In water treatment, anyone of the above membranes can be used individually for a specific purpose or these membrane can be combined and work as a unit in a multiple-stage processing line. For example, NF/RO membranes are designed to work under higher pressures and to remove small molecules effectively. Thus the requirements for both membrane fabrication and membrane materials are comparatively harsher. The theme of this thesis is to obtain a better insight into the relationship between the NF/RO membrane structures and their performances. Some novel methods, which can improve membrane performance and ready for industrial scale-up, are being investigated by experiments.

1.2 Separation mechanism and transport

There are many models to explain the separation and transport mechanisms in membranes. Some well-established models related to this thesis are briefed below.

For MF and UF applications, the feed solution is purified by the sieving retention, as the particle size of the contaminant is larger than the pore size of the membrane. Liquid flow in MF/UF membranes generally follows the Hagen-Poiseuille equation [4]:

$$J = \frac{\varepsilon r^2}{8\eta\tau}\frac{\Delta P}{\Delta x} \quad (1.1)$$

where **J** is liquid flux, **ε** is pore structure factor related to pore size and porosity, **τ** is tortuousity factor, which is unity in the case of cylindrical pores, **η** is dynamic viscosity, **ΔP** is pressure drop across the membrane and **Δx** is the membrane thickness.

For RO membranes, both solute and solvent diffuse across the nonporous RO barrier layer driven by concentration and pressure gradient based on the Fick's law. Separation is achieved in the membrane by different diffusion rates of solvent and solute. Based on the above assumptions, the solution-diffusion model yields fluxes of solute and solvent as follows [5]:

$$J_w = A(\Delta P - \Delta\pi) \quad (1.2)$$

$$J_s = B(C_F - C_P) \quad (1.3)$$

where $\mathbf{J_w}$ is water (solvent) flux, **A** is the water permeability coefficient which is related to water diffusivity in the membrane and the membrane thickness. **Δπ** is osmosis pressure across the membrane, $\mathbf{J_s}$ is salt (solute) flux, **B** is the solute permeability coefficient which is determined by salt diffusion coefficient, salt solubility in the membrane and the membrane thickness; $\mathbf{C_F}$ and $\mathbf{C_P}$ are concentrations of feed solution and permeate, respectively. Values of **A** and **B** are the two important attributes to evaluate the RO membrane performance. Usually, membranes with good performance have a large **A** value but a small **B** value.

NF membrane is located between RO and UF in terms of the pore-size scale. It is believed that liquid transport and separation behavior in NF membranes follow both Hagen-Poiseuille and solution-diffusion relationships. Besides that, the Donnan effect is another factor for membrane selectivity. Interfacial polymerized polyamide layers are reported to contain negative charges on

their surface, which retard anions in the feed solution passing across the membranes [6, 7]. The Donnan-Setric pore model (DSPM) has been built to take all the above factors into account. In DSPM, the water transport in the membrane follows the Hagen-Poiseuille relationship (equation 1.1) and the salt flux is described as follows [8, 9]:

$$J_s = -\underbrace{D\frac{dc}{dx}}_{\text{Diffusion}} - \underbrace{\frac{zcDF}{RT}\frac{d\varphi}{dx}}_{\text{Donnan effect}} + \underbrace{KcJ_w}_{\text{Pore flow}} \qquad (1.4)$$

where **D** is the salt diffusivity in the membrane, **x** and **c** are a certain point in the barrier layer and the corresponding salt concentration at point **x**; **z** is the valence of salt ions; **F**, **R**, **T** are the Faraday constant, the universal gas constant and the absolute temperature, respectively; **φ** is the Donnan potential; **K** is a hindrance factor based on the sieving mechanism.

1.3 Materials for membrane top barrier layers

Usually, interfacial polymerization is the first choice to prepare NF/RO membranes due to its self-limited process. The thin polymer layer formed at the interface between the two immiscible reacting phases (through condensation polymerization) and controls the thickness of the barrier layer to around 100 nm [10]. A brief review on interfacial polymerization and materials, as well as alternative methods for fabricating the barrier layer in NF/RO membranes is given below.

1.3.1 Materials for NF membranes

For fabricating the barrier layer in NF membranes by interfacial polymerization, the frequently used monomers are piperazine (PIP) in water and 1,3,5-Benzenetricarbonyl trichloride (TMC) in hexane. Permeability of resulting membranes could be as high as 0.71 L/(m^2 h psi)

with the salt ($MgSO_4$) rejection above 97% [11]. Poly(amidoamine) dendrimer was reported to replace PIP, leading to a membrane with permeability of 0.63 L/(m^2 h psi) and 85% rejection on $MgSO_4$ [12]. When triethanol amine was used as an aqueous monomer to react with TMC, a polyester barrier layer could be produced. The resulting membrane had a permeability of 0.59 L/(m^2 h psi) and a $MgSO_4$ rejection of 76.5% [13]. A positively charged NF membrane was prepared by using the reaction of poly (N,N-dimethylaminoethyl methacrylate) and p-xylene dichloride. The membrane had higher rejections on $MgCl_2$ (98%) than on $MgSO_4$ (86%) with a permeability of ~ 0.07 L/(m^2 h psi) [14].

Besides interfacial polymerization, layer-by-layer (LBL) can be another technique to fabricate ultrathin NF membranes. For example, two polyelectrolytes, containing opposite charges, are deposited alternatively and a dense barrier layer is self-assembled by electrostatic interactions. Membrane thickness is controlled by the repetitions of the deposition process. 60 bilayers of 18-azacrown-6/polyvinylsulfate had permeability of 1.8×10^{-3} L/(m^2 h psi) and sulfate ion rejection of 98.6% [15]. An ultrathin barrier layer, a 4.5 bilayer of poly(styrene sulfonate) (PSS)/protonated poly(allyl amine) was deposited on a UF substrate leading to membrane permeability as high as 0.51 L/(m^2 h psi) and sulfate ions rejection of 95%. The 4.5 bilayer of PSS/poly (diallyldimethyl ammonium chloride) further improved the permeability to 0.95 L/(m^2 h psi) with a comparable rejection on sulfate [16]. Due to the comparatively loose molecular structure, it was hard to achieve high NaCl rejection with LBL membranes. For example, a membrane with 60 bilayers of poly(vinylamine)/ poly(vinylsulfate potassium salt) was reported to have a complete rejection on multivalent ions and only 84% rejection on NaCl with permeability of 7.8×10^{-3} L/(m^2 h psi) [17].

The pore size of UF membranes can be narrowed down to NF scale by some chemical/physical ways. The resulting NF membranes are usually useful for filtration of dye or sugar molecules rather than salt ions because of their comparatively large pore sizes. The surface of polyethersulfone (PES) UF membrane was reported to be annealed by high power (900 W) microwave irradiation for 130 s and its rejection on NaCl was improved from 0 to 30% [18]. The surface grafting reaction was initiated on the surface of PES UF membrane in acrylic acid solution. Its retention on maltose was improved from 38% to 62% [19].

1.3.2 Materials for RO membranes

Cellulose acetate was the first generation of RO barrier material and was soon replaced by other materials because it had very low permeability (~ 0.01 L/(m^2 h psi)) and vulnerable to halogen-based disinfectants [20]. Some materials with good resistance to disinfectants were reported, such as polyoxadiazole, polybenzimidazoline, polyether-polyfurane and sulfonated polysulfone [21]. Unfortunately, permeabilities of RO membranes made by these materials were still very low, resulting in the replacement of these materials to the interfacial polymerized polyamide. The molecular structure of polyamide could be varied by using different kinds of monomers. Among them, polyamide prepared by aromatic amine and aromatic acyl chloride possessed both high salt rejection and high permeability [22]. For example, C.K. Kim, et. al prepared RO membranes by using a series of aromatic amines (e.g. 1,2-phenylenediamine, 1,3-phenylenediamine and1,4-phenylenediamine) and aromatic acyl chlorides (e.g. benzoyl chloride, phthaloyl chloride, isophthaloyl chloride, terephthaloyl chloride and trimesoyl chloride). The results demonstrated that RO membranes prepared by using 1,3-phenylenediamine (MPD) and trimesoyl chloride (TMC) had the best performance in terms of salt rejection and permeability

[23]. Therefore, most recent works on RO membranes have been focused on optimizing the formulation of MPD/TMC based polyamides.

A noticeable development has been to embed Linde type A zeolite nanoparticles into the polyamide barrier layer through interfacial polymerization. Comparing with neat polyamide membranes, the permeability of such composite membranes was doubled with no side effects on salt rejection because the hydrophilic zeolite particles provided water pathways and its negative charges enhanced the Donnan exclusion [24-26]. Another composite for RO membrane was prepared by conducting interfacial polymerization with an aqueous phase containing silica nanoparticles. Being different from zeolites, an increase in the amount of loading of silica nanoparticles could demonstrate a definite tradeoff between salt rejection and permeability [27]. Aside from the use of nanoparticles, small molecules can also be used as additives. The RO membrane permeability was reported to be tripled without decline of salt rejection by using isopropyl alcohol in the aqueous phase [28]. Acetone was added into the aqueous phase to work as a co-solvent. When the acetone concentration reached to 2 wt%, the membrane permeability was raised four times with no considerable rejection loss [29]. Some new aqueous additives, such as o-aminobenzoic acid, m-aminobenzoic acid, 2-(2-hydroxyethyl) pyridine and 4-(2-hydroxyethyl) morpholine were used to build hydrophilic water pathways in RO membranes. The membrane permeability was improved to around 0.4 L/(m^2 h psi) with 98.8% salt rejection, which was better than the performance of commercial membranes [30].

1.4 Strategy to improve NF/RO membrane performances

Though some new materials and additives for NF/RO membranes have been introduced in section 1.3, improvements on membrane efficiency brought by those formulations have, so far,

been limited on a small scale. As has been described briefly in section 1.2, water molecules have to diffuse across the membrane along tortuous pathways, which are formed by polymer free volumes, in NF/RO membranes. One innovative strategy to significantly lower down the pressure drop in the barrier layer was to introduce directed water channels which can provide selectivity for the sieving mechanism and straight pathways for water molecules. [31]. Multiwall carbon nanotubes (CNTs) were aligned by chemical vapor deposition and the oriented CNTs were embedded into a polymer matrix. To enhance the nanotube transport efficiency, carboxylate functionalization was achieved at the tips of CNTs. The diffusion of metal ions (Ru $(NH_3)_6^+$) in the membrane was studied [32]. In another experiment, aligned CNTs were embedded into an inorganic material, Si_3N_4 by chemical vapor deposition, with the permeability of the resulting membrane being four to five orders of magnitude higher than commercial polycarbon membranes [33]. Aquaporin was another attractive material as a sort of protein in the form of water-selective channels in cell membranes. Aquaporin Z proteins were reported to be embedded into self-assembled polymer vesicles. Membranes of the vesicles had permeability around one order of magnitude higher than commercial RO membranes [34]. Membranes with cylindrical channels were prepared by phase-segregated assemblies of lyotropic liquid crystal (LLC). The channel diameter was varied with the crystal structure of LLC. The inverted hexagonal LLC membrane had channel diameter of 1.2 nm and the bicontinuous cubic (Q_I) LLC membrane had 0.75 nm. It was noticeable that the Q_I LLC had around 95% rejection on NaCl and water permeability comparable to commercial RO membranes [35, 36].

A new water channel structure was proposed by our group. As is shown in Figure 1.1, the barrier layer of the NF/RO membranes could be fabricated by combing ultrafine cellulose nanofibers (CNs) and polymer matrix. Water-channels were formed in the interface between the

polymer matrix and CNs. Water molecules could then be transported faster through the interconnected channels rather than the tortuous pathways via molecular cavities in the polymer matrix. In practice, the nanocomposite barrier layer structure can be achieved by conducting interfacial polymerization inside the CN substrate. Such an approach is more feasible for scale-up productions than those preceding approaches. The experimental details will be introduced in Chapter 3.

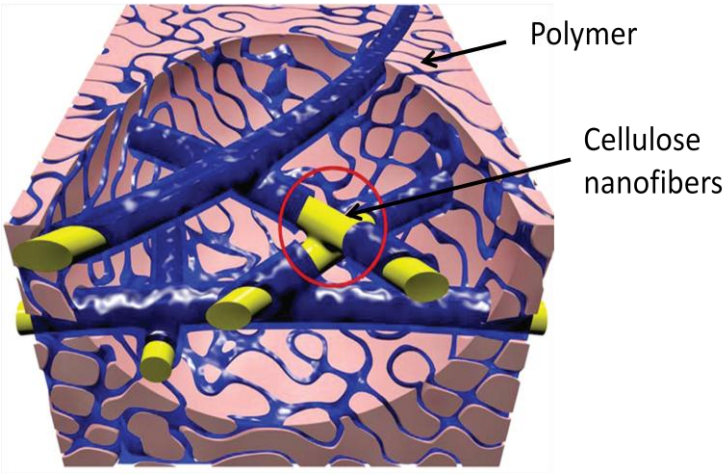

Figure 1.1 Schematic representation of the nature of water channels in the nanocomposite barrier layer [37]

1.5 CNs for water purification

Cellulose is a renewable and abundant natural material, being readily accessible from plants, animals and bacteria. It has been used as engineering materials for hundreds of years and even to this day, it is still an important industrial material in textile, paper, etc. Cellulose fibers are the core constitution of cellulose and fibers with different dimensional sizes can be obtained from different cellulose sources and methods of preparation. Cellulose nanofibers with diameters in the nanoscale (3 ~ 50 nm) can be obtained by refining wood or plant micro-fibers through chemical or biological treatment [37]. Due to the large surface area per volume and abundant

surface groups that can be functionalized, cellulose nanofibers have great potentials to be applied for water treatment.

A recent study by our research group reported that 2,2,6,6-tetramethylpiperidine-1-oxylradical (TEMPO) oxidized CNs amidated by polyvinylamine (PVAm) could be infused into an elect-spun polyacrylonitrile (PAN) scaffold to prepare a unique MF filter with virus removal capability. The resulting filter was capable of completely removing Eschrichia coli (by size exclusion) and exhbited 4 log reduction value (LRV) on the MS2 virus (by adsorption). The same study indicated that each gram of the TEMPO oxidized CNs (without further modification) could absorb 100 mg Cr (V) or 260 mg Pb (II) in water [38]. The MF filter based on electrospun PAN scaffold containing TEMPO oxidized CNs was reported to have high absorption capacity of a positively charged dye, crystal violet (around 4mg/g) [39]. TEMPO oxidized CNs absorbed uranyl acetate and precipitated from the suspension to form gelatin. The gelatin containing the radioactive metal ions could then be easily removed by filtration. The UO_2^+ absorption capacity of CNs was 167 mg/g, being 2-3 times higher than the conventional absorbents [40]. A thin layer (around 100 nm) of CNs was deposited on PAN electrospun scaffold to prepare a UF membrane with an average diameter of ~12.4 nm. Due to the large porosity and the interconnected pores in the CN layer, the CN UF membrane had a 10-fold higher permeability than commercial UF membranes with 99.5% rejection on oil/water emulsion [41].

1.6 Performances of commercial NF/RO membranes

One main specific research aim in my PhD research project is to explore approaches of improving NF/RO membrane work efficiency. Information of all accessible commercial

membranes was collected and compared with our lab-made membranes and to use the best commercial product as a reference.

1.6.1 Commercial NF membranes

As shown in Figure 1.2, rejection and permeability of membranes from different sources are summarized in one plot. Reference of points in Figure 1.2 and corresponding membrane sources are listed in Table 1.1. All the membranes were prepared by depositing a thin polyamide layer on the porous polymeric substrate by means of interfacial polymerization. The NF membranes were evaluated under a comparatively uniform condition: 2000 ppm $MgSO_4$ in water, 25 ^oC and 70 - 100 psi. Membrane rejection was varied in the range of 97% - 100% and permeability could reach 0.9 L/(m^2 h psi). Among all the commercial membranes in Figure 1.2, Se1 (NF-1, Sepro), Se2 (NF-2, Sepro) and D3 (NF 270, DOW) were the top three in terms of permeability. NF 270 was selected as the reference because it was more accessible from membrane providers than the other two. It should be noted that the permeability of all the new materials mentioned in section 1.4.1 was comparable to or mostly smaller than polyamide-based commercial membranes. Therefore, polyamide was used in the PhD thesis research. A1 and A2 are our lab-made membranes with electrospun scaffolds as substrates [42]. Comparing with D3 (NF 270), A2 had a slightly higher permeability and comparable salt rejection, implying a potential of using nanofibers for the improvement of membrane performances. Ultrafine cellulose nanofibers were introduced as a new substrate, on which B1 and B2 were prepared through machine coating. B2 had a significantly higher permeability, around 100% higher than that of NF 270. The details to obtain B1 and B2 are introduced in Chapter 3.

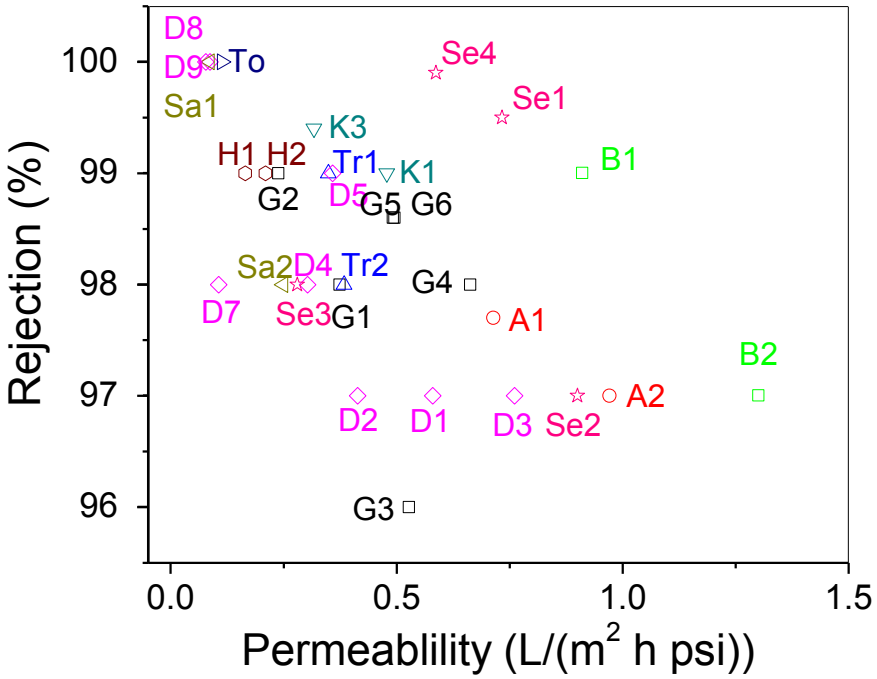

Figure 1.2 Performances of commercial NF membranes (data were obtained from membrane providers' websites) and lab-made NF membranes (data were obtained from cross-flow test)

Table 1.1 List of the points in Figure 1.2 and their corresponding membrane names

Point	Company	Membrane	Point	Company	Membrane	Point	Company	Membrane
G1	GE	DK	D1	Dow	NF90	Se1	Sepro	NF-1
G2		AK	D2		NF200	Se2		NF-2
G3		DL	D3		NF270	Se3		NF-3
G4		HL	D4		NF70	Se4		NF-4
G5			D5		NF400			
G6		Duraslick NFHS	D6		NF			
Tr1	Trisep	TS80	D7		XLE-400			
Tr2		TS83	D8		LE-400			
Tr3		XN45	D9		BW-400			
K1	Koch	TFC-S	Sa1	Saehan	RE-BLR	A1	lab-made	manual coating on Electro-spun PAN
K2		TFC-SR2	Sa2		NE-90	A2		manual coating on Electro-spun PAN, BP added
K3		TFC-SR3	To	Toray	UTC-70	B1		slot die coating on CN
			H1	Hydranautics	ESPA	B2		slot die coating on CN, BP added
			H2		ESNA			

1.6.2 Commercial RO membranes

Results of rejection and permeability of varying RO membranes are plotted in Figure 1.3 and their corresponding sources are listed in Table 1.2. All the membranes are polyamide based and classified in three sorts according to their operating pressures. High pressure membranes are designed for desalination of seawater (32,000 ppm NaCl) at 800 psi. Medium pressure membranes are for brackish water (2000 ppm NaCl) at 225 psi. Low pressure membranes are for brackish water (500 ppm) as well at 100 -150 psi. The main difference among the sorts is the

molecular structures of membrane barrier layers. Some preliminary research results on low pressure RO membranes are reported in Chapter 5 with D6 (XLE, DOW) as the reference.

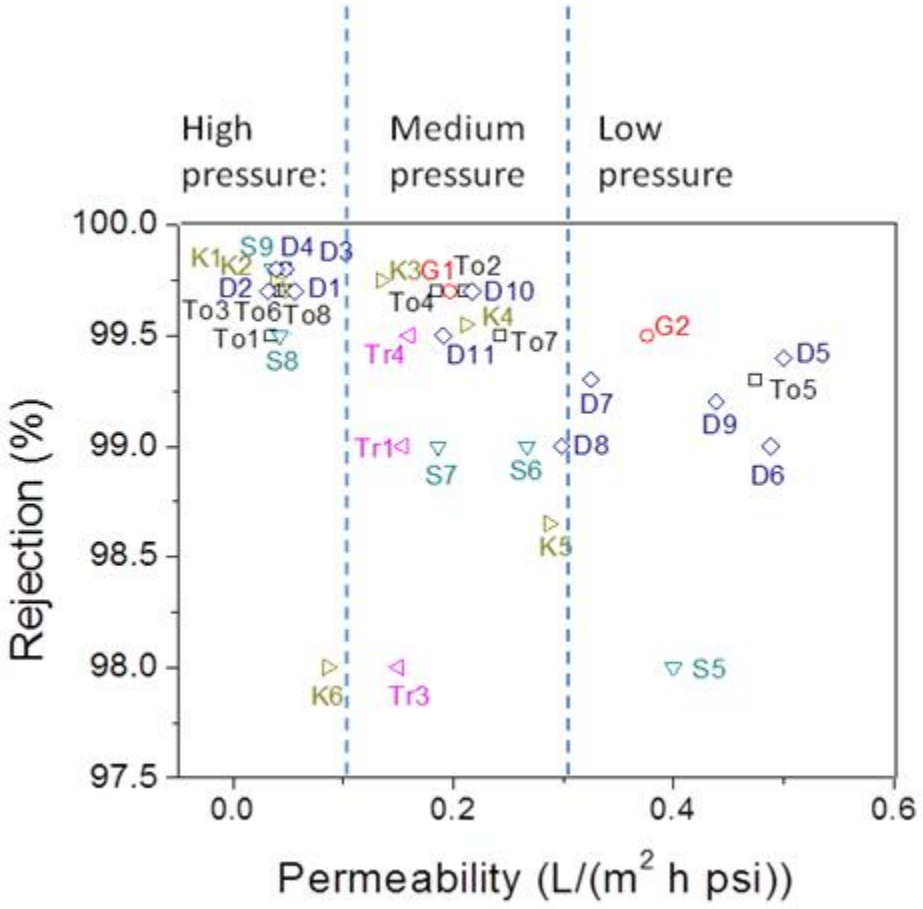

Figure 1.3 Performances of commercial RO membranes (data were obtained from membrane providers' websites)

Table 1.2 List of the points in Figure 1.3 and their corresponding RO membrane names

Point	Company	Membrane	Point	Company	Membrane
To1	Toray	TM 800C	Tr1	Trisep	X-20
To2		TM700	Tr2		ACM
To3		TMG	Tr3		SB20
To4		TML	Tr4		SB50
To5		TMH			
To6		TM800F	K1	Koch	TFC-SW
To7		TM700L	K2		TFC-HF
To8		TM800S	K3		TFC-XR
			K4		TFC-HR
G1	GE	AG HR	K5		TFC-ULP
G2		AK HR	K6		ROGA-HR
G3		desal51HL			
H	Hoechst	N30F	D1	Dow	SW30ULE
			D2		SW30XLE
			D3		SW30XHR
S1	Sepro	NF-1	D4		SW30HR-LE
S2		NF-2	D5		SW30
S3		NF-3	D6		XLE-400
S4		NF-5	D7		LE-440
S5		RO-1	D8		BW30LE-440
S6		RO-2	D9		LP-4040
S7		RO-3	D10		BW30HR
S8		RO-4	D11		TW30
S9		RO-6	D12		NF270

References

[1] M. Mulder, Basic principles of membrane technology, in, Kluwer Academic, Dordrecht ; Boston, 1996, pp. 235.

[2] A. Fane, Ultrafiltration: factors influencing flux and rejection, Progress in filtration and separation, 4 (1986) 101-179.

[3] N. Hilal, H. Al-Zoubi, N. Darwish, A. Mohamma, M. Abu Arabi, A comprehensive review of nanofiltration membranes: Treatment, pretreatment, modelling, and atomic force microscopy, Desalination, 170 (2004) 281-308.

[4] M. Mulder, Basic principles of membrane technology, in, Kluwer Academic, Dordrecht ; Boston, 1996, pp. 287.

[5] M.E. Williams, A review of reverse osmosis theory, EET Corporation and Williams Engineering Services Company, Inc, (2003).

[6] A.E. Childress, M. Elimelech, Effect of solution chemistry on the surface charge of polymeric reverse osmosis and nanofiltration membranes, Journal of Membrane Science, 119 (1996) 253-268.

[7] A.E. Childress, M. Elimelech, Relating nanofiltration membrane performance to membrane charge (electrokinetic) characteristics, Environmental Science & Technology, 34 (2000) 3710-3716.

[8] J.M. Gozálvez-Zafrilla, B. Gómez-Martínez, A. Santafé-Moros, Evaluation of nanofiltration processes for brackish water treatment using the DSPM model, Computer Aided Chemical Engineering, 20 (2005) 457-462.

[9] W. Richard Bowen, A. Wahab Mohammad, Diafiltration by nanofiltration: prediction and optimization, AIChE Journal, 44 (1998) 1799-1812.

[10] V. Freger, Swelling and Morphology of the Skin Layer of Polyamide Composite Membranes: An Atomic Force Microscopy Study, Environmental Science & Technology, 38 (2004) 3168-3175.

[11] L. Yung, H. Ma, X. Wang, K. Yoon, R. Wang, B.S. Hsiao, B. Chu, Fabrication of thin-film nanofibrous composite membranes by interfacial polymerization using ionic liquids as additives, Journal of Membrane Science, 365 (2010) 52-58.

[12] L. Lianchao, W. Baoguo, T. Huimin, C. Tianlu, X. Jiping, A novel nanofiltration membrane prepared with PAMAM and TMC by in situ interfacial polymerization on PEK-C ultrafiltration membrane, Journal of Membrane Science, 269 (2006) 84-93.

[13] B. Tang, Z. Huo, P. Wu, Study on a novel polyester composite nanofiltration membrane by interfacial polymerization of triethanolamine (TEOA) and trimesoyl chloride (TMC): I. Preparation, characterization and nanofiltration properties test of membrane, Journal of Membrane Science, 320 (2008) 198-205.

[14] R. Du, J. Zhao, Properties of poly (N, N-dimethylaminoethyl methacrylate)/polysulfone positively charged composite nanofiltration membrane, Journal of Membrane Science, 239 (2004) 183-188.

[15] A. El-Hashani, A. Toutianoush, B. Tieke, Use of layer-by-layer assembled ultrathin membranes of dicopper-[18] azacrown-N_6 complex and polyvinylsulfate for water desalination under nanofiltration conditions, Journal of Membrane Science, 318 (2008) 65-70.

[16] R. Malaisamy, M.L. Bruening, High-Flux Nanofiltration Membranes Prepared by Adsorption of Multilayer Polyelectrolyte Membranes on Polymeric Supports, Langmuir, 21 (2005) 10587-10592.

[17] W. Jin, A. Toutianoush, B. Tieke, Use of polyelectrolyte layer-by-layer assemblies as nanofiltration and reverse osmosis membranes, Langmuir, 19 (2003) 2550-2553.
[18] Y. Mansourpanah, S. Madaeni, A. Rahimpour, Preparation and investigation of separation properties of polyethersulfone supported poly (piperazineamide) nanofiltration membrane using microwave-assisted polymerization, Separation and Purification Technology, 69 (2009) 234-242.
[19] B. Van der Bruggen, Comparison of redox initiated graft polymerisation and sulfonation for hydrophilisation of polyethersulfone nanofiltration membranes, European Polymer Journal, 45 (2009) 1873-1882.
[20] P. Robert J, Composite reverse osmosis and nanofiltration membranes, Journal of Membrane Science, 83 (1993) 81-150.
[21] K.P. Lee, T.C. Arnot, D. Mattia, A review of reverse osmosis membrane materials for desalination—development to date and future potential, Journal of Membrane Science, 370 (2011) 1-22.
[22] N. Saha, S. Joshi, Performance evaluation of thin film composite polyamide nanofiltration membrane with variation in monomer type, Journal of Membrane Science, 342 (2009) 60-69.
[23] C. Kim, J. Kim, I. Roh, J. Kim, The changes of membrane performance with polyamide molecular structure in the reverse osmosis process, Journal of Membrane Science, 165 (2000) 189-199.
[24] M.L. Lind, D. Eumine Suk, T.-V. Nguyen, E.M. Hoek, Tailoring the structure of thin film nanocomposite membranes to achieve seawater RO membrane performance, Environmental Science & Technology, 44 (2010) 8230-8235.

[25] M.L. Lind, A.K. Ghosh, A. Jawor, X. Huang, W. Hou, Y. Yang, E.M. Hoek, Influence of zeolite crystal size on zeolite-polyamide thin film nanocomposite membranes, Langmuir, 25 (2009) 10139-10145.

[26] B.-H. Jeong, E. Hoek, Y. Yan, A. Subramani, X. Huang, G. Hurwitz, A.K. Ghosh, A. Jawor, Interfacial polymerization of thin film nanocomposites: A new concept for reverse osmosis membranes, Journal of Membrane Science, 294 (2007) 1-7.

[27] G.L. Jadav, P.S. Singh, Synthesis of novel silica-polyamide nanocomposite membrane with enhanced properties, Journal of Membrane Science, 328 (2009) 257-267.

[28] S. Qiu, L. Wu, L. Zhang, H. Chen, C. Gao, Preparation of reverse osmosis composite membrane with high flux by interfacial polymerization of MPD and TMC, Journal of Applied Polymer Science, 112 (2009) 2066-2072.

[29] C. Kong, M. Kanezashi, T. Yamomoto, T. Shintani, T. Tsuru, Controlled synthesis of high performance polyamide membrane with thin dense layer for water desalination, Journal of Membrane Science, 362 (2010) 76-80.

[30] L. Zhao, P.C.-Y. Chang, W. Ho, High-flux reverse osmosis membranes incorporated with hydrophilic additives for brackish water desalination, Desalination, (2012).

[31] M.A. Shannon, P.W. Bohn, M. Elimelech, J.G. Georgiadis, B.J. Marinas, A.M. Mayes, Science and technology for water purification in the coming decades, Nature, 452 (2008) 301-310.

[32] B.J. Hinds, N. Chopra, T. Rantell, R. Andrews, V. Gavalas, L.G. Bachas, Aligned multiwalled carbon nanotube membranes, Science, 303 (2004) 62-65.

[33] J.K. Holt, H.G. Park, Y. Wang, M. Stadermann, A.B. Artyukhin, C.P. Grigoropoulos, A. Noy, O. Bakajin, Fast mass transport through sub-2-nanometer carbon nanotubes, Science, 312 (2006) 1034-1037.

[34] M. Kumar, M. Grzelakowski, J. Zilles, M. Clark, W. Meier, Highly permeable polymeric membranes based on the incorporation of the functional water channel protein Aquaporin Z, Proceedings of the National Academy of Sciences, 104 (2007) 20719-20724.

[35] M. Zhou, P.R. Nemade, X. Lu, X. Zeng, E.S. Hatakeyama, R.D. Noble, D.L. Gin, New Type of Membrane Material for Water Desalination Based on a Cross-Linked Bicontinuous Cubic Lyotropic Liquid Crystal Assembly, Journal of the American Chemical Society, 129 (2007) 9574-9575.

[36] M.-j. Zhou, T.J. Kidd, R.D. Noble, D.L. Gin, Supported Lyotropic Liquid-Crystal Polymer Membranes: Promising Materials for Molecular-Size-Selective Aqueous Nanofiltration, Advanced Materials, 17 (2005) 1850-1853.

[37] H. Ma, C. Burger, B.S. Hsiao, B. Chu, Highly Permeable Polymer Membranes Containing Directed Channels for Water Purification, ACS Macro Letters, 1 (2012) 723-726.

[38] R.J. Moon, A. Martini, J. Nairn, J. Simonsen, J. Youngblood, Cellulose nanomaterials review: structure, properties and nanocomposites, Chemical Society Reviews, 40 (2011) 3941-3994.

[39] R. Wang, S. Guan, A. Sato, X. Wang, Z. Wang, R. Yang, B.S. Hsiao, B. Chu, Nanofibrous microfiltration membranes capable of removing bacteria, viruses and heavy metal ions, Journal of Membrane Science, 446 (2013) 376-382.

[40] H. Ma, C. Burger, B.S. Hsiao, B. Chu, Nanofibrous Microfiltration Membrane Based on Cellulose Nanowhiskers, Biomacromolecules, 13 (2011) 180-186.

[41] H. Ma, B.S. Hsiao, B. Chu, Ultrafine Cellulose Nanofibers as Efficient Adsorbents for Removal of UO_2^{2+} in Water, ACS Macro Letters, 1 (2011) 213-216.

[42] H. Ma, C. Burger, B.S. Hsiao, B. Chu, Ultrafine Polysaccharide Nanofibrous Membranes for Water Purification, Biomacromolecules, 12 (2011) 970-976.

[43] K. Yoon, B.S. Hsiao, B. Chu, High flux nanofiltration membranes based on interfacially polymerized polyamide barrier layer on polyacrylonitrile nanofibrous scaffolds, Journal of Membrane Science, 326 (2009) 484-492.

Chapter 2 Design of Slot-die Apparatus for Fabrication of the Barrier Layer

2.1 Introduction

The coating technology is a process to introduce one or multiple functional layers onto an object for the purpose of decoration, protection, surface modification and so forth. In industry, coating processes are usually classified into two sorts: self-metered coating and pre-metered coating [1]. The mass of the coating liquid in the former is not pre-determined by the desired wet film thickness. The coating thickness is varied according to many factors, such as dimensions of the coating device, characteristics of the coating liquid, and coating conditions. Examples for the self-metered coating process are knife coating, roll coating and dip coating. On the contrary, the wet coating thickness in the pre-metered coating process can be calculated from the coating speed and the flow rate of the coating liquid. Typical pre-metered coating methods in industry are slot-die coating, curtain coating and slide coating. Among them, the slot-die coating process is regarded as the one able to achieve the most precise control on the coating layer [2] and is reported to be able obtain a wet coating thickness of lower than 10 μm [3].

In industry, the barrier layers in reverse osmosis (RO)/nanofiltration (NF) membranes are usually prepared by using the dip coating method [4]. During fabrication, the membrane support is first impregnated in an aqueous solution and subsequently dipped into an organic solution to

carry out interfacial polymerization. Once the polymer layer is formed at the interface, it will retard further reaction of monomers from the two phases. Hence, the membrane growth becomes "self-limiting". The typical research plan for fabrication of high-flux NF membranes usually involves the controlling of the amount of organic solution introduced for the reaction. Under this condition, monomers in the organic solution work as the "limiting reagent" and the membrane growth can be stopped when the membrane is still very thin. The barrier layer of a conventional NF membrane is typically prepared by a certain amount of piperazine (two functional groups) in water and 0.1% (w/v) trimesoyl chloride (three functional groups) in organic solvent. When the thickness of the resulting polymer layer is 200 nm and the polymer, the aqueous solution and the organic solution have similar densities, the maximum wet coating thickness of the organic solution is estimated to be 80 μm. This means that the membrane growth is controlled only when the wet coating thickness is lower than 80 μm. To tune the wet coating thickness quantitatively over a large range, the method of slot-die coating has been investigated for the production of high flux NF membranes in this study. Besides the improvement of membrane efficiency, the slot-die coating process should also provide the realistic opportunities to introduce our new NF membranes for commercialization. Compared with dip coating, the slot- die coating process has the following merits [5]:

- Precise control on the delivered volume. The fluid delivery system delivers a constant supply of coating fluid and the variation in the volume delivered can be controlled by regulating the pumping rate and the line speed ratio.
- A narrow cross-web liquid distribution. The internal manifold geometry of the slot-die delivery system is designed to uniformly distribute the coating fluid. In a fixed lip slot die, the body shim can work in combination with the manifold to provide an even distribution.

• Improved waste management. All of the coating fluid is applied to the substrate. A slot-die system is a closed system, which can reduce contamination from the coating fluid.

In this chapter, the construction of slot-die coating system and the study on slot-die coating performance were conducted under Dr. Dufei Fang's guidance. The preliminary designing work, such as the calculation of pressure drops in the slot die head, checking the working capability of the slot-die influenced by syringe pump and the construction of coating windows were completed by me. The dimensions of the slot-die head were determined and the entire coating system was constructed by Dr. Fang.

2.2 Design of the slot-die head

2.2.1 Design methods

To simplify the design of a custom-built slot-die head, an approach known as "infinite cavity design" proposed by Gutoff et al. [6, 7] has been used. This design assumed that the cavity was large enough to reduce the liquid pressure drop from the feed port to the two ends. The larger the cavity size, the better the flow distribution. As shown on the left diagram in Figure 2.1, this method led to a T-shaped die structure with no compensation on the slot length. However, the "infinite cavity design" can only allow the flow distribution close to but never achieve uniformity in theory [2]. In practical conditions, the residence time is increased with the cavity size and the flow at the ends is nearly stagnant in a large cavity. The design can be corrected to form a die with a coat hanger structure, as shown in Figure 2.1, through the method proposed by Tadmor et al.[8].

In the current design, the preliminary dimensions of slot-die were obtained from experimental requirements and the designs in successful slot die examples reported in the

literature. Errors and boundary states were calculated according to the "infinite cavity design" to ensure that the die had good cooperation with the lab device. The final dimensions of the design were corrected for the construction of a die with the coat hanger structure.

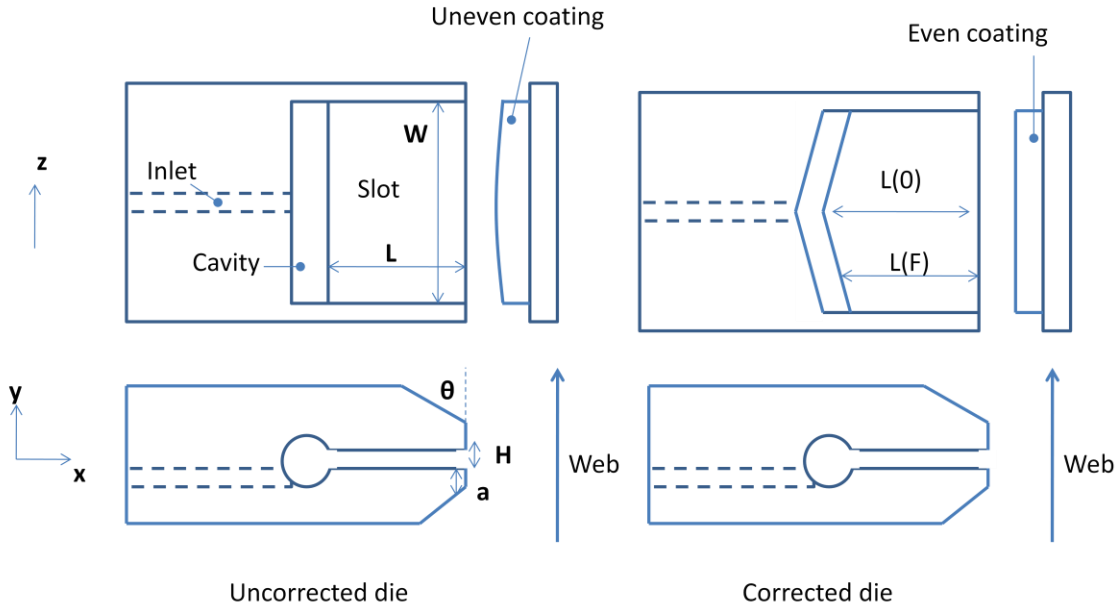

Figure 2.1 Schematics of internal structures, side views and coating profiles of slot die. The one on the left is uncorrected T-shape die and on the right is corrected coat hanger die.**W** is the width of coating slot. **L** is the length of slot in direction of flow. **H** is height or slot opening. **a** and **θ** are lip length and lip angle respectively. **F** is the fraction distance from the feed port to the edge. **L (F)** is the length of the slot as a function of **F** and **L(0)** is the length at the feed port. **x** is the direction down the slot. **y** is the direction perpendicular to liquid flow. **z** is the direction down the cavity channel from feed port in T-shape die.

The preliminary dimensions of the uncorrected T-shaped slot die are listed in Table 2.1. The slot dies for industrial production usually have width in the meter scale, which was a big challenge in both design and manufacturing for laboratory scale up. The purpose of the present design was to check the capability of slot-die coating in order to improve the NF membrane efficiency. It was anticipated that each batch of production could provide coating area large enough for two NF tests. This requirement was met when the width was chosen to be 14.5 cm. The left dimensional sizes were all obtained from the slot die used by the Liu group [9].

Table 2.1 Preliminary dimensions of uncorrected T-shaped slot die

Die Parameters	Dimensions
Die Width (W)	14.5 cm
Slot gap (H)	100 μm
Slot length (L)	3.5 cm
Cavity radius (r)	1 cm
Lip angle (θ)	45^{o}
Lip length (a)	1 mm

2.2.2 Pressure distribution in the cavity of uncorrected T-shaped die

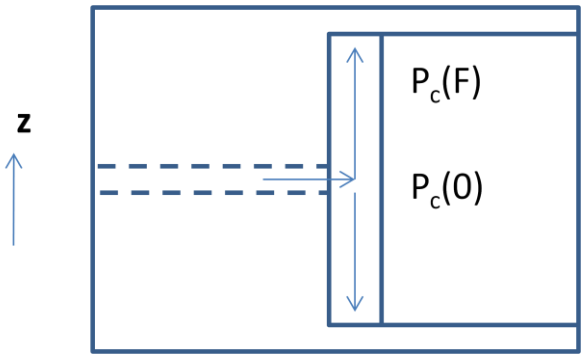

Figure 2.2 Liquid flow in the cavity and its pressure drop along z direction.**P_c (0)** and **P_c (F)** are the liquid pressure at the feed port and at the end of cavity respectively.

As shown in Figure 2.2, the liquid was introduced into the slot die by pumping through the inlet and fill the cavity with the flow along the **z** direction. Because the cavity size in the uncorrected T-shaped die was sufficiently large, resistance from the cavity could be ignored. The main reason for the non-uniform pressure distribution was the variation of flow in the velocity head. At the feed port, the fluid had a velocity along **z** and at the ends of cavity, the velocity was

zero. The pressure in the cavity at the feed port was referred to as $\mathbf{P_c(0)}$ and at the end was $\mathbf{P_c(F)}$. **F** was the fraction distance calculated by the following equation:

$$F = \frac{z}{W/2} \tag{2.1}$$

According to Bernoulli's equation, the kinetic energy can be converted into pressure and at the ends of cavity channel. If the velocity head is converted into the pressure head, the pressure rise in the cavity is:

$$P_c(F) - P_c(0) = \frac{1}{2}\rho v^2 = \frac{1}{2}\rho\left(\frac{Q_{\max}}{\pi r^2}\right)^2 \tag{2.2}$$

where **ρ** is the liquid density and $\mathbf{Q_{max}}$ is the maximum flow rate, which is determined by the pump. When the liquid was decane, it has a density of 0.73 g/cm^3 and a viscosity of 0.92 cP at 20 ^{o}C. The pump used in the experiment was the KD220 syringe pump (KD Scientific) with amaximum flow rate of 2.4 mL/s (http://www.kdscientific.com/products/pumps/kds220.asp). Based on the above values, the pressure difference between the feed port and the cavity end was only 0.34 Pa. Therefore, the T-shaped die had a uniform pressure distribution in its cavity.

2.2.3 Pressure distribution in the slot of the uncorrected T-shaped die

The liquid pressure varies along the directions of **x** and **z,** respectively. The pressure drop along x can be described by the model of flow between two parallel and infinitely extended plates:

$$-\Delta P_{sx} = \frac{12\eta q_{sx} L}{H^3} \tag{2.3}$$

where **η** is the liquid viscosity and $\mathbf{q_{sx}}$ is the flow rate per unit width. When the flow rate arrives at the maximum, $\mathbf{q_{sx}}$ is calculated to be 1.66×10^{-5} m^2/s and the corresponding $-\Delta P_{sx}$ is as high as 6.5×10^{3} Pa.

The flow rate at the die exit varies in the z direction due to the decline of liquid pressure from the center to the two ends. The pressure at its corresponding position is described by the following equation:

$$\frac{P_s(z)}{P_s(0)} = \frac{\exp\left[C^{0.5}(1-F)\right] + \exp\left[-C^{0.5}(1-F)\right]}{\exp(C^{0.5}) + \exp(-C^{0.5})} \qquad (2.4)$$

where **C** is a constant determined by the die dimensions:

$$C = \frac{8H^3W^2}{3\pi D_e{}^4 L} \qquad (2.5)$$

$\mathbf{D_e}$ is the equivalent diameter, which is defined as 4 times of cross-section area over the perimeter. In our condition, $\mathbf{D_e}$ is the cavity diameter (1 cm). When the die dimensions in Table 2.1 are applied to equation 2.5, **C** is calculated to be 5.1×10^{-5}. The result of equation 2.4 with the **C** value is 0.99998, which means that the pressure difference between the center and the ends is only 0.002%. A significant variation of pressure at die exit can be found when the die width (**W**) is in meter scale. The distribution of pressure in our die slot was uniform.

When the T-shaped die is corrected into a coat hanger die, the constant **C** is the correction value:

$$\frac{L(F)}{L(0)} = 1 - C \qquad (2.6)$$

L(F) is the length of the slot as a function of **F**. At the ends of the die, **F**=1, **C** is 5.1×10^{-5} and the value of L(1)/L(0) is close to 1. This result dedicates that the uncorrected and corrected die structures are the same in our case and they both possess a T-shaped structure.

Besides the die internal structure, variations of pressure along the **z** direction could be achieved by using the different design and/or operating conditions as follows.

If we take the natural logs of both sides from equation 2.3, the following expression can be obtained.

$$\ln q_{sx} = -\ln 12 - \ln L - \ln \eta + \ln \Delta P_{sx} + 3\ln H \qquad (2.7)$$

Take the derivatives of both sides, we get

$$\frac{dq_{sx}}{q_{sx}} = -\frac{dL}{L} - \frac{d\eta}{\eta} + \frac{d\Delta P_{sx}}{\Delta P_{sx}} + 3\frac{dH}{H} \qquad (2.8)$$

We can replace the differentials by finite differences

$$\frac{\Delta q}{q} = -\frac{\Delta L}{L} - \frac{\Delta \eta}{\eta} + \frac{\Delta(\Delta P)}{\Delta P} + 3\frac{\Delta H}{H} \qquad (2.9)$$

If we take the square operation on both sides, and if the errors are random, the cross production will average to zero.

$$(\frac{\Delta q_{sx}}{q_{sx}})^2 = (\frac{\Delta L}{L})^2 + (\frac{\Delta \eta}{\eta})^2 + (\frac{\Delta(\Delta P_{sx})}{\Delta P_{sx}})^2 + (\frac{3\Delta H}{H})^2 \qquad (2.10)$$

As the solution used in our experiment was Newtonian like, and temperature could be regarded as constant because of a very short coating time period (i.e., in few seconds), the variation of viscosity could be neglected. Furthermore, as $\mathbf{\Delta P_{sx}}$ along the **z** direction has been

shown to be a constant due to the small value of **W** (the pump in our experiment was a scientific syringe pump, which provided a smooth liquid delivery to avoid fluctuations), the error of $\mathbf{\Delta P_{sx}}$ from the liquid delivery system could also be neglected. The left two terms thus mainly depend on the manufacturing accuracy. Gutoff suggested that the variation of slot length (ΔL) could be controlled to within 25 μm and the slot flatness (ΔH) to within 2.5 μm [7]. The variation of flow rate along the **z** direction was calculated to be around 7.5%, which came mainly from manufacturing errors.

2.2.4 Working capability of the slot die and its dependence of the liquid delivery system

It has been shown that the slot die head with the dimensions listed in Table 2.1 could produce a uniform coating profile. The next step was to guarantee that the targeted coating conditions could be achieved with the chosen liquid delivery system. The driving force in this delivery system was provided by a pump, which was connected to the slot-die head by a plastic tube. The pump was KD220 syringe pump (KD Scientific) with the maximum output linear force of 18 kg. Plastic syringes were provided by the Becton, Dickinson and Company (BD). The diameters of the syringes at different volumes (data obtained from http://www.harvardapparatus.com/hapdfs/HAI_DOCCAT_4/Syringe%20Selection%20Guide.pdf) and their maximum flow rates are listed in Table 2.2. The pressure drops in the slot die and tube together with the velocity at the slot exit were calculated at the maximum flow rates and the results are listed in Table 2.2. For each syringe with a specific volume, the maximum flow rate could be achieved when the total value of the pressure drops and the velocity heads became smaller than the maximum affordable pressure. The KD220 syringe pump was found to be strong enough to delivery decane onto the membrane substrate surface through the slot die at the working flow rate of the pump.

Table 2.2 Diameters of BD syringes at different volumes and their corresponding maximum flow rates

Syringe volume (mL)	Syringe diameter (mm)	Area of syringe plug (cm^2)	Maximum flow rate* (mL/s)
140	38.4	11.6	2.4
100	34.9	9.6	2
60	26.7	5.6	1.2
30	21.7	3.7	0.8
20	19.1	2.9	0.6
10	14.3	1.6	0.3

*The maximum flow rate is calculated from the max step rate of KD220 and the syringe plug area.

Table 2.3 Pressure drops and velocity heads calculated in the liquid delivery system

Syringe volume	Maximum pressure drop in slot die [1] (Pa)	Maximum pressure drop in tube [2] (Pa)	Maximum velocity head at slot exit [3] (Pa)	Total [4] (Pa)	Maximum affordable pressure [5] (Pa)
140 mL	6.50×10^3	389	2.13×10^3	9.02×10^3	1.5×10^4
100 mL	5.40×10^3	324	1.48×10^3	7.20×10^3	1.8×10^4
60 mL	3.30×10^3	194	5.33×10^2	4.03×10^3	3.2×10^4
30 mL	2.10×10^3	129	2.37×10^2	2.47×10^3	4.8×10^4
20 mL	1.60×10^3	97.3	1.33×10^2	1.83×10^3	6.1×10^4
10 mL	8.10×10^2	48.6	3.33×10	8.92×10^3	1.1×10^5

[1] The maximum pressure drop in slot die is calculated by equation 2.3 with the maximum flow rate and the dimensions in Table 2.1.

[2] The maximum pressure drop in tube is calculated by on-line DP Pressure Drop Calculator (http://www.pressure-drop.com/). The tube has inner diameter of 3.28 mm (1/8") and length of 0.5 m. When the plastic tube is used, the tube's roughness is 0.007 mm (http://www.engineeringtoolbox.com/major-loss-ducts-tubes-d_459.html). The flow medium is decane with density of 0.73 g/cm^3 and viscosity of 0.92 cP at 20^{o}C.

[3] The maximum velocity head equals to $\frac{1}{2}\rho(\frac{Q_{max}}{\pi H^2})^2$, where the Q_{max} is the maximum flow rate in Table 2.2.

[4] The total value is the sum of the maximum pressure drop in slot die, the maximum pressure drop in tube and the maximum velocity head at slot exit.

[5] The maximum affordable pressure is obtained the max linear force of the pump and syringe plug area in Table 2.2.

The above equations and calculations are all based on one important assumption in the delivery system, i.e. the laminar flow. To confirm this assumption, Reynold's numbers (Re) were calculated to check the flow state. This is because Re is proportional to the flow rate, where the laminar flow could be ensured for all the coating conditions as long as the flow rate of the coating liquid was below the maximum flow rate (2.4 mL/s).

For this purpose, the Reynold's number (Re_c) was calculated in the slot die cavity using the following equation [7]:

$$\mathrm{Re}_c = \frac{2Q\rho}{\eta\pi r} \tag{2.11}$$

where in the slot gap, the Reynold's number (Re_s) could be calculated as follows [10]:

$$\mathrm{Re}_s = \frac{\rho Q}{\eta W} \tag{2.12}$$

When the flow rate Q=2.4 mL/s, the Re_c and Re_s were found to be 50.5 and 3.5, respectively. Hence, the liquid flow in the slot die during the coating process was always laminar flow.

2.3 Coating window design

2.3.1 Profile of the slot die coating system

Having been checked in the above sections, the dimensions of the slot die head in Table 2.1 was used directly to construct the lab-scale coating system. The outline drawing of the slot die head is shown in Figure 2.3. The slot gap was controlled by the shim having a thickness of 100 μm.

Figure 2.4 shows the photographic image of the experimental coating set-up. The coating solution was controlled and delivered (by a KD220 syringe pump) to the slot die head through a 0.5 m long plastic tube with an inner diameter of 1/8 inches (3.28 mm). The slot die head was mounted onto a frame with the solution introduced downward vertically onto a moving steel plate. The plate was settled on a high precision positioning stage (LW7-48, Rockwell Automation). The maximum travel distance and velocity of the plate were 1.2 m and 3 m/s, respectively. The specific travel distance and the velocity were controlled by a laptop computer. The coating gap between the slot die exit and the membrane substrate was measured by a sheet metal thickness gauge (usually around 100 μm). The die head was lift up and down together with the connected frame by screws on two sides. There was a steel ware under the slot die to hold the extra solution during the coating process.

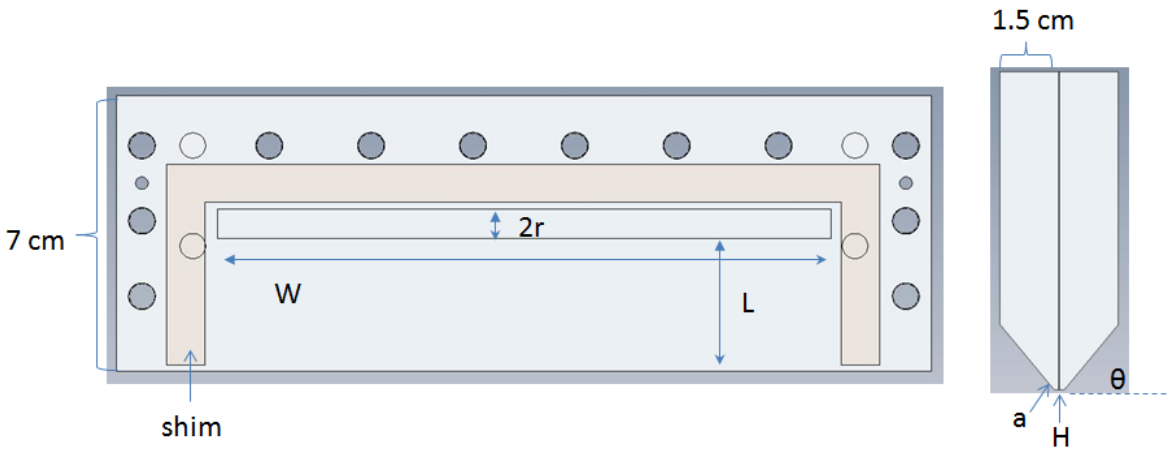

Figure 2.3 Outline drawing of slot die head (drawn in Solid Work by Dr. Dufei Fang)

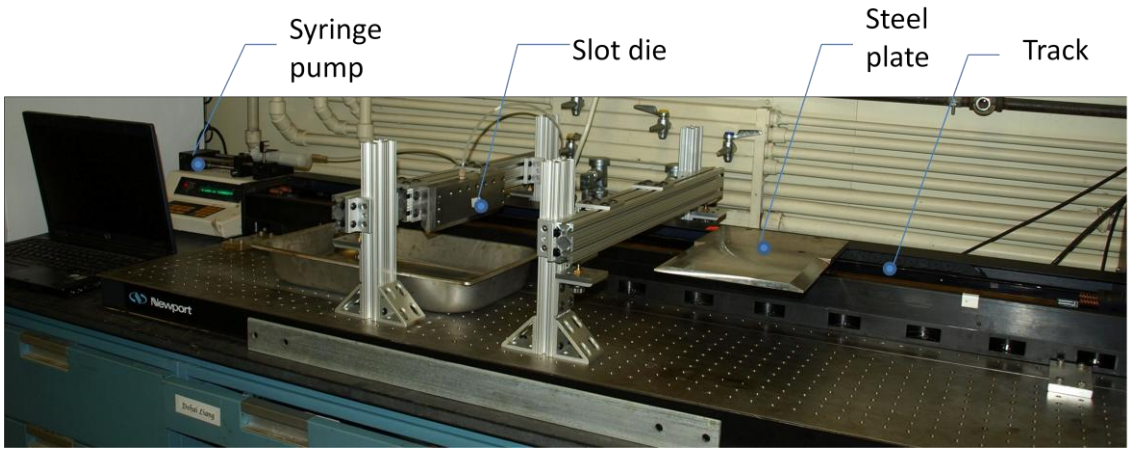

Figure 2.4 Photo image of the lab-scale coating system (built by Dr. Dufei Fang)

2.3.2 Construction of coating windows through experiments

2.3.2.1 Experimental

The region of acceptable coating quality in the space of the operating parameters represents the coating window. In this region, a thin liquid film is cast by the slot die with the cooperation of web velocity and liquid flow rate. The coating window can be constructed with the two parameters to determine the minimum wet coating thickness. These parameters can be obtained

through theoretical modeling or experimentation [11]. In this study, coating experiments were carried out to produce the two parameters for the construction of coating window to optimize the membrane production.

The experimental study was carried out using the coating system in Figure 2.4. The coating liquid, decane, was pumped from a 60 mL BD syringe into the slot die with a flow rate in the range of 40 mL/min to 70 mL/min. The membrane substrate, a piece of cellulose nanofibrous (CN) ultrafiltration (UF) membrane (20 cm×30 cm) was fixed tightly on top of the steel plate by tapes. The coating gap between the die exit and the UF membrane was set to be 40 μm, 60 μm and 100 μm. The starting position of the UF membrane was at 60 cm away from the slot die. The syringe pump was first run for a few seconds to allow a stable flow at the die exit. The UF membrane was moved in sync with the steel plate under the slot die at a velocity in the range of 0.2 m/s to 0.6 m/s. The coating result was determined by visual observation. As shown in Figure 2.5(A), when a uniform thin decane film was covered on CN UF membrane, the shining surface turned out to be dimmer. There was an unstable coating area produced at the beginning of coating, where decane was found to coagulate and penetrated into the substrate. This behavior was referred to as "dripping". A higher velocity or a lower flow rate could produce some uncovered area on the coated substrate, which was the "ribbing" in Figure 2.5(B).

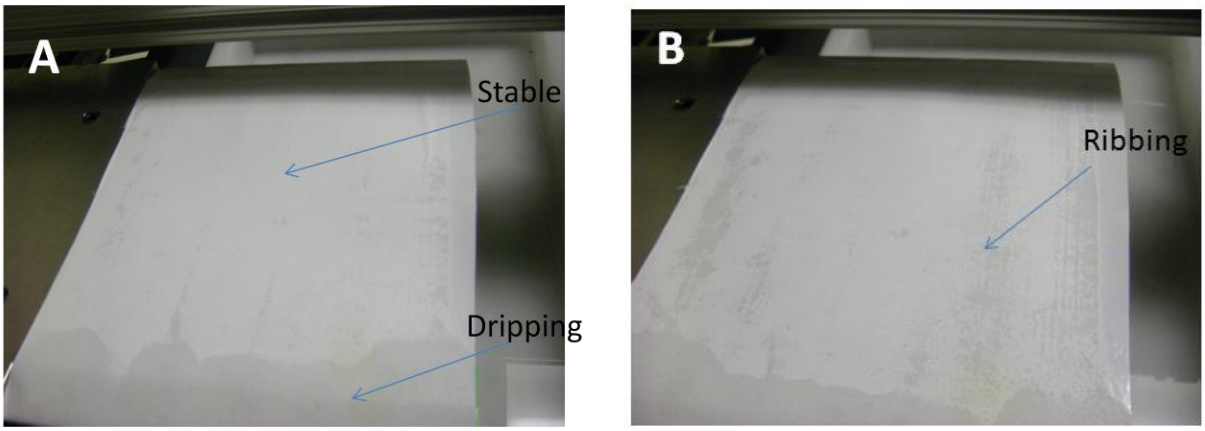

Figure 2.5 Photographs of different coating results, (A) a stable coating with dripping occurred at the beginning of coating and (B) ribbings caused by part of uncovered area.

2.3.2.2 Results and discussion

For industrial production, the membrane substrate is driven by a rotating roll and coated by the slot die continuously. In our experiment, the slot die coating process was designed for batch production to control the consumption of the membrane substrate. It should be noted that in Figure 2.5, there always existed an unstable coating area, located at the steep area on the steel plate. In this area, the coating gap was much larger than 100 microns and the introduced liquid failed to form a thin film by the shearing force. The same condition was also discovered when the introduced liquid was more than enough at the lower coating speed and higher flow rate area (as seen in Figure 2.6). With an increase in the coating gap, the slot die coating window was narrowed and its stable minimum wet coating thickness was increased. According to the model presented by Carvalho et al., the minimum wet coating thickness was mainly determined by the coating gap H_c and thecapillary number (Ca). Their relationship can be described by the following equation [1]:

$$Ca = \frac{\eta V_w}{\sigma} = 0.65\left(\frac{2}{H_c / t_{\min} - 1}\right)^{3/2} \tag{2.13}$$

where V_w is the web velocity or the coating speed, σ is surface tension of the coating liquid (decane is 23.83 mN/m). H_c is the coating gap and t_{min} is the minimum wet coating thickness.

To obtain a successful film coating, the coating gap should always be larger than the targeted thickness. For a specific coating speed, the increase in the coating gap would lead to an increase in the minimum wet coating thickness. This trend was observed in our experiments as shown in Figure 2.6. When the specific coating speed was 400 mm/s, the coating gaps and their corresponding minimum wet coating thickness were 40 µm (8.2 µm), 60 µm (9.9 µm), 100 µm (14.4 µm), respectively.

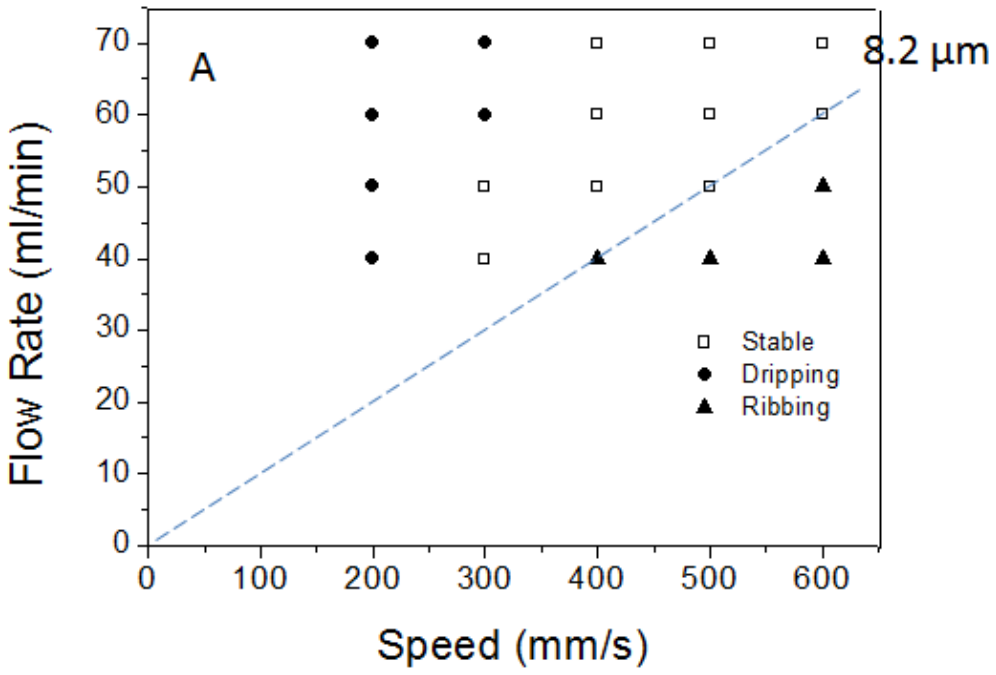

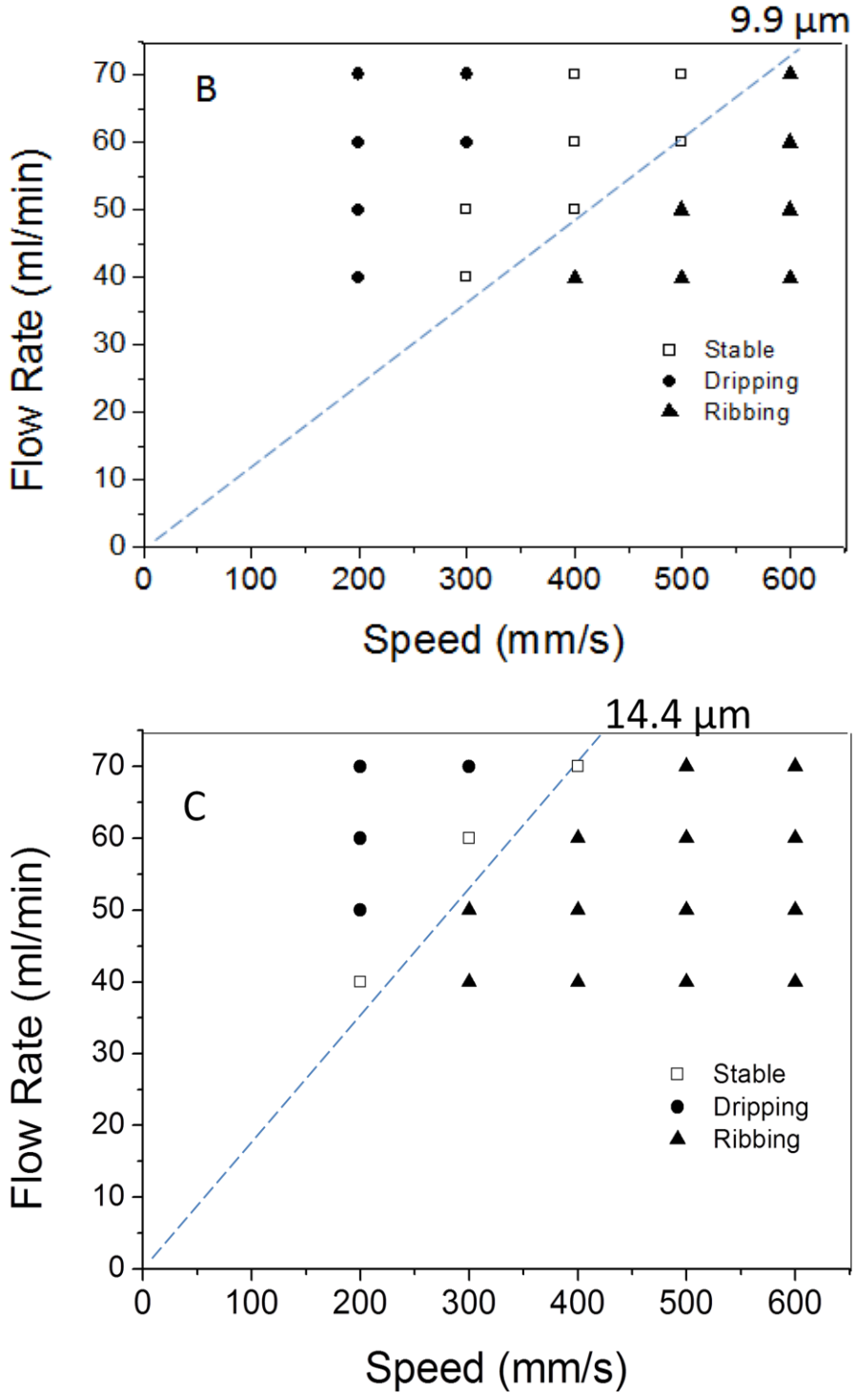

Figure 2.6 Slot die coating windows with coating gaps of (A) 40 µm (B) 60 µm (C) 100 µm. The stable minimum wet coating thicknesses of (A), (B) and (C) are 8.2 µm, 9.9 µm and 14.4 µm respectively.

2.4 Conclusions

A slot die coating head was designed for the preparation of NF membrane through interfacial polymerization. Dimensions of the slot die head were determined based on the successful die design example reported in the literature and the specific requirements in our membrane preparation. It was found that the variation in the pressure drop along the slot width was below 0.002% in the uncorrected T-shaped model due to the small value of the slot width. Under this condition, no more correction on the slot length was needed to compensate for the pressure difference. The coating error could mainly come from the manufacturing of the die head, which was anticipated to be in the 7.5% range. The syringe pump KD220, BD syringes and 0.5 m plastic tube with inner diameter of 3.28 mm were used to deliver the coating liquid (decane). Having checked the pressure drops and the velocity heads, we found that the syringe pump was strong enough to achieve the maximum flow rate of 2.4 mL/s. Reynold numbers were calculated to confirm that the state of decane in the delivery system was always under laminar flow. The slot die coating system was thus constructed, where its coating windows were obtained through experimentation. It was found that increasing the coating gap could increase the minimum stable coating thickness and reduce the coating window.

Nomenclature

C	a constant determined by slot dimensions
Ca	capillary number
De	equivalent diameter
F	fraction distance down the slot channel along z direction
H	slot gap

$\mathbf{H_c}$	coating gap between slot exit and membrane substrate
L	length of slot channel along the flow direction
$\mathbf{P_c}$	pressure in slot cavity
$\mathbf{P_s}$	pressure drop in slot channel in the direction of z
$\mathbf{P_{sx}}$	pressure drop in slot channel in the direction of x
Q	liquid flow rate
$\mathbf{q_{sx}}$	flow rate per unit width in slot channel in the direction of x
$\mathbf{Q_{max}}$	maximum flow rate
$\mathbf{Re_c}$	Reynold's number in slot gap
$\mathbf{Re_s}$	Reynold's number in slot cavity
R	cavity radius of slot die
$\mathbf{t_{min}}$	minimum wet coating thickness
$\mathbf{V_m}$	coating speed
W	width of slot die along z direction
x	direction down the slot
y	direction perpendicular to the flow
z	direction down the cavity channel from feed port
ρ	liquid density
θ	lip angle
σ	surface tension of coating liquid
η	liquid viscosity

References

[1] M.S. Carvalho, H.S. Kheshgi, Low-flow limit in slot coating: Theory and experiments, AIChE Journal, 46 (2000) 1907-1917.

[2] H.G. Lippert, Slot die coating for low viscosity fluids, Coatings Technology Handbook, (1991) 1559-1564.

[3] H. Benkreira, J. Ikin, Pushing the limits of slot Coating with the application of low viscosity Gases.

[4] M. Liu, S. Yu, M. Qi, Q. Pan, C. Gao, Impact of manufacture technique on seawater desalination performance of thin-film composite polyamide-urethane reverse osmosis membranes and their spiral wound elements, Journal of Membrane Science, 348 (2010) 268-276.

[5] S.I. Youn, S.Y. Kim, D.M. Shin, J.S. Lee, H.W. Jung, J.C. Hyun, A review on viscocapillary models of pre-metered coating flows, Korea-Australia Rheology Journal, 18 (2006) 209-215.

[6] E.B. Gutoff, Comparison of infinite cavity and corrected designs for coating die internals, The Journal of imaging science and technology, 38 (1994) 584-593.

[7] E.B. Gutoff, Simplified design of coating die internals, The Journal of imaging science and technology, 37 (1993) 615-627.

[8] Z. Tadmor, C.G. Gogos, Principles of polymer processing, Wiley. com, 2006.

[9] H.M. Chang, Y.R. Chang, C.F. Lin, T.J. Liu, Comparison of vertical and horizontal slot die coatings, Polymer Engineering & Science, 47 (2007) 1927-1936.

[10] S.J. Weinstein, K.J. Ruschak, One-dimensional equations governing single-cavity die design, AIChE Journal, 42 (1996) 2401-2414.

[11] Y.-R. Chang, C.-F. Lin, T.-J. Liu, Start-up of slot die coating, Polymer Engineering & Science, 49 (2009) 1158-1167.

Chapter 3 Nanofiltration Membranes Based on Thin-Film Nanofibrous Composites

A thin-film nanofibrous composite (TFNC) membrane for nanofiltration (NF) with substrates fabricated entirely by fibers has been developed. From bottom to top, the membrane consisted of a poly (ethylene terephthalate) (PET) non-woven cloth, a polyacrylonitrile (PAN) electrospun scaffold, a cellulose nanofiber (CN) layer and a polyamide (PA) top barrier layer, partially integrated with the CN layer. Under the same test condition (70 psi, 2000 ppm $MgSO_4$ as feed solution), all the manually coated NF membranes possessed high rejections (above 99%) but different fluxes. TFNC NF membrane had a flux of 44.7 l/m^2-h (LMH) while NF membranes by using the traditional phase-inversion substrate had a flux of 27.6 l/m^2-h (LMH). Transmission electron microscopy (TEM) showed that the CN could be partially combined with the PA barrier layer to form a structure simulating directed water channels that may result in achieving a higher flux for the barrier layer. Slot die coating was then introduced to further improve the membrane performance. Its main function was to control the growth of barrier layer by metering the amount of organic solution delivered for interfacial polymerization. When the thickness of the organic phase was controlled to 19 μm, the TFNC NF membrane was able to achieve a flux of 71.7 LMH and a rejection ratio of 98.5% for the 2000 ppm $MgSO_4$ solution. Comparing with the commercial membrane NF 270 (Filmtec), whose rejection ratio is 97%, the flux of TFNC NF membrane still had potential to get improved. 20% bipiperidine (BP) with respect to the weight

of total amine monomers was added during the slot-die-coated interfacial polymerization process. With a rejection ratio of 96.7%, the TFNC NF membrane finally obtained a flux of 94.3 LMH, doubling the flux of NF 270. Based on the pore size distribution analysis and the amount of surface charge density, the slot die coating process controlled mainly the membrane thickness. At present, the selected coating conditions seems to have led to about twice as thick barrier layer as NF 270, suggesting that the membrane efficiency still has room for further improvement.

3.1 Introduction

Nanofiltration (NF) membranes can be regarded as "loose" reverse osmosis (RO) membranes (i.e., with larger pore sizes than those of RO membranes) and have been used to soften water for more than 30 years. [1] Similar to RO, NF needs pressures but often in the lower pressure range (5 -20 bar [2]) to overcome the osmotic pressure to obtain the permeate. Two critical issues can be addressed to improve the membrane efficiency, i.e., cost effectiveness and energy efficiency. The thin-film composite (TFC) membrane with a thin polyamide (PA) barrier layer achieved by means of interfacial polymerization and properly deposited on top of an ultrafiltration (UF) substrate made by phase inversion is the state-of-the-art desalination technology. [3] Recently, some new membrane materials [4-9] have been introduced. However, their practical performance still has a distance to go when compared with commercial TFC membranes. An alternative way to obtain high-performance membranes is to optimize the existing TFC membrane, such as changing reaction conditions [10], or/and introducing nanoparticles [11], surfactants [12] or other small molecules [13] into the barrier layer. Membrane permeability could be optimized in the reported attempts, but the barrier layer became looser (i.e., with a reduction in selectivity).

The current study is an attempt to provide an alternative approach to enhance membrane permeability without affecting the salt rejection capability

According to the Donnan-steric pore model (DSPM) [14], the pure water flux of a NF membrane can be described by the Hagen-Poiseuille equation, where at fixed test conditions, the pure water flux is proportional to the square of the pore radius and inversely proportional to the membrane thickness. If the mean pore size and the porosity of the barrier layer remain unchanged, the membrane permeability can be controlled by adjusting the thickness of the barrier layer. The polymer layer formed at the interface by using interfacial polymerization is self-limiting and tends to resist further reaction between the two phases, thereby limiting the membrane thickness. [15] Reagents in either the organic phase or the aqueous phase for interfacial polymerization are crucial factors that can predetermine the barrier layer thickness. To achieve further thickness control, the volume of one phase can be reduced to such an extent that the monomers in the corresponding phase become the limiting reagent (i.e. the barrier layer thickness can be reduced with the volume of the phase delivered.) Hence, a new membrane manufacturing process is being proposed to replace the conventional dip coating process. The slot die coating process belongs to a class of coating methods known as pre-metered coating. The thickness of the metered liquid layer is set by a prescribed flow rate, making this approach ideal for controlling the coating thickness. [16] The most important feature of this coating operation is the minimum wet coating thickness at a given condition. [17]

The thin-film nanofibrous composite (TFNC) has a new, often more porous, membrane structure based on the nanofibrous substrate. In our previous studies, the nanofibrous substrate was prepared by depositing electrospun fibers onto a substrate with strong mechanical properties, e.g., a poly(ethylene terephthalate) (PET) non-woven cloth. Compared with conventional

substrates fabricated by using the phase inversion method, the electrospun substrate possesses lower resistance to fluid flow. The NF membrane on the electrospun substrate had a greater flux than those membranes using the phase-inversion substrates, including NF270 (Flimtec, Dow). [18] X. Song et al. reported that this fibrous substrate could overcome internal concentration polarization and therefore, could improve membrane efficiency for forward osmosis (FO). [19] Recently, a novel natural material being isolated from cellulose, often referred to as ultra-thin cellulose nanofibers (CN), was introduced onto the top of the electrospun layer to form a barrier layer for ultrafiltration (UF) membranes. When fabricated with ultra-fine CN having diameters of about 5 nm, the CN UF membrane was able to achieve a 10-fold increase in the permeate flux over similar commercial membranes (PAN 10, Sepro) with the comparable rejection ratio, when dealing with oil/water emulsions. [20] As a substrate for NF membranes, the CN layer not only provided a smoother surface to support the ultra-thin barrier layer, but could also act as embedded water channels in the barrier layer. The water channels could be located at the interface between the embedded nanofibers and the polymer matrix forming the barrier layer in order to provide the flow of water molecules over shorter distances through the interconnected interface, rather than through the tortuous paths in the polymer matrix forming the barrier layer. [21]

In this chapter, three substrates, a PAN elecro-spun membrane, a CN UF membrane and a commercial UF membrane (PS 20, Sepro), were used to prepare NF membranes. To show the influence from substrates on the NF barrier layer, their morphology and surface roughness were detected by scanning electron microscopy (SEM) and atomic force microscopy (AFM), respectively. The performances of NF membranes with those three substrates were compared to show the unique advantages of TFNC. A slot die coater was designed, constructed, tested, and

then applied to control the thickness of the NF barrier layer for further improvements on the membrane performance. The pore size distribution and the surface charge density of the NF membrane were measured in order to provide a rationale for the increased efficiency of the TFNC NF membrane.

3.2 Experimental work

3.2.1 Materials and reagents

Poly(ethylene terephthalate) (PET) non-woven cloth was supplied by Sanko Junyaku Co., Ltd. (Japan) for use as the bottom substrate. Polyacrylonitrile (PAN) (M_w = 1.50 x 10^5 g/mole) from Polysciences, Inc. was dissolved in dimethyl formamide (DMF) and deposited onto the PET substrate by means of electrospinning technology. 2,2,6,6-tetramethyl-1-piperidinyloxy (TEMPO) was purchased from Acros Organics. Sodium bromide (NaBr), 10-15% sodium hypochlorite (NaClO) solution, and sodium hydroxide (NaOH) were used to oxidize cellulose samples (wood pulps from Fisher Scientific Company and Biofloc 96 from Thembec Tartas in France). Oxidized pulps were dispersed into de-ionized water (DI) and used to coat the top of a PAN electrospun layer to form the cellulose nanofiber (CN) layer. To prepare the polyamide (PA) barrier layer, the aqueous phase was prepared by dissolving piperazine (PIP), bipiperidine (BP) and triethylamine (TEA) into deionized (DI) water. The organic phase was prepared by dissolving trimesoyl chloride (TMC) into decane. Ethanol, cyclohexanone, galactose, maltose, rafinose were used to measure the pore size distribution of NF membranes. Except when mentioned, all above chemicals were bought from Sigma-Aldrich and used without further purification.

3.2.2 Preparation of PAN electrospun layer

PAN was dissolved in DMF with occasional string for two days at 60 ^{o}C to obtain a 10 wt% homogenous solution. The PAN solution was electrospun at 20 kV onto a PET non-woven cloth using a custom-built multiple-jet instrument. [22] The polymer solution flow rate for each jet was 20 μl/min and the distance between each jet and the PET support was 7 cm. This product was referred to as PAN/PET later.

3.2.3 Fabrication of CN layer

A CN suspension was prepared following the protocol reported by Hongyang Ma et al. [23] 10 g wood pulps (Biofloc 96) were cut into small pieces and dispersed into 192 g DI water. 0.2 g sodium bromide and 0.04 g TEMPO were dissolved into the mixture and 30 g 10 ~ 15% NaClO aqueous solution was added to start the reaction. The pH value was adjusted in the range of 10.0 to 10.3 by adding 1M NaOH aqueous solution. After 8 hours, the reaction was stopped by adding 10 mL of ethanol. The mixture was centrifuged at 1960 g to obtain the modified CN. The CN slurry was washed with DI water and separated by centrifugation. The washing and separation were repeated five times to remove salts in the slurry. 5 g of modified CN slurry was dispersed into 100 g DI water by using a homogenizer (Cole Parmer VCX-400) for 5 min. The suspension was centrifuged at 1960 g and the supernatant was taken for further use. The CN concentration in the suspension was obtained by using a total organic carbon analyzer (TOC-5000, Shimadzu).

PAN/PET was first saturated with an aqueous HCl solution (pH = 2). A rubber roller was used to remove bubbles on the substrate and residual HCl solution from the surface. A 0.1 wt% CN suspension was introduced on top of the PAN electrospun scaffold and coated by using a draw-down machine (Gardco DP-8301). The coating thickness of the suspension was controlled

to around 200 μm and the coated membrane was dried in a 90 ^{o}C oven for 20 min. The product was referred to as CN/PAN.

3.2.4 Preparation of NF membranes on different substrates with manual coating method/slot die process

The aqueous phase solution was prepared by dissolving PIP (1 wt%) and TEA (1 wt%) in DI water. A proper amount of BP could be added into the aqueous solution to adjust the pore size of the NF top barrier layer. The organic phase solution was prepared by dissolving 0.1 g TMC into 100 ml decane. PAN/PET, CN/PAN and PS 20 (Sepro) were adapted as the NF support.

The manual coating process was as follows. A piece of substrate (8 cm × 8 cm) was soaked and saturated in the aqueous phase and squeezed by using a rubber roller to remove extra solution from the surface. The wetted support layer was fixed at the flat bottom (19 cm × 12 cm) glass plate with the four edges of the support layer being sealed with tapes of known thickness. 46 mL organic solution was introduced on the top. After 10 s, the organic solution was drained and the membrane was treated with a heat gun to remove the residual organic solution. Afterwards, the membrane was dried at 80 ^{o}C for 10 min. It should be noted that the amount of solution and the 10 s time period were of some importance because the combination should coincide fairly closely to the depth of penetration needed for the interfacial polymerization, even though the excess amount of the organic solution was drained.

The slot die coating system consisted of three parts, computer control station, solution deliver part (including syringe pump and slot die head) and membrane deliver part (including steel plate and track). When coated by using the slot die process, the substrate was first fixed onto the steel plate with tapes. The fixed substrate was wetted with the aqueous phase manually and then

squeezed with a rubber roller to remove excess solution from the substrate surface and the bubbles between the steel plate and the substrate. The organic solution was injected into the slot die with a 60 ml syringe and the flow rate was controlled using a syringe pump (Harvard apparatus HA22I). The velocity of the steel plate moving on the track was computer controlled. The organic solution was delivered uniformly along the slot die with the support layer moving quickly and uniformly beneath the slot die in order to achieve an ultra-thin coating layer. The thickness of the coated organic solution layer was estimated by the following equation:

$$t = \frac{F}{L \times \mathrm{v_s}} \qquad (3.1)$$

where t is thickness of coated organic solution. F (0-70 ml/min), L (14.5 cm) and v_s (0-400 mm/s) are flow rate of organic solution, length of slot (as shown in Figure 2.3) and velocity of steel plate, respectively. The coated organic phase was left alone for 10 s and removed by cold air flow provided by a heat gun. Afterwards, the membrane was dried at 80 ^{o}C for 10 min.

The NF membranes with PAN/PET, CN/PAN and PS 20 as substrates are referred to as PA/PAN, PA/CN and PA/PS, respectively.

3.2.5 Pore size distribution test

The pore size distribution for the NF membrane was measured by following the procedure reported by J. A. Otero et al. [24] Six solutes (i.e. ethanol, cyclohexanone, galactose, maltose, rafinose, α-cyclodextrine) with different Stokes radius were dissolved in DI water to prepare a 500 ppm feed solution. The NF membrane was cut and put into a dead-end stirred cell (Amicon 8050) and 50 psi hydraulic pressure was applied using compressed nitrogen gas. The concentration of the feed solution and the permeate solution were measured by a total organic

carbon (TOC) analyzer to obtain the rejection ratio. The results were plotted and fitted by the following equation [24]:

$$f = 1 - \frac{1}{1 + (r / B)^C} \qquad (3.2)$$

where f and r are the number fraction of pore size and pore size (i.e. Stokes radius), respectively. B and C are constants, which were obtained through non-linear fitting in the Origin software. The plot of d*f*/d*r* versus r is drawn to show the pore size distribution of the NF membrane.

3.2.6 Carboxylic groups on NF membrane surface quantified by toluidine blue O (TBO) technique

The test was carried out by following the protocol published by Tiraferri et al. [25] The only difference was that the absorbance of the TBO solution was measured by using Ultraviolet-visible (UV, USB 2000 UV/vis) spectroscopy (Ocean Optics), instead of a micro-plate reader.

3.2.7 NF performance test

A custom-built cross-flow nanofiltration system with an active filtration area of 42 cm^2 was used to characterize the membrane performance. [8] The feed solution was a 2000 ppm $MgSO_4$ aqueous solution and circulated through the system at a flow rate of 0.1 gallon per minute (GPM) and 70 psi. The temperature of the solution was controlled to 25 ± 2 ^oC by using a recirculating chiller (Thermoflex 1400). The NF membrane worked under the above conditions for 3 hours to ensure a stable performance. Permeate flux and conductivity were measured every 5 min, which were monitored by using a top loading balance (Cole-Parmer Symmetry ECII-800) and a

conductivity meter (Oakton CON 110), respectively. Salt rejection (R) was calculated by using the following equation.

$$R = (1 - \frac{C_P}{C_F}) \times 100\% \quad (3.3)$$

where C_P and C_F are the conductivity of the permeate solution and the feed solution, respectively.

3.2.8 Scanning electron microscopy (SEM) measurements

The membrane morphology was observed by SEM (LEO 1550, Carl Zeiss) with a Schottky field emission gun and a Robinson backscatter detector. Cross-sectioned samples were prepared by fracturing water-wetted membranes in liquid nitrogen. All specimens received a one-minute of gold coating.

3.2.9 Cross-section of CN/PAN and PA/CN detected by transmission electron microscopy (TEM)

The sample was prepared by peeling the PET non-woven cloth from the top layers carefully. The top layers were then transferred into a flat embedding mold, filled with fresh epoxy Spur resin and polymerized at 70 ^{o}C. The cross-sections were obtained by cutting the resin-wrapped membranes with an ultra-microtome and mounted onto a copper grid. The samples were observed by FEI BioTwinG^2 TEM at an accelerating voltage of 120 kV. Images were acquired with an AMT XR-60 CCD Digital Camera System.

3.2.10 Atomic force microscopy (AFM) measurements

Surface roughness of PAN/PET, CN/PAN and PS 20 were measured by using a Nanoscope III atomic force microscope (DI 3000, Digital Instruments) in the contact mode.

3.3 Results and discussion

3.3.1 Morphology of NF substrate

The typical NF substrate consists of two layers, with the PET non-woven cloth being the bottom layer which can provide the mechanical strength to afford high hydraulic pressures during filtration. The mid-layer, settling on the non-woven cloth and contacting with the top barrier layer, usually possesses a porous structure to reduce the resistance to water flow. The mid-layer has smaller pore sizes when compared with the bottom substrate in order to provide support for the ultra-thin NF barrier layer. Figure 3.1 shows, respectively, the three different NF mid-layer structures. PS 20 is a commercial UF membrane prepared by phase inversion with a molecular weight cutoff (MWCO) of 20 KDa [26]. Figure 3.1 (a) shows that PS 20 has a sponge-like porous structure. From bottom to top, the membrane porosity decreases gradually and the neighboring small pores are not interconnected. A similar structure can be found in Figure 3.1(d) for the cross section of a high-performance NF commercial membrane, NF270, whose polysulfone (PS) mid-layer is fabricated by using phase inversion. [27] Different from the phase inversion method, the TFNC membrane, with the mid-layer being fabricated by using the electrospinning technology, has an interconnected porous structure with relatively lager pore sizes in the microfiltration (MF) range. Figure 3.1(b) shows a PAN electrospun scaffold with fiber diameters of around 220 nm (Figure 3.2), an average thickness of 37 μm (Table 3.1) and a mean pore size of 0.65 μm (Figure 3.8). Figure 3.1(c) is our newly-developed CN UF membrane. The UF barrier layer with a thickness of 240 nm (Table 3.1) was set on the PAN electrospun

scaffold. Fabricated by using ultra-fine cellulose nanofibers (with mean diameters of about 5 nm), the CN layer possesses interconnected pores and a much smaller average pore size (~21 nm with MWCO of around 2000 kDa) than the electrospun scaffold [23].

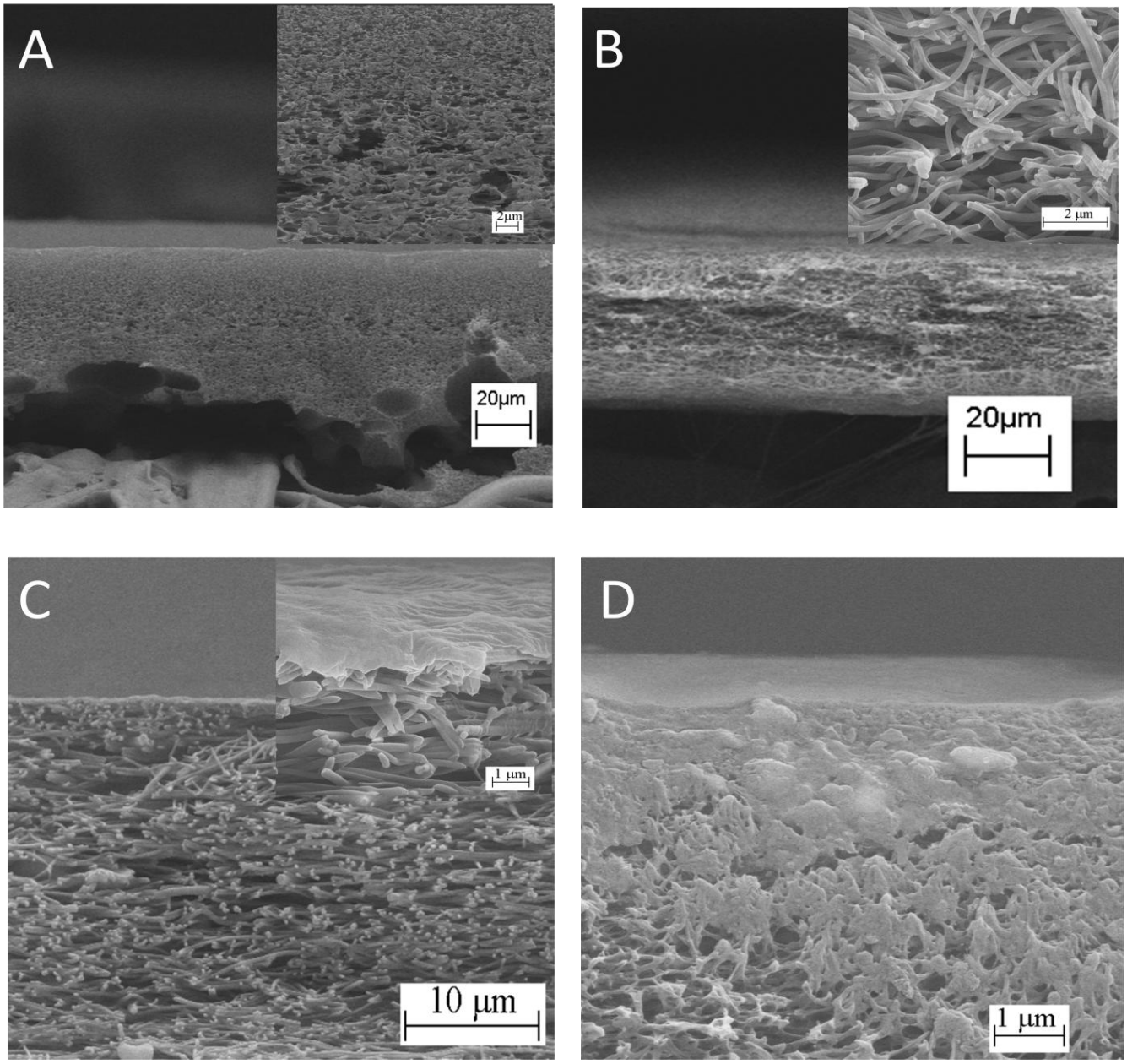

Figure 3.1 SEM images of membranes with PET non-woven cloth removed: (a) PSf 20, (b) PAN electrospun scaffold, (c) CN on PAN electrospun scaffold, (d) NF 270.

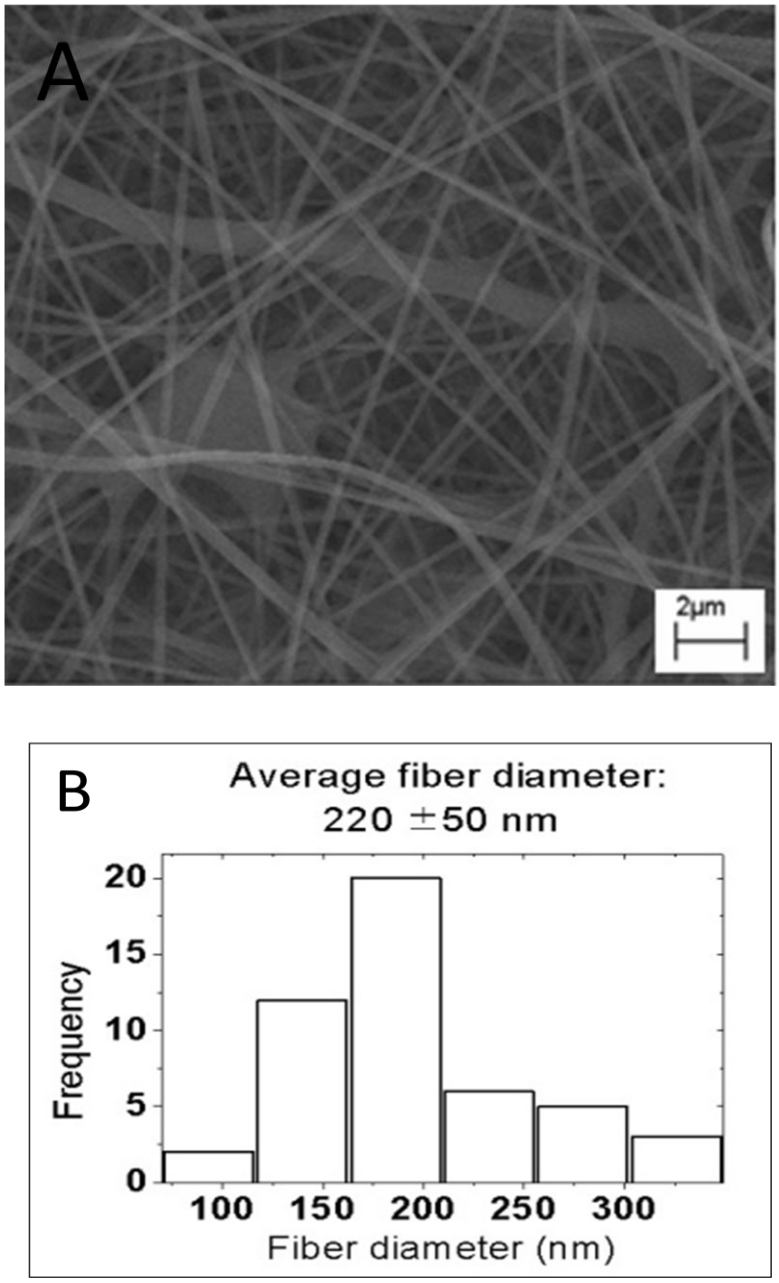

Figure 3.2 (a) SEM top view image of PAN electrospun scaffold and (b) distribution of fiber diameters.

Table 3.1 Properties of PAN electrospun scaffold, cellulose nanofiber (CN) ultrafiltration (UF) layer and commercial UF membrane PSf 20.

	PAN electrospun scaffold	**CN UF layer**	**PSf 20**
Thickness of substrate contacting with barrier layer (μm)	37.3 ± 6.4	0.24 ± 0.03	57.2 ± 5.1
pure water flux L/(m^2•h•psi)	3.02 x 10^3 [a]	15.3 [b]	6.3 [b]

The thickness was determined from the cross sectional image in Figure 3.1 by using the Leika image analysis software.

[a] Pure water was driven under 2.28 psi by gravity to flow through membrane in a dead-end cell. Water was collected in 1 min and measured by using a top loading balance.

[b] Pure water flux was measured in a dead-end stirred cell (Amicon 8050) under 30 psi provided by compressed air. Water was collected in 1 min and weighed by using a top loading balance.

3.3.2 Performance of hand-coated NF membrane with different substrates

With the barrier layer of NF 270 being piperazine-based polyamide [27], PIP and TMC were selected as the two monomers for the barrier layer preparation by means of interfacial polymerization. In order to compare the effects of the substrates (i.e., PS20, CN/PAN and PAN/PET), all interfacial polymerization on those substrates were carried out under the same conditions. The membrane performance is presented in Figure 3.3. All hand-coated NF membranes have impressive higher salt rejection (above 99%) than NF 270 (97.4%), but lower permeability. The reason for a higher flux for NF 270 is not clear because specific procedure(s) on the membrane preparation for NF270 is unknown. However, under the same preparation conditions, both PA/PAN (39.6 LMH) and PA/CN (44.7 LMH) obtained higher fluxes than that of PA/PS (27.6 LMH), suggesting the inherent advantages of using fibrous substrates for the NF support. Moreover, the newly-developed CN/PAN appeared to have more potential than PAN /PET because PA/CN had the highest flux.

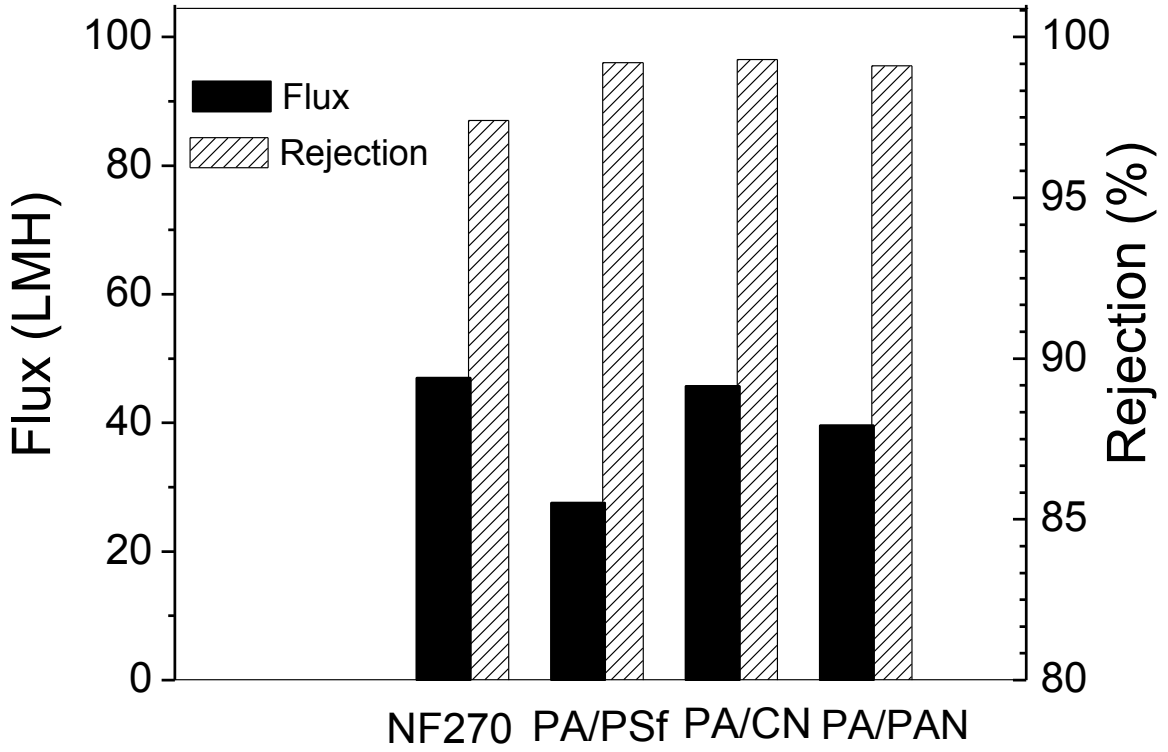

Figure 3.3 Comparison of NF fluxes and rejections among NF270 and manually-coated NF membranes on different substrates: PSf 20 (PA/PSf), cellulose nanofiber UF membrane (PA/CN), PAN electrospun membrane (PA/PAN).
The test conditions were as follows: 2000 ppm $MgSO_4$ feed solution, 70 psi and 25 ^oC.

Pure water permeability of different substrates increased in order of PS 20, CN/PAN and PAN/PET (Table 3.1). As the NF substrate, PAN/PET achieved the lowest resistance to water flow. Thus, with the same recipe and the same preparation conditions, the performance of the membrane should change with the thickness of the NF barrier layer. It was reported that the substrate with larger hydrophobic pores in the skin layer produced a more permeable NF membrane because of the thinner barrier layer from interfacial polymerization. [28] PAN/PET had hydrophobic skin pores (with surface contact angle of 151.2 ± 2^{o} [29]) and the largest pore

size. The barrier layer on PAN/PET should be thinner than those on PS 20 and CN/PAN. Hence, PA/PAN was anticipated to have the best efficiency because of the thinner barrier layer. However, PA/CN actually had the highest flux. The advantage of PA/CN could be attributed to the presence of cellulose nanofibers in the barrier layer, which was utilized to create directed water channels. [21] During the interfacial polymerization process, polyamide formed not only on top of the CN layer but also partially interpenetrated into the CN layer to form a composite barrier layer. As shown in Figure 3.4(b), PA had only a layer with a thickness of about 50 nm on the top. We can identify a dark layer with a thickness of around 30 nm beneath the PA layer as the composite area and postulate that, in this dark layer, directed water channels have been formed in the gaps between CN and polyamide matrix. As illustrated in Figure 3.4(c), molecules with sizes smaller than the gap length scale (e.g., water) should be able to pass through the directed water channels in the composite layer, in addition to the tortuous path via molecular cavities in the polyamide matrix. SEM image in the previous study showed that the polyamide layer bumping on the PAN/PET support without the composite layer. [18] The water-channel structure in PA/CN should correspond to an effective decrease in the nominal thickness of the polyamide barrier layer and thereby improve the membrane throughput. In practice, we have not yet optimized the use of directed water channels, in terms of density of water channels (including polymer matrix pore sizes), thickness of the nanocomposite barrier layer, and the interface structure (including charge density) for the directed water channels. It is also anticipated that, with the nanocomposite barrier layer, we do not need the pure polyamide barrier layer.

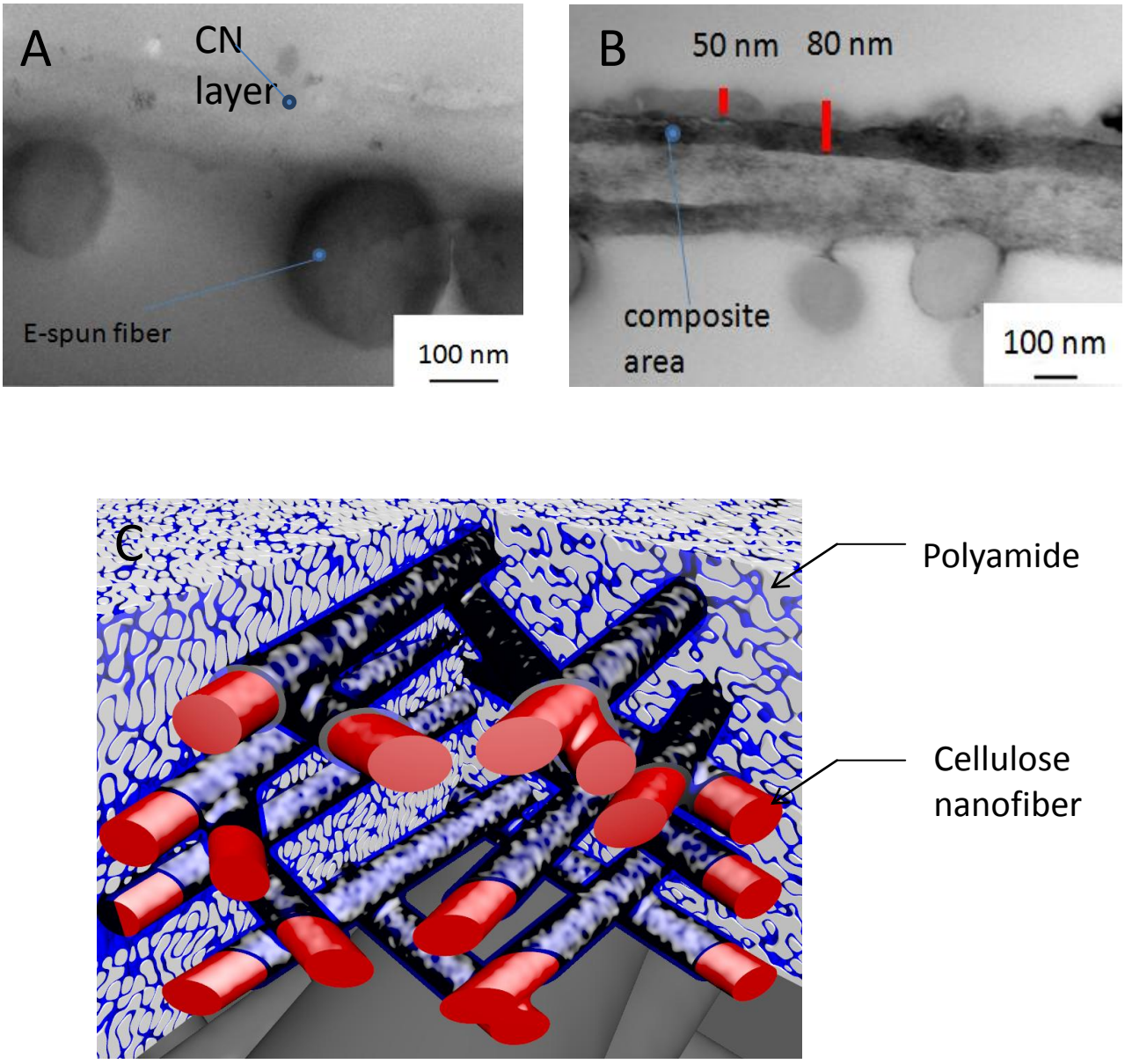

Figure 3.4 TEM image of (a) NF substrate (CN/PAN), (b) NF membrane from manual coating (PA/CN) and (c) schematic of water-channel structure in composite area.

3.3.3 Wet coating thickness controlled by slot die process

Although the fibrous structure of CN/PAN could bring an improvement on the membrane efficiency, the most important factor to the NF membrane performance is the characteristics related to the top barrier layer. Membrane formation in the interfacial polymerization process occurs over a very short time period, making control of the membrane thickness difficult to achieve. Rachel et al. [15] , by computer simulation, reported that during the interfacial polymerization, the monomers in the aqueous phase diffused into the organic phase and reacted with other monomers there to form a dense polymer layer. Later, aqueous monomers could keep reacting in the organic phase to increase the membrane thickness by diffusing through the initial denser layer to form a looser layer. It should be noted that the membrane selectivity comes mainly from the initial denser layer. Thus, the growth of the looser layer has less effect on the salt rejection. As it is difficult to achieve the control on the growth of the barrier layer through reacting time because the membrane is formed in a very short period of time (~2 ms [15]). While lower concentration in the aqueous phase can control the membrane thickness, it also leads to a lower salt rejection. [18] It is noted that the density of the denser layer is determined by the initial monomer concentrations in the two phases. [15] Thus, to ensure good salt rejection, the monomer concentrations in the two phases cannot be decreased independently. However, as the monomer concentration in the organic phase is often much lower than that in the aqueous phase, controlling the volume of the organic phase can limit further growth of the loose layer. A custom-built slot die coater was used to control the volume of the organic phase.

Figure 3.5 shows the performances of NF membranes with wet thickness of the organic phase on CN/PAN. The range of thickness was varied from 2 mm to 11 μm. The 2-mm thickness process was carried out by hand while the remaining thicknesses were achieved by using the slot

die process. From 2 mm to 78 μm, the permeate flux was only improved from 44.7 LMH to 45.7 LMH while the salt rejection remained unchanged. However, when the thickness was decreased to 39 μm, the flux was improved to 58.0 LMH without sacrificing the salt rejection. At a thickness of 19 μm, the flux was increased to 71.7 LMH but the salt rejection was declined to 98.5%. When the thickness was decreased to 11 μm, the salt rejection went down to 96.9% while the flux was increased to 77.1 LMH. NF 270 was introduced as a reference, whose typical rejection ratio for 2000 ppm $MgSO_4$ was 97%. Later, bipiperidine (BP) was added into the aqueous solution as co-monomers to improve the membrane flux. To balance the trade-off between flux and rejection, the wet thickness of 19 μm was selected as a satisfactory coating condition and adopted in further studies.

Figure 3.6 shows performances of NF membranes coated on PS 20 and CN by using the slot die process. With the salt rejection of 97.1% and the flux of 45.1 LMH, the performance of PA/PS was fairly close to that NF 270. Compared with the manual coating method, the slot die coating process improved the flux of PA/PS by 63%. To PA/CN, the flux of the NF membrane prepared by slot die was about 60% higher than that by manual coating. In a previous study, BP was found to be a kind of effective co-monomer to improve membrane flux without scarifying much on salt rejection. [18] 20 wt% BP with respect to the total amount of aqueous monomer concentration was added. The result showed an improvement on the membrane flux up to 94.3 LMH, which was twice as high as that of NF 270 (47.0 LMH), with the salt rejection ratio of PA (20%BP)/CN being 96.7%, comparable to that of NF 270 (97.4%).

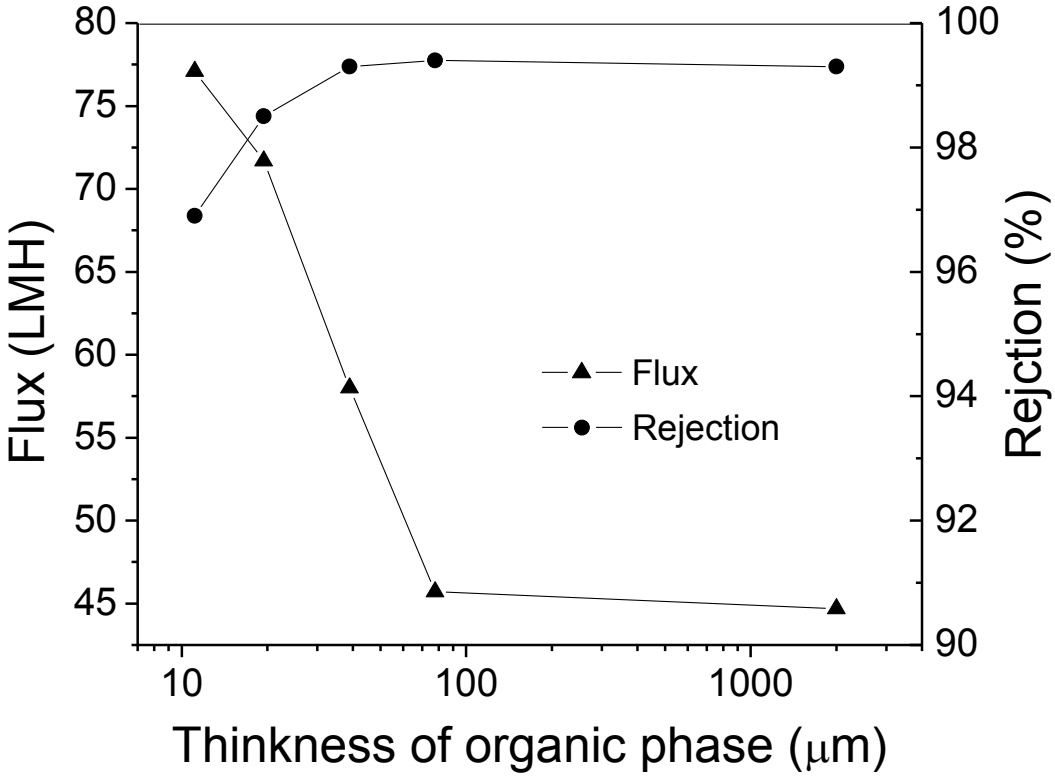

Figure 3.5 Organic phase thickness dependence of NF membrane flux and rejection in interfacial polymerization on CN substrate. Test conditions were as follows: 2000 ppm $MgSO_4$ feed solution, 70 psi and 25 ^{o}C.

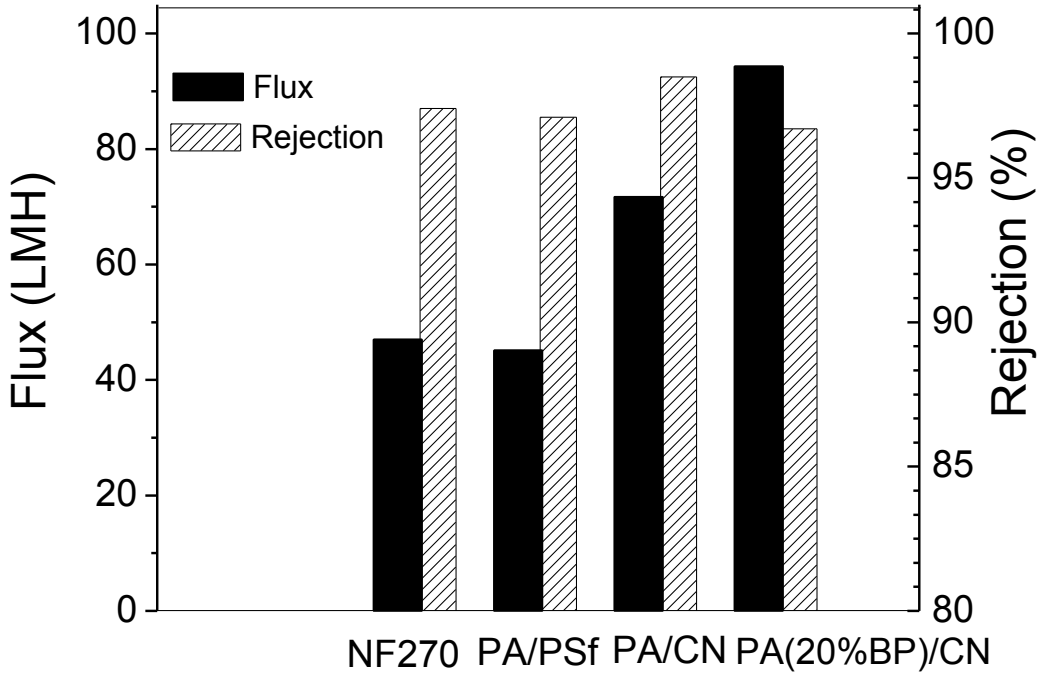

Figure 3.6 Comparison of NF fluxes and rejections among NF270 and slot die coated NF membranes on different substrates. The thickness of organic phase for interfacial polymerization was 19 μm. PA(20%BP)/CN was the NF membrane on CN prepared by 0.1% (w/v) TMC in decane and 0.8 wt% PIP, 0.2% BP, 1% TEA in water. The test conditions were as follows: 2000 ppm $MgSO_4$ feed solution, 70 psi applied pressure and 25 ^oC.

The improvements brought by the slot die coating process could be observed by using both PS 20 and CN/PAN substrates. However, no defect-free NF membrane was obtained on PAN/PET after many attempts when the wet thickness of the organic phase was set at 19 μm. Figure 3.7 shows AFM images of three different NF supports, with corresponding quantitative insights on their roughness being listed in Table 3.2. PAN/PET had the roughest surface and the distance between the valley and the peak on its surface was 11.9 μm, being comparable to the wet coating thickness of the organic solution (19 μm). Some areas on PAN/PET could not be well covered by the organic solution during the interfacial polymerization as practiced by the slot die process, leading to the failure of NF membrane preparation. Another reason for the failure

was the relatively larger pore size (0.65 μm, Figure 3.8), which led to less mechanical support to the top barrier layer. When its thickness was decreased by the slot die coater, the barrier layer became more vulnerable to the hydraulic pressure (70 psi).

Table 3.2 Surface roughness of NF substrates

Substrate	R_a (nm)	R_q (nm)	R_{max} (nm)
PAN electrospun	8.93×10^2	1.18×10^3	1.19×10^4
CN	41.6	56.0	5.07×10^2
PS 20	6.36	7.87	54.0

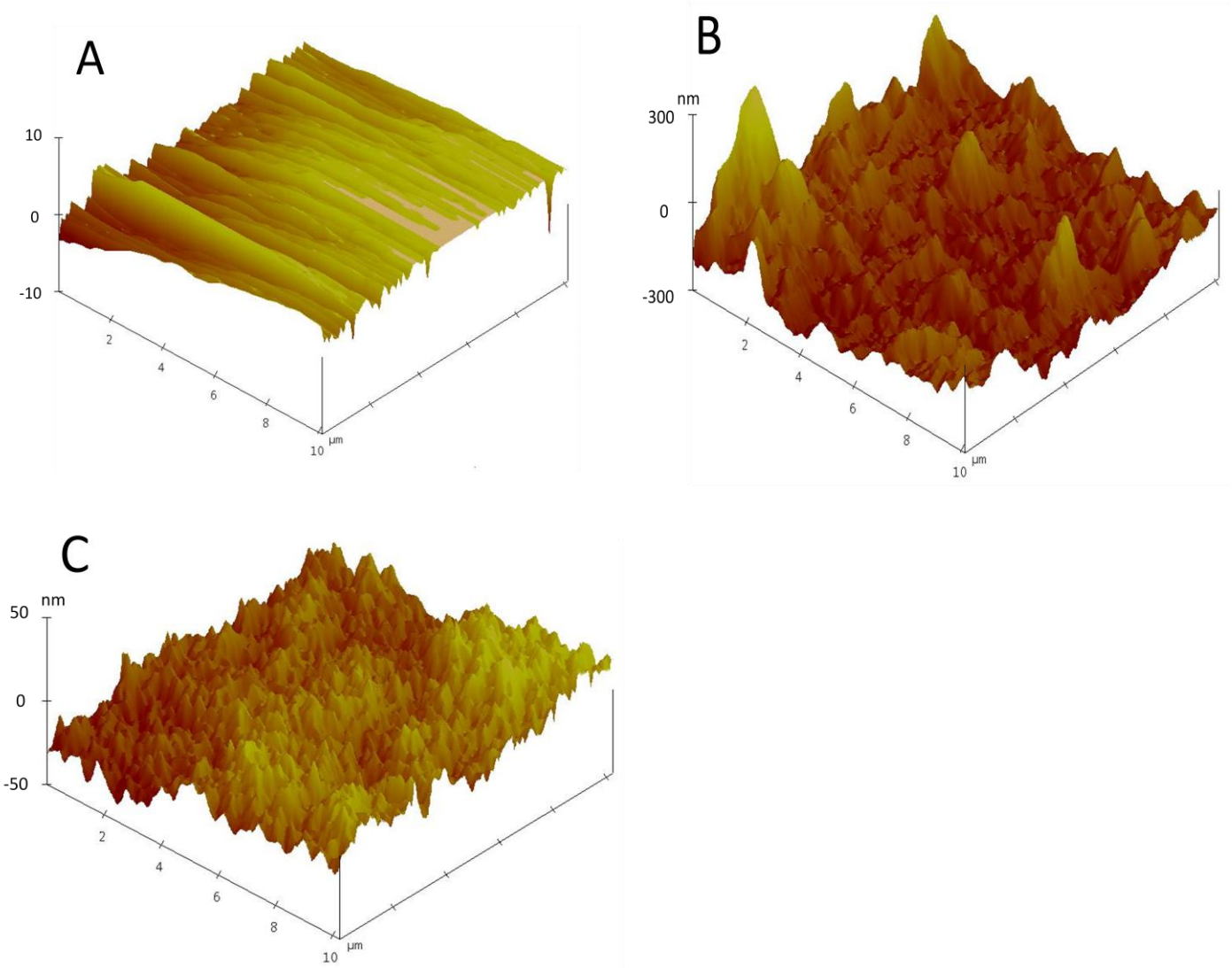

Figure 3.7 Three-dimensional AFM images of different substrates: (a) PAN electrospun scaffold, (b) CN, (c) PSf 20.

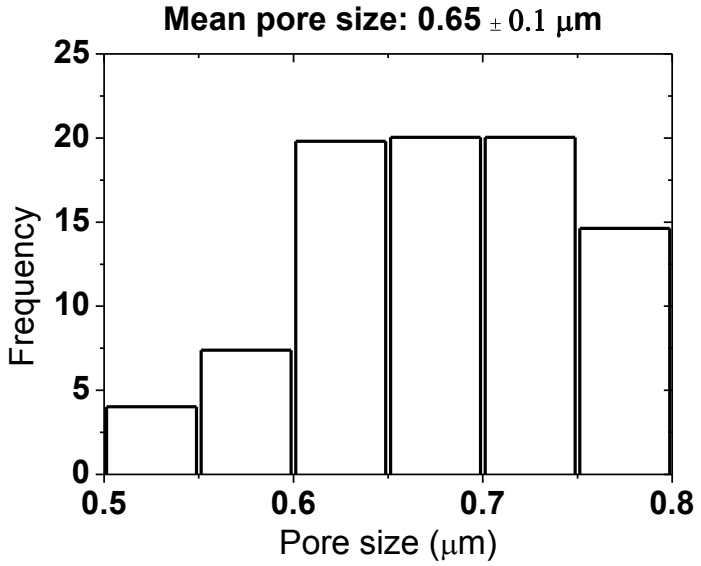

Figure 3.8 Pore size distribution of PAN electrospun scaffold.

3.3.4 Pore size distribution and quantification of surface carboxyl groups

Although the improvements on the membrane performance by using the slot die coater have been attributed to the control of the barrier layer thickness, the statement is difficult to confirm by using only microscopy. According to the Donnan-steric pore model (DSPM) [14], the permeate flux is determined by pore size and membrane thickness under the same test conditions. The change in the membrane thickness can be reflected by monitoring the changes in the pore size and the membrane flux. The membrane flux is shown in Figure 3.5 and the pore size distribution can be obtained by using aqueous solutions containing different uncharged solutes. The molecular radii of the uncharged organic solutes are listed in Table 3.3. In this test, the sieving mechanism is assumed to be the only reason for the retention. The rejection of a given organic solute is equal to the fraction of pores in the membrane being smaller than the

molecular radius of the organic solute. With a series of solutes having different molecular radii, the pore size distribution curve was obtained and fitted with Equation 3.2, as shown in Figure 3.10(a) and (b). Figure 3.10(c) shows the pore size distributions of NF membranes prepared by using the slot die coating process and manual coating. The four distribution curves were quite close to each other and their average pore sizes (radii) were all around 0.3 nm. Since the pore sizes were not changed by using the slot die coating process, the only factor contributing to the flux improvement could be the controlled thickness of the barrier layer.

Table 3.3 Molecular Radii of the organic solutes used in pore size distribution test [68].

500 ppm feed solution	**r (nm)**
Ethanol	0.2
Cyclohexanone	0.23
Galactose	0.35
Maltose	0.47
Rafinose	0.58
α-Cyclodextrine	0.77

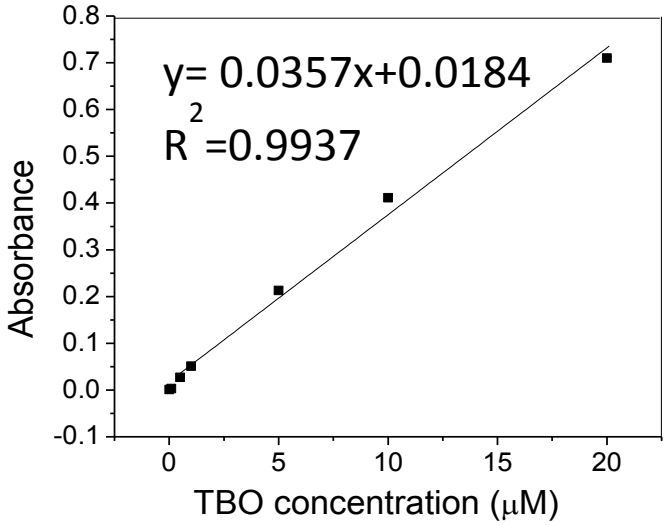

Figure 3.9 Calibration curve for quantification of carboxylic groups on NF membrane surface at 630 nm with 1 cm light path length.

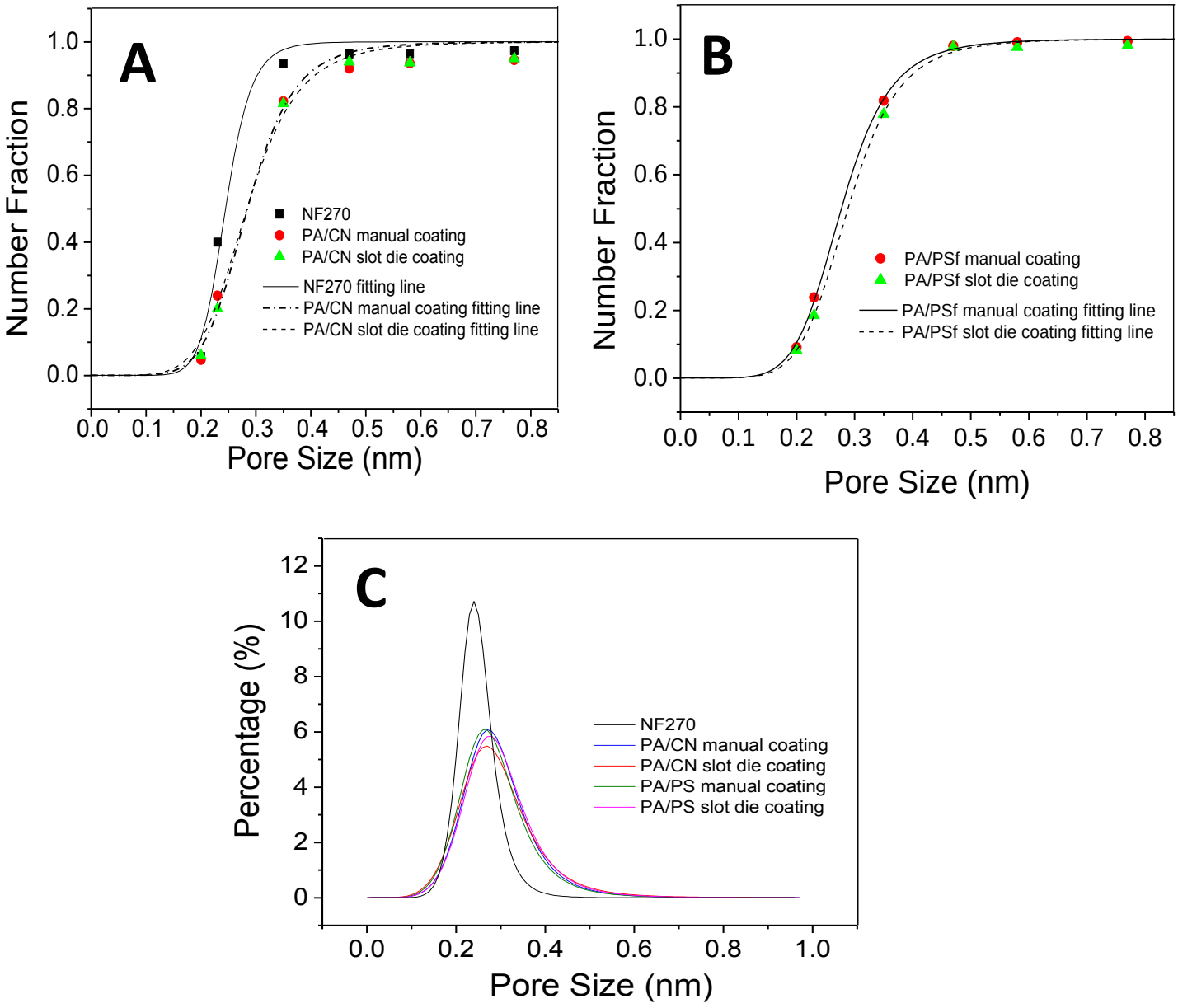

Figure 3.10 Cumulative pore size distributions of (a) NF270, PA/CN prepared by manual coating and slot die coating, (b) PA/PSf prepared by manual coating and slot die coating, and (c) pore size distributions of the membranes from (a) and (b). To the membranes coated by slot die, the thickness of organic phase for interfacial polymerization was 19 μm. The pore size is the mean radius of pores.

PA/CN prepared by manual coating (Figure 3.3) or slot die coating (Figure 3.6) could always yield a higher salt rejection ratio than that of NF270. However, its average pore size was larger than that of NF270. DSPM showed that the salt flux of NF membrane was determined not only by the membrane pore size, but also by the surface charge density and the thickness of the barrier layer. [14] While the streaming potential test could only provide an indirect or qualitative measurement on surface charge [25], the toluidine blue O (TBO) method was applied to quantify the NF surface charge. Figure 3.9 shows the calibration curve of TBO solution, with the test result being listed in Table 3.4. Compared with NF270, PA/CN had a little higher surface charge density, which remained about the same as by the slot die coating process. The thickness of the PA top barrier layer, as shown in Figure 3.4(b), was measured to be 50 nm and the thickness of the PA layer in PA/CN, as prepared by slot die coating (with a wet thickness of 19 μm), was estimated to be 31 nm, according to the DSPM and the flux ratios in Figure 3.5. Both PA/CN barrier layers were all thicker than the reported NF 270 barrier layer (13.9 nm [30]). Hence, the high surface charge density and the thick barrier layer compensated the large pore size in PA/CN and led to a higher salt rejection ratio than that of NF 270, as shown in Figures 3.3 and 3.6.

Table 3.4 Surface charge densities of NF membranes

Membrane	**Density of carboxyl groups (nm^{-2})**
NF270	0.8-1.6
PA/CN from manual coating	1.6-2.0
PA/CN from slot die coating [a]	1.5-2.0

[a] Thickness of organic phase was 19 μm during interfacial polymerization

3.4 Conclusions

NF membranes were prepared on the three different substrates manually and performances of both TFNC membranes were better than TFC. NF membrane with the newly developed CN/PAN substrate yielded the best performance possibly because of the water-channel structure to decrease the effective distance of water pathway in the composite area between CN and polyamide. With the slot die operation, the wet thickness of the organic phase could be controlled as thin as 19 μm during interfacial polymerization to confine the monomer diffusion. The fluxes of membranes prepared by using the slot-die coating process were improved around 60% when compared with those by using the manual coating process. Comparing with PAN electrospun scaffold, smaller pore size and smoother surface enabled CN/PAN to be coated by using the slot-die coating process. The improvement on membrane efficiency brought by the slot-die coating process could be attributed to better control on the thickness of the barrier layer through measurement tests on pore size distribution and surface charge density. 20% BP with respect to the total weight of amine monomers was added to further improve the membrane permeability. With the use of CN substrate, a combination of slot-die coating and addition of comonomer (BP), the NF membrane permeability could be improved to twice as high as the commercial one (NF270). The demonstration illustrates the feasibility of using the fibrous format for barrier support. Further improvements based on proper matching of substrate pore size and thinner barrier layer, together with proper use of directed water channels could improve the membrane performance to the next level.

References

[1] P. Robert J, Composite reverse osmosis and nanofiltration membranes, Journal of Membrane Science, 83 (1993) 81-150.

[2] M. Mulder, Basic principles of membrane technology, in, Kluwer Academic, Dordrecht ; Boston, 1996, pp. 17-18.

[3] M.A. Shannon, P.W. Bohn, M. Elimelech, J.G. Georgiadis, B.J. Marinas, A.M. Mayes, Science and technology for water purification in the coming decades, Nature, 452 (2008) 301-310.

[4] R. Du, J. Zhao, Properties of poly (N,N-dimethylaminoethyl methacrylate)/polysulfone positively charged composite nanofiltration membrane, Journal of Membrane Science, 239 (2004) 183-188.

[5] M. Homayoonfal, A. Akbari, M.R. Mehrnia, Preparation of polysulfone nanofiltration membranes by UV-assisted grafting polymerization for water softening, Desalination, 263 (2010) 217-225.

[6] L. Lianchao, W. Baoguo, T. Huimin, C. Tianlu, X. Jiping, A novel nanofiltration membrane prepared with PAMAM and TMC by in situ interfacial polymerization on PEK-C ultrafiltration membrane, Journal of Membrane Science, 269 (2006) 84-93.

[7] Y. Lu, T. Suzuki, W. Zhang, J.S. Moore, B.J. Mariñas, Nanofiltration Membranes Based on Rigid Star Amphiphiles, Chemistry of Materials, 19 (2007) 3194-3204.

[8] J. Miao, G. Chen, L. Li, S. Dong, Formation and Characterization of Carboxymethyl Cellulose Sodium (CMC‐Na)/Poly (vinylidene fluoroide) (PVDF) Composite Nanofiltration Membranes, Separation Science and Technology, 42 (2007) 3085-3099.

[9] M. Zhou, P.R. Nemade, X. Lu, X. Zeng, E.S. Hatakeyama, R.D. Noble, D.L. Gin, New Type of Membrane Material for Water Desalination Based on a Cross-Linked Bicontinuous Cubic Lyotropic Liquid Crystal Assembly, Journal of the American Chemical Society, 129 (2007) 9574-9575.

[10] L. Meihong, Y. Sanchuan, Z. Yong, G. Congjie, Study on the thin-film composite nanofiltration membrane for the removal of sulfate from concentrated salt aqueous: Preparation and performance, Journal of Membrane Science, 310 (2008) 289-295.

[11] M.L. Lind, A.K. Ghosh, A. Jawor, X. Huang, W. Hou, Y. Yang, E.M.V. Hoek, Influence of Zeolite Crystal Size on Zeolite-Polyamide Thin Film Nanocomposite Membranes, Langmuir, 25 (2009) 10139-10145.

[12] Y. Mansourpanah, S.S. Madaeni, A. Rahimpour, Fabrication and development of interfacial polymerized thin-film composite nanofiltration membrane using different surfactants in organic phase; study of morphology and performance, Journal of Membrane Science, 343 (2009) 219-228.

[13] L. Yung, H. Ma, X. Wang, K. Yoon, R. Wang, B.S. Hsiao, B. Chu, Fabrication of thin-film nanofibrous composite membranes by interfacial polymerization using ionic liquids as additives, Journal of Membrane Science, 365 (2010) 52-58.

[14] W. Richard Bowen, A. Wahab Mohammad, Diafiltration by nanofiltration: Prediction and optimization, AIChE Journal, 44 (1998) 1799-1812.

[15] R. Oizerovich-Honig, V. Raim, S. Srebnik, Simulation of Thin Film Membranes Formed by Interfacial Polymerization, Langmuir, 26 (2009) 299-306.

[16] Y.-R. Chang, C.-F. Lin, T.-J. Liu, Start-up of slot die coating, Polymer Engineering & Science, 49 (2009) 1158-1167.

[17] C.-F. Lin, D.S. Hill Wong, T.-J. Liu, P.-Y. Wu, Operating windows of slot die coating: Comparison of theoretical predictions with experimental observations, Advances in Polymer Technology, 29 (2010) 31-44.

[18] K. Yoon, B.S. Hsiao, B. Chu, High flux nanofiltration membranes based on interfacially polymerized polyamide barrier layer on polyacrylonitrile nanofibrous scaffolds, Journal of Membrane Science, 326 (2009) 484-492.

[19] X. Song, Z. Liu, D.D. Sun, Nano gives the answer: breaking the bottleneck of internal concentration polarization with a nanofiber composite forward osmosis membrane for a high water production rate, Adv Mater, 23 (2011) 3256-3260.

[20] H. Ma, C. Burger, B.S. Hsiao, B. Chu, Ultrafine polysaccharide nanofibrous membranes for water purification, Biomacromolecules, 12 (2011) 970-976.

[21] H. Ma, C. Burger, B.S. Hsiao, B. Chu, Highly Permeable Polymer Membranes Containing Directed Channels for Water Purification, ACS Macro Letters, 1 (2012) 723-726.

[22] B. Chu, B.S. Hsiao, D. Fang, Apparatus and methods for electrospinning polymeric fibers and membranes, in, The Research Foundation of State University of New York, USA . 2002, pp. 55 pp.

[23] H. Ma, C. Burger, B.S. Hsiao, B. Chu, Ultrafine Polysaccharide Nanofibrous Membranes for Water Purification, Biomacromolecules, 12 (2011) 970-976.

[24] J.A. Otero, O. Mazarrasa, J. Villasante, V. Silva, P. Prádanos, J.I. Calvo, A. Hernández, Three independent ways to obtain information on pore size distributions of nanofiltration membranes, Journal of Membrane Science, 309 (2008) 17-27.

[25] A. Tiraferri, M. Elimelech, Direct quantification of negatively charged functional groups on membrane surfaces, Journal of Membrane Science, 389 (2012) 499-508.

[26] B.D. McCloskey, H.B. Park, H. Ju, B.W. Rowe, D.J. Miller, B.J. Chun, K. Kin, B.D. Freeman, Influence of polydopamine deposition conditions on pure water flux and foulant adhesion resistance of reverse osmosis, ultrafiltration, and microfiltration membranes, Polymer, 51 (2010) 3472-3485.

[27] FILMTEC™ Reverse Osmosis Membranes Technical Manual, in, pp. 17.

[28] A.K. Ghosh, E.M.V. Hoek, Impacts of support membrane structure and chemistry on polyamide–polysulfone interfacial composite membranes, Journal of Membrane Science, 336 (2009) 140-148.

[29] H.S. Lim, S.H. Park, S.H. Koo, Y.-J. Kwark, E.L. Thomas, Y. Jeong, J.H. Cho, Superamphiphilic Janus Fabric, Langmuir, 26 (2010) 19159-19162.

[30] V. Freger, Swelling and Morphology of the Skin Layer of Polyamide Composite Membranes: An Atomic Force Microscopy Study, Environmental Science & Technology, 38 (2004) 3168-3175.

Chapter 4 Nanofiltration Membranes Prepared by Interfacial Polymerization through Two Different Methods

Nanofiltration (NF) membranes, consisting of a composite barrier layer prepared by interfacial polymerization of polyamide around the ultra-fine cellulose nanofibers (CN) layer in a thin-film nanofibrous composite (TFNC) scaffold, were demonstrated. Two interfacial polymerization pathways (termed IP and IP-R), regarding the arrangement of the aqueous and organic phases, were investigated. It was found that interfacial polymerization with the aqueous phase above the organic phase (IP-R) yielded better filtration performance, i.e., IP-R based membranes exhibited a higher $MgCl_2$ rejection than IP based membranes. Transmission electron microscopy (TEM) observation indicated that the denser part of the barrier layer was on the CN layer surface of IP-R based membranes, whereas this portion was deeply immersed in the CN layer of IP based membranes. To investigate the structure and property relationship of the composite barrier layer, both IP and IP-R based membranes were treated with 1% trimesoyl chloride (TMC) in hexane. After treatment, the rejection of NaCl was found to increase from 74% to 91% for IP-R based membranes, while remained unchanged (~75%) for IP based membranes. This behavior can be explained by the decrease in pore size due to the cross-linking of TMC and secondary amino groups in the barrier layer of IP-R based membranes, while the permeability in IP based membranes was probably mainly controlled by the water passage through channels

formed at the interface between CN and polymer matrix in the barrier layer of IP based membranes, which is not dependent of the cross-linking reaction.

4.1 Introduction

Desalination technologies for producing fresh water from sea water and brackish water have become increasingly important [1]. However, conventional desalination technologies usually involve energy-intensive processes, whereas the pressure-driven membrane separation process is the most energy efficient one [2]. The efficiency of the membrane technology can be further improved by developing new materials with higher permeability while maintaining good salt rejection capability. Currently, thin film composite (TFC) membrane, having a thin polymer barrier layer deposited on a porous substrate and thus forming an asymmetric structure, is considered one of the most energy efficient membrane systems [3] for applications such as nanofiltration (NF) and reverse osmosis (RO). Extensive research efforts have been made to improve the TFC membrane performance through interfacial polymerization (IP) to fabricate the barrier layer. These efforts include the introduction of new monomers [4], incorporation of non-reactive additives (e.g., surfactant [5], ionic liquid [6], nanoparticles [7] and small organic molecules [8, 9]), variation of reaction conditions (e.g., concentrations of organic phase or aqueous phase [10], types of organic phases [11] and surface property of the substrate [12]). These efforts indicate that there is the clear trade-off between permeability and rejection capability, i.e., the improvement on membrane efficiency always came with the loss of salt rejection capability, and vice versa.

The concept of “directed water channel” in the barrier layer [13] is a newly proposed pathway to improve the membrane efficiency without sacrificing the rejection capability. In brief,

the existence of directed water channel can facilitate the transport of water molecules, thus reducing the membrane resistance to water flow. However, the gap of the channel is sufficiently small to maintain the selectivity and rejection capability of contaminant molecules. It has been shown that materials, such as carbon nanotubes and Aquaporin proteins, can be used to introduce directed water channels in the barrier layer [14], suitable for NF and RO applications. Another nanoporous polymer system, containing interconnected channel-like structure, was demonstrated by cross-linking of lyotropic liquid crystal [15], in which the resulting structure consisted of a mean pore size of about 0.75 nm with permeability comparable to commercial RO. It was noted that the major obstacles in using the above materials for practical applications are the scale up processing schemes to produce high quality membranes at a competitive cost.

One practical pathway to introduce directed water channels is through the nanocomposite formation in the barrier layer, where natural occurring surface between the interconnecting filler scaffold (e.g. nanofibers) and polymer matrix (e.g. by interfacial polymerization) can be used to transport water molecules. In a previous study, we demonstrated that thin-film nanofibrous composite (TFNC) membranes can be used for this purpose [16]. Typically, the TFNC format contains an asymmetric layered structure having fibrous scaffolds with different fiber diameters (e.g. from a few nanometers to tens of nanometers). Different from conventional membranes, where the top barrier or support layer are prepared by phase-inversion, the nanofibrous layer can offer larger surface porosity and interconnected pores to reduce trans-membrane pressure drop while maintaining the same selectivity [17]. Recently, ultra-fine polysaccharide nanofibers (i.e., cellulose and chitin) were demonstrated as effective barrier layers supported by an electrospun scaffold for ultrafiltration (UF) applications [18]. These barrier layers offered smooth surface and pore size typically in the range of 20-50 nm. We have further demonstrated that the pore size

in these barrier layers could be further reduced to achieve NF/RO performance through interfacial polymerization on top. The thickness of NF/RO barrier layer was well controlled by slot die coating, which effectively enhanced the membrane efficiency [19]. In addition, the presence of a nanocomposite barrier layer, containing ultra-fine nanofibrous scaffold and space-filling polymer matrix layer, could provide opportunity to introduce directed water channels at the fiber/matrix surface [13].

Since the introduction of directed water channels in the barrier layer can significantly improve the membrane permeability, an in-depth investigation of this subject has become a focused area in our laboratory. In a previous study, we discovered that when interfacial polymerization of polyamide was carried out near the ultra-fine nanofibrous top layer, only a small portion of the polyamide was able to penetrate into the nanofibrous scaffold [19], which is similar to the condition in the substrate made by the phase-inversion method [12]. To effectively incorporate polyamide into the ultra-fine nanofibrous scaffold, positions of two phases (aqueous and organic) during interfacilally polymerization could be exchanged accordingly. This process was first demonstrated by Kaur, et al., who obtained the rejection of $MgSO_4$ at around 75%, when p-phenylenediamine and TMC were used as reactants on poly(vinylidene fluoride) (PVDF) electrospun scaffold [20]. These two interfacial polymerization pathways were termed IP (the organic phase on top of the aqueous phase) and IP-R (the aqueous phase on top of the organic phase), respectively. As the polyamide/cellulose nanofibers (CN) composite barrier layer could be produced with difference morphology and effective thickness [21] through the IP or IP-R route, the corresponding permeability could be quite different. It was thought that the IP-R based membrane could possess extra amino groups at the surface of the barrier layer (because the barrier layer facing the aqueous solution should have more amino groups than carboxylic groups),

while the IP based membrane would possess extra carboxylic groups [22]. In addition, the IP and IP-R based membranes should possess barrier layers with different polymer cross-linking topology and distributions. This is because a dense polymer barrier layer is firstly formed at the aqueous/organic interface during reaction, whereby the polymer subsequently grows into the organic phase and form a relatively loose layer [23].

In this study, the comparison of NF performance of TFNC-based membranes prepared by IP and IP-R pathways under the same reactive conditions (but at different concentrations of aqueous solutions) was carried out. The TFNC scaffold contained three fibrous layers: a top ultra-fine CN layer, an electrospun nanofibrous mid-layer and a non-woven fibrous substrate support. To determine the composition of functional groups in the barrier layer and its dependency on the membrane selectivity, the stream potential test was used to characterize the surface charges. In addition, surface modification was also introduced to eliminate extra amino groups on the IP-R based membrane, where the performances of modified and unmodified membranes were compared. The pore size distribution test and transmission electron microscopy was also used to correlate with the salt rejection capability of IP-R and IP based membranes. Based on the experimental results, a model was proposed to correlate the polymerization, structure and property for this system.

4.2 Experimental

4.2.1 Materials and reagents

The TFNC bottom substrate was a polyethylene terephthalate (PET) non-woven cloth from Junyaku Co., Ltd. (Japan). Polyacrylonitrile (PAN) (Mw=150,000, Polysciences Inc.) was first dissolved in dimethylformamide (DMF), where the solution was used to produce the TFNC mid-layer by electrospinning. Wood pulps, Biofloc 96 from Thembec Tartas factory (French) was

used to prepare ultra-fine cellulose nanofibers (CN), based on a scheme described elsewhere [18], to fabricate the TFNC top layer. The chemicals used in the CN preparation scheme were 2,2,6,6-tetramethyl-1-piperidinyloxy (TEMPO, Acros Organics), sodium bromide (NaBr, Fisher Scientific Company), 10-15% sodium hypochlorite (NaClO) solution and sodium hydroxide (NaOH). The barrier layer of the TFNC membrane was prepared by interfacial polymerization of the top CN layer involving two immiscible phases. The aqueous phase was prepared by dissolving piperazine (PIP) and triethylamine (TEA) into de-ionized (DI) water, whereas the organic phase was prepared by dissolving trimesoyl chloride (TMC) into hexane. The solution of 2-ethylhexanoyl chloride in hexane was also introduced to capture the secondary amino groups on the surface of IP-R based NF membrane. 500 ppm standard solutions (i.e., ethanol, cyclohexanone, galactose, maltose and rafinose in DI water) were used to measure the pore size distribution of the resulting TFNC membranes. The NF performance of these membranes was further tested by feed solution, containing magnesium sulfate ($MgSO_4$), magnesium chloride ($MgCl_2$), and sodium chloride (NaCl), respectively. Except mentioned, all above chemicals were purchased from Sigma-Aldrich and used without further purification.

4.2.2 Preparation of electrospun PAN mid-layer

The 10 wt% PAN/DMF solutions were stirred at 60 ^{O}C for two days to achieve a homogenous state. The PAN solution was electrospun at 20 KV onto the PET non-woven cloth by a custom-built multiple-jet machine [24]. Flow rate in each jet was 20 μl/min and the distance between the spinnerets and the PET support was 7 cm. The product will be referred to as the PAN/PET scaffold.

4.2.3 Fabrication of the CN top layer

CN suspension was prepared following the protocol reported earlier [18]. The concentration of the CN suspensions was measured by using the total organic carbon (TOC) analysis. The procedure to cast the CN suspension onto the PAN/PET scaffold was as follows. The PAN/PET scaffold was first saturated in HCl aqueous solution (pH = 2). A rubber roller was used to remove bubbles inside the substrate and extra HCl solution on the surface. 0.1% CN suspension was subsequently cast onto the electrospun PAN scaffold using a draw-down machine (Gardco DP-8301). The wet coating thickness was controlled at about 200 μm. The cast membrane was then equilibrated in a 90 ^{o}C oven till dry. The product will be referred to as the CN/PAN/PET scaffold.

4.2.4 Preparation of polyamide barrier layer by interfacial polymerization

Two different routes of interfacial polymerization were carried out on top of the CN/PAN/PET scaffold. The aqueous phase was prepared by dissolving PIP (0.2%-3%) and TEA (1%) into DI water, where the organic phase was prepared by dissolving 0.1 g TMC into 100 mL hexane. The IP route was carried out in a glass ware having flat bottom (19 cm × 12 cm). In this process, a piece of CN/PAN/PET scaffold (8 cm × 8 cm) was soaked and saturated in the aqueous phase first and subsequently squeezed by rubber a roller to remove extra solution on the surface. The wetted substrate was fixed in the glass ware with four edges sealed by tapes and left in air for 5 min. About 50 mL organic solution was then introduced gently on the top of the reactive wet CN/PAN/PET scaffold. After 1 min, the organic solution was drained out and the membrane was cured in an 80 ^{o}C oven for 10 min.

For IP-R, the substrate was first fixed on the glassware bottom by tape and impregnated by using the organic phase. Subsequently, about 200 ml aqueous solution was introduced to cover the substrate from one side to the other gradually before a thin layer of the organic solution on the substrate surface disappeared. After 1min, the aqueous solution was drained out and the membrane was cured in an 80 ^{o}C oven for 10 min.

4.2.5 Surface modification of IP-R based TFNC membrane

To remove extra amino groups on the IP-R based membrane, the following surface modification scheme was carried out. 1 g TMC or 1 g 2-ethylhexanoyl chloride was dissolved in 100 mL hexane. A piece of cured IP-R based TFNC membrane was then soaked in the hexane solution for 1 min and dried in the hood at room temperature. The modified TFNC membranes were subsequently washed and stored in DI water before tests.

4.2.6 Pore size distribution test on NF membranes

Pore size distribution test on NF membranes was pursued by following the procedure reported by J. A. Otero et al [25]. This test has assumed that the retention to organic solute is purely due to the sieving mechanism. For each solute, there is a fraction of totally retaining pores and the rest is allowed a free pass of the solute. Six organic solutes with different stokes radius were dissolved in DI water, respectively, to prepare 500 ppm feed solutions. The NF membrane was mounted into a dead-end stirred cell (Amicon 8050) and 3.4 bar hydraulic pressure was applied as driving force by using compressed nitrogen gas. Concentrations of the feed solution and permeate solution were measured by TOC for the determination of obtain solute rejections. The results were plotted and fitted by the Equation 3.2.

4.2.7 Membrane performance test

A custom-built cross-flow NF system with an active filtration area of 42 cm^2 was used to characterize the membrane performance. The feed aqueous solutions were 2000 ppm $MgSO_4$, 2000 ppm $MgCl_2$ or 500 ppm NaCl, respectively. The feed solution was circulated through the system at a flow rate of 0.38 liter per minute under 4.8 bar pressure. Continuous circulation using DI water was carried out for 3 hours to ensure stable membrane performance before testing. The temperature of the feed solution was controlled at 25 ± 2 ^{o}C by using a recirculating chiller (Thermoflex 1400). The filtrate solution was collected every 10 min and weighed using a top-loading balance (Cole-Parmer Symmetry ECII-800). The value of solution conductivity was monitored by using a conductivity meter (Oakton CON 110). The salt rejection (R) was calculated by using Equation 3.3.

4.2.8 Scanning electron microscopy (SEM)

The morphology of the samples was observed by using SEM (LEO 1550) with a Schottky field emission gun and a Robinson backscatter detector. Cross-sectioned samples were prepared by fracturing water-wetted membrane in liquid nitrogen. All specimens received a 1 min gold coating.

4.2.9 Transmission electron microscopy (TEM)

For TEM sample preparation, the upper layer of the TFNC membrane was first separated from the PET non-woven cloth and then cured in epoxy resin (Spur) at 70 ^{o}C. Cross-sections of the cured specimen were prepared by ultra-microtoming, where the cross-sectioned specimen was mounted on a copper grid. The samples were observed by a FEI BioTwinG2

TEM instrument operating at an accelerating voltage of 120 kV. Images were acquired using an AMT XR-60 CCD Digital Camera System.

4.2.10 Water contact angle measurement on NF membranes

The contact angle for a water droplet was measured by a CAM200 Optical Contact Angle Meter (KSV Instruments, LTD). For this measurement, the TFNC membrane was attached to a glass slide by scotch tape, where a 5 μL drop of water was placed on the sample for 30 seconds. Digital images of the water droplet were taken by the CAM software. The water contact angle was calculated by a curve fitting method [13].

4.2.11 Membrane surface zeta potential

Streaming current measurements were performed with the SurPASS Electrokinetic Analyzer (Anton Paar, USA) using an adjustable gap cell (AGC). For each measurement, a sample (10 mm x 20 mm) was carefully affixed onto each of the two sample holders using double sided adhesive tape. The sample holders were inserted into the AGC and the gap between the samples was adjusted to 50 - 150 μm. Each sample was first rinsed at a maximum pressure of 300 mbar for 180 seconds before the streaming current test at a target pressure of 300 mbar for 20 seconds. The pH value was automatically titrated with NaOH and HCl standard solutions. 1 mM KCl solution was used as the background electrolyte.

4.3 Results and Discussion

4.3.1 Morphology of TFNC membrane scaffold prior to interfacial polymerization

TFNC membranes, consisting of a top ultra-fine cellulose nanofibrous (CN) layer, an electrospun nanofibrous mid-layer and a non-woven fibrous substrate support, were prepared using the procedures described earlier [17]. These membranes were used as scaffolds to support the interfacial polymerization process to produce the barrier layer. Figure 4.1(a) illustrates the top-viewed SEM image of the electrospun PAN mid-layer. The mean fiber diameter in this scaffolding layer was 250±80 nm, which was measured from the Leika image analysis software [26]. When the thickness of the electrospun mid-layer layer (supported by the PET non-woven substrate) was 35±6 μm, the effective mean pore size became 0.65±0.1 μm having a pure water flux of 3.67×10^4 L/(m^2•h•bar) (Table 4.1), which was about 2-3 times higher than that of the commercial microfiltration (MF) membrane (e.g. Millipore GSWP) having the same rejection of carboxylate micro-particles with diameter of 1.0 μm, 0.5 μm and 0.2 μm respectively [26].

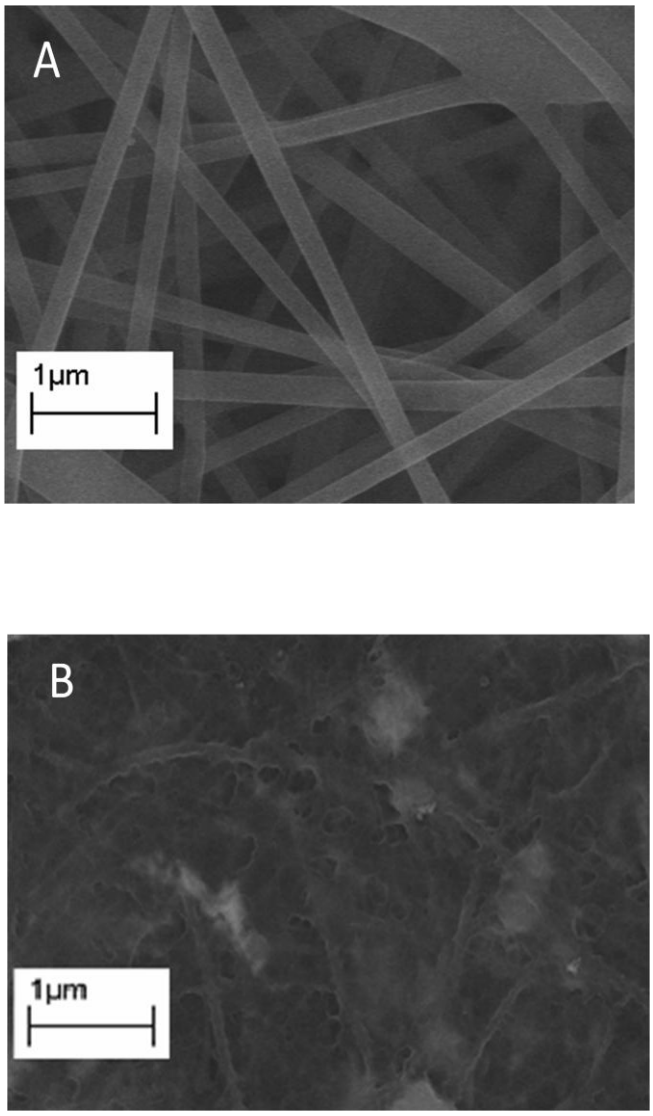

Figure 4.1 SEM top view images of (a) electrospun PAN scaffold and (b) CN layer on top of the electrospun PAN scaffold**.**

Table 4.1 Properties of the two nanofibrous substrates

	Thickness of top layer (μm)	**Pore size/MWCO**	**Pure water flux L/(m^2•h•bar)**
PAN/PET	35 ±6 [a]	0.65±0.1 μm [c]	3.67 ×10^4 [e]
CN/PAN/PET	0.25 ±0.03 [b]	5000 K Da [d]	238 [f]

[a] PAN electrospun scaffold was peeled off and measured by micrometer.
[b] Thickness of the CN layer was measured in its SEM cross-section image by Leika image analysis software
[c] The pore size was measured in a capillary flow porometer (CFP-1500A from PMI porous material, Inc). Wet air flow rate was measured by rinsing the sample with Galwick wetting fluid.
[d] The molecular weight cut off (MWCO) was measured with series of 1000 ppm dextran standard solutions. Each solution was driven through the membrane sample by compressed air (3.4 bar). Molecular weights of dextran vary in the range of 200 K – 5000 K. Concentrations of both feed and permeate were monitored by TOC.
[e] Pure water was driven through the membrane in a dead-end cell by gravity (0.157 bar). The permeate water was collected in 1 min and weighed on a top loading balance.
[f] Pure water flux was measured in a dead-end cell (Amicon 8050) under 2.1 bar provided by compressed air. The permeate water was collected in 1 min and weighted on top loading balance.

The PAN/PET scaffold offers the advantage of higher porosity over the substrate of conventional UF membrane (made by phase inversion) for NF [17] and forward osmosis (FO) applications [27]. Recently, fine cellulose nanofibers (with diameter of 5-10 nm) were cast onto the surface of PAN/PET scaffold, where the 3-layered composite scaffold possessed the pore sizes in the UF range [18]. Figure 4.1(b) shows the top view of the CN layer (thickness 250 ±30 nm) and the corresponding filtration performance is listed in Table 4.1. Although the surface pore size became smaller and the trans-membrane pressure drop increased quite significantly, the CN/PAN/PET scaffold turned out to be a better NF substrate than the PAN/PET scaffold because

of smoother surface and possible introduction of directed water-channels between ultra-thin CN and barrier polymer matrix for NF applications [19].

4.3.2 Performances of TFNC NF membranes prepared by IP and IP-R methods

For IP based membrane preparation, it was relatively easy to obtain defect-free NF barrier layers by introducing organic solution (i.e. TMC in hexane) on top of the CN/PAN/PET scaffold containing aqueous solution. However, during IP-R based membrane preparation, many pin-holes could be produced in the barrier layer because both density and surface energy of the organic solution were lower than those of the aqueous solution. To alleviate the pin-hole problem, a comparatively large amount of aqueous solution was gently introduced on top of the substrate, where hexane solution in the substrate was used to fill the pores of the cellulose substrate so that the polymerization reaction could take place at the interface between hexane and the aqueous solution. This step was intended to prevent hexane from moving upward at the interface which tends to produce defects in the barrier layer. Figure 4.2 shows the cross-sectioned images of the barrier layers prepared through IP and IP-R methods, respectively. It is clear that a dense defect-free layer was present on top of the PAN/PET scaffold in both Figures 4.2(a) or (b). However, the locations of the two barrier layers with respect to the substrates were different. In Figure 4.2(a), the barrier layer was essentially intact on top of the electrospun nanofibrous layer and the boundary between the electrospun fibers and the polymer layer were visually distinct, whereas the barrier layer was partially penetrated into the electrospun nanofibrous layer in Figure 4.2(b). The above difference could be attributed to the fact that the aqueous monomer appeared to diffuse into the organic phase, where polyamide was formed from the solvent interface into the organic phase [3]. Figures 4.3 and 4.4 show the NF performance of IP and IP-R based

membranes, respectively. When the TMC concentration in hexane was fixed at 0.1 (w/v) %, the NF performance exhibited a systematic change with the variation of PIP concentration (i.e. rejections increased and flux decreased with increasing PIP). Using $MgSO_4$ as the feed solution, there was little difference in the membrane performance between Figures 4.3(a) and 4.4(a), except that the rejection in Figure 4.3(a) was lower than that in Figure 4.4(a) at the concentrations of 0.2% and 0.6%. However, when the feed solution was switched to $MgCl_2$, the difference between Figures 4.3(b) and 4.4(b) became definitive. The IP based membranes always exhibited a lower rejection than the IP-R based membranes at the PIP concentration lower than 2%. For example, at the 1% PIP concentration, the IP-R based membrane had a rejection of 91.6% and the IP based membrane only had a rejection of 67.6%. The advantage of IP-R based membrane was maintained on CN/PAN/PET even at lower PIP concentrations. For example, Figures 4.5(b) and 4.6(b), the IP-R based membrane exhibited a rejection of 95.6% with the IP based membrane only 67.2% at the 1% PIP concentration. However, this difference disappeared when the PIP concentration became high, which explanation will be discussed next.

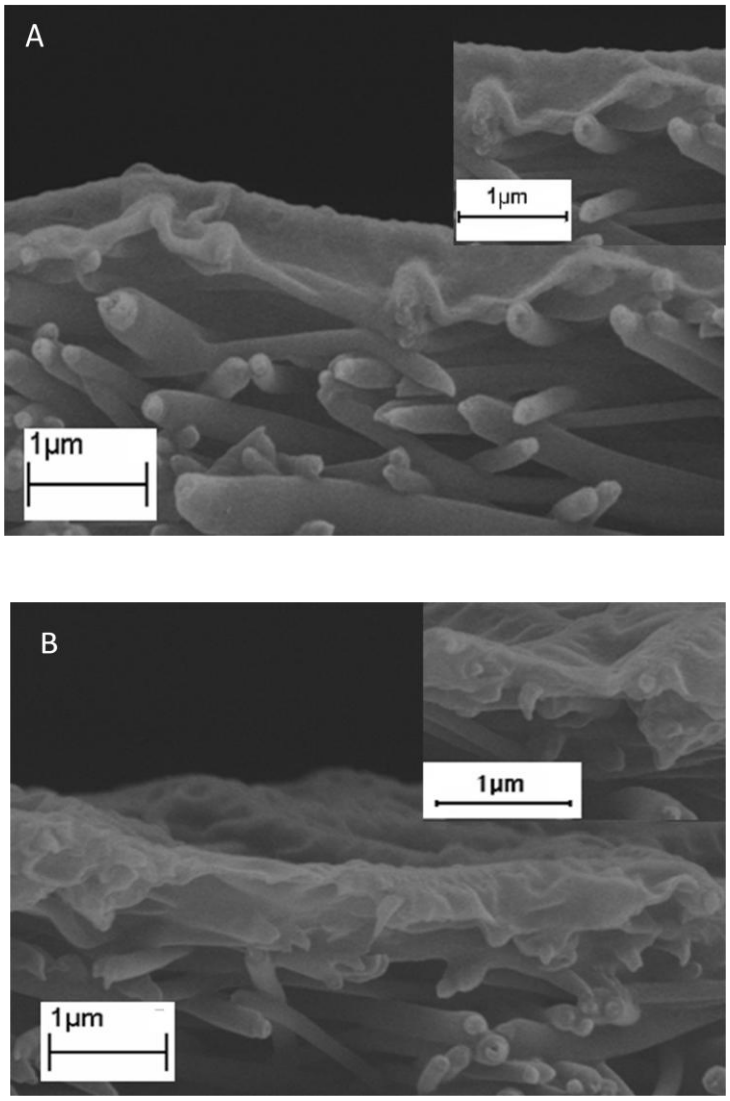

Figure 4.2 SEM cross-sectione images of composite barrier layers on top of electrospun PAN scaffolds in (a) IP based membrane and (b) IP-R based membrane.

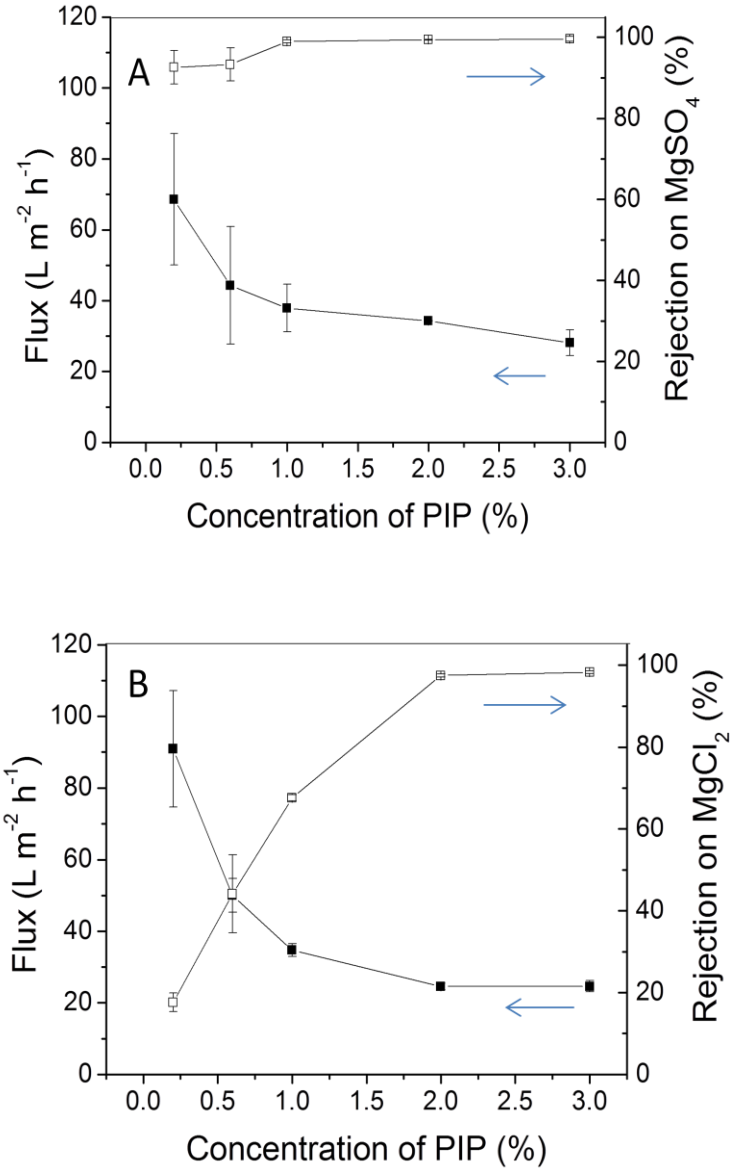

Figure 4.3 The PIP concentration dependence of flux and rejection in IP based membranes on PAN/PET scaffold using feed solutions of (a) $MgSO_4$ and (b) $MgCl_2$. The organic solution used to prepare the barriers layer was 0.1 (w/v) % TMC in hexane. The test conditions were as follows: 2000 ppm feed solution, 4.8 bar applied pressure and temperature of 25 ^{o}C.

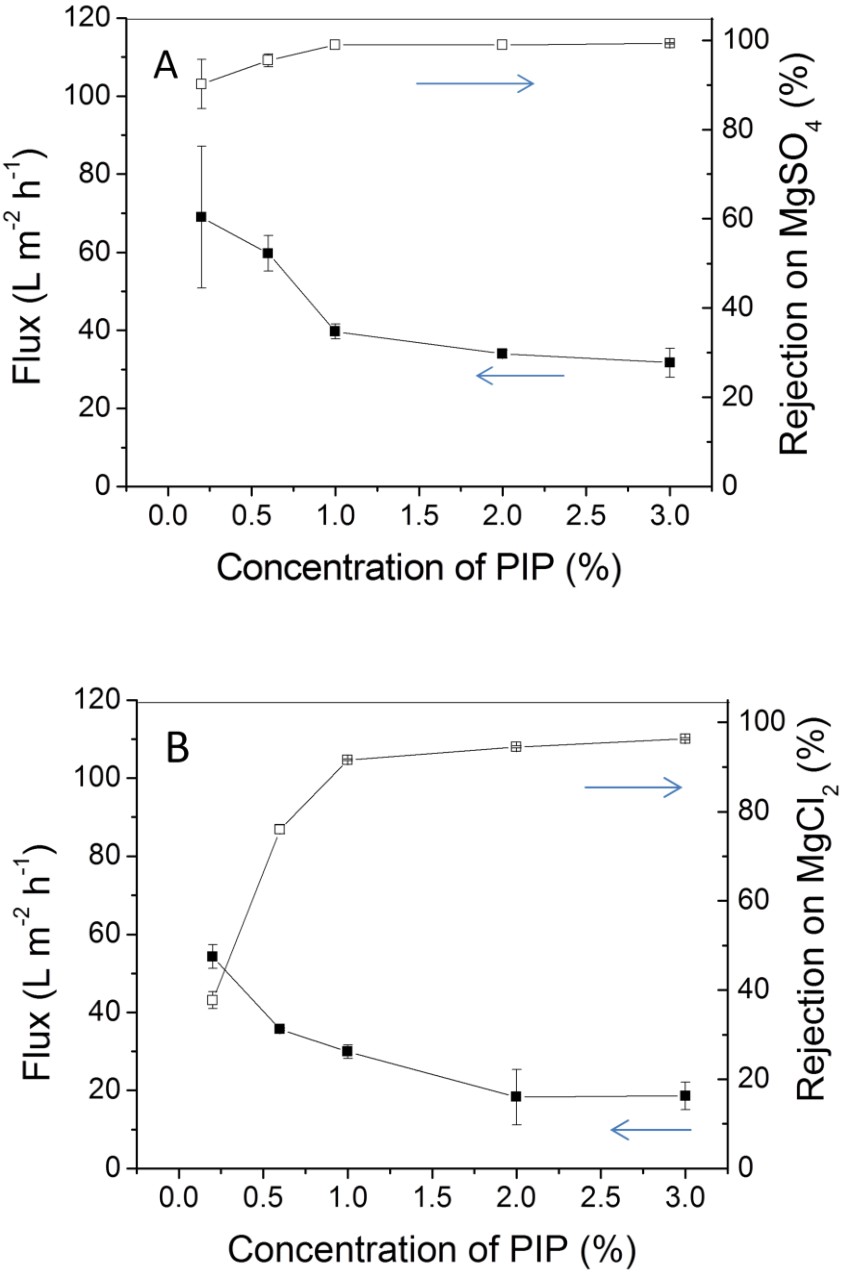

Figure 4.4 The PIP concentration dependence of flux and rejection in IP-R based membranes on PAN/PET scaffold using feed solutions of (a) $MgSO_4$ and (b) $MgCl_2$. The organic solution used to prepare the barriers layer was 0.1 (w/v) % TMC in hexane. The test conditions were as follows: 2000 ppm feed solution, 4.8 bar applied pressure and temperature of 25 ^{o}C.

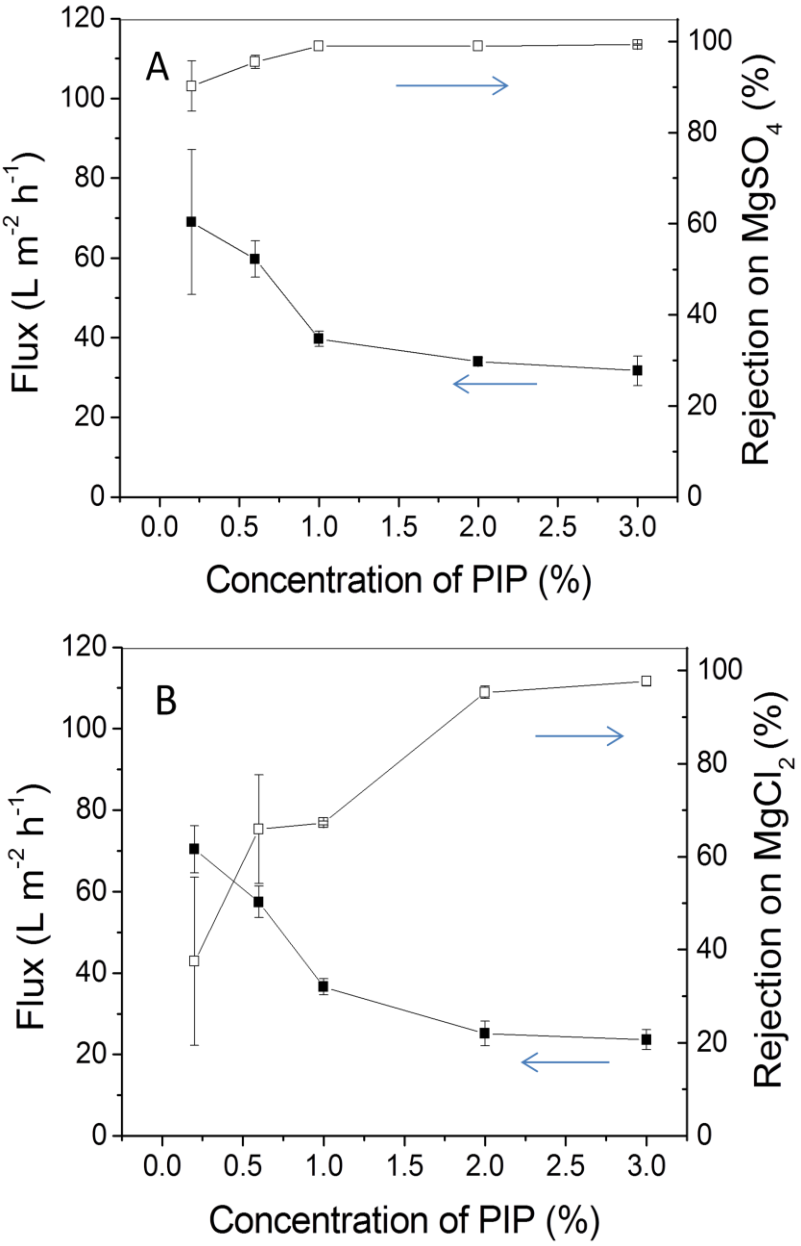

Figure 4.5 The PIP concentration dependence of flux and rejection in IP based membranes on CN/PAN/PET scaffold using feed solutions of (a) $MgSO_4$ and (b) $MgCl_2$. The organic solution used to prepare the barriers layer was 0.1 (w/v) % TMC in hexane. The test conditions were as follows: 2000 ppm feed solution, 4.8 bar applied pressure and temperature of 25 ^{o}C.

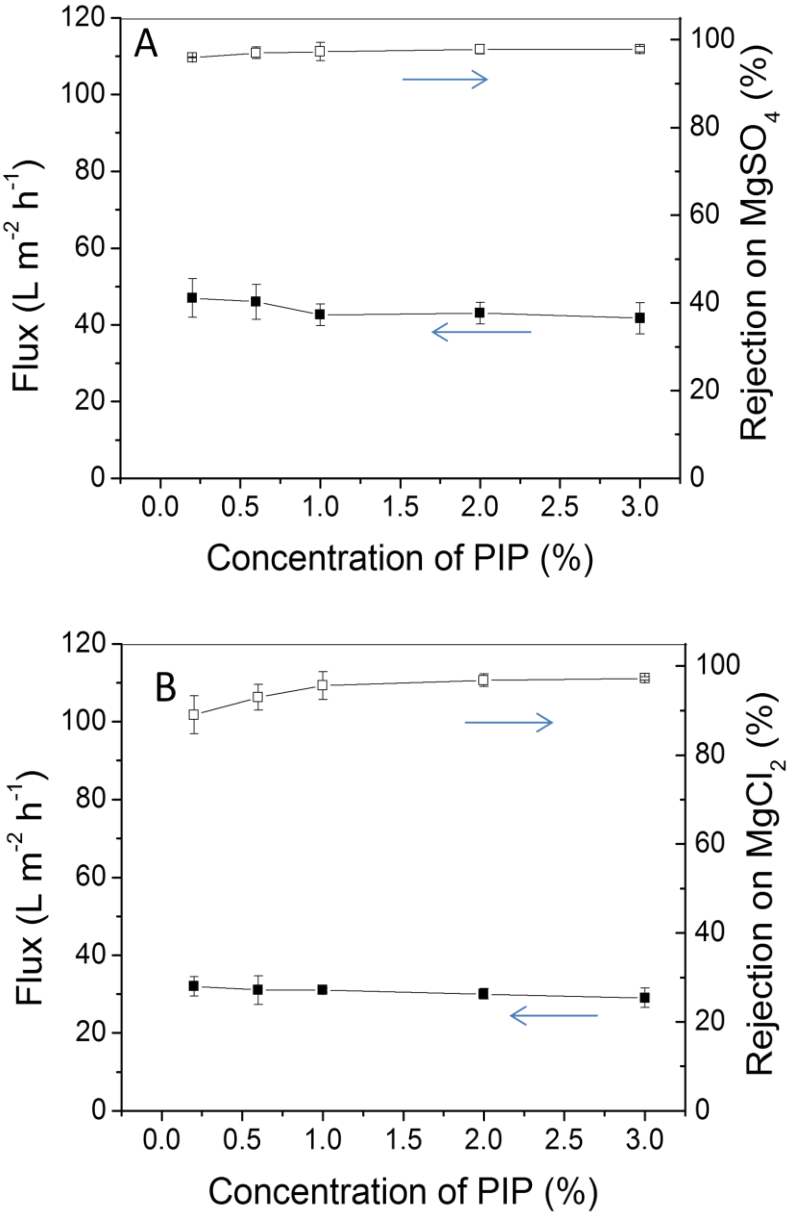

Figure 4.6 The PIP concentration dependence of flux and rejection in IP-R based membranes on CN/PAN/PET scaffold using feed solutions of (a) $MgSO_4$ and (b) $MgCl_2$. The organic solution used to prepare the barriers layer was 0.1 (w/v) % TMC in hexane. The test conditions were as follows: 2000 ppm feed solution, 4.8 bar applied pressure and temperature of 25 ^{o}C.

It is noticeable in Figures 4.5 & 4.6 that the flux of IP-R based membrane was significantly higher than that of IP based membrane at high PIP concentrations (>1%) on CN/PAN/PET. For example, when the PIP concentration was 2%, fluxes of IP-R based membranes were 43.0 L m^{-2} h^{-1} ($MgSO_4$) and 30.1 L m^{-2} h^{-1} ($MgCl_2$), while fluxes of IP based membrane were 34.2 L m^{-2} h^{-1} ($MgSO_4$) and 25.1 ($MgCl_2$). However, these differences on PAN/PET in Figures 4.3 & 4.4 were negligible. For example, when the PIP concentration was 2%, fluxes of IP-R membranes were 35.1 L m^{-2} h^{-1} ($MgSO_4$) and 25.3 L m^{-2} h^{-1} ($MgCl_2$), while fluxes of IP based membrane were 34.0 L m^{-2} h^{-1} ($MgSO_4$) and 24.6 ($MgCl_2$). The IP-R based membrane on CN/PAN/PET had the best efficiency. The reason behind it will be discussed in the following section.

4.3.3 Reasons behind the high performance of IP-R based membranes

4.3.3.1 Donnan effect

Typical NF membranes usually possess much a lower rejection against $MgCl_2$ than $MgSO_4$ [28]. Under the same test conditions as those in Figure 6, NF 270 (Filmtec, DOW) exhibited a rejection of 97.0% (flux of 50.2 L m^{-2} h^{-1}) against $MgSO_4$ and 72.4% (flux of 43.9 L m^{-2} h^{-1}) against $MgCl_2$. According to the Donnan ion repulsion effect [29], negative charges in the barrier layer can influence the ion-exchange equilibrium and impede the passage of anions in the feed solution. Since the sequence of hydrated ion sizes is SO_4^{2-} > Mg^{2+} > Cl^- [30], the negative surface charges could thus repel $MgSO_4$ more effectively than $MgCl_2$. However, as the surface charges are switched from negative to positive, Mg^{2+} could be repelled and the rejection against $MgCl_2$ would be enhanced [31]. It has been demonstrated that the polyamide barrier layer possessed excess carboxylic groups in the IP based membranes and that possessed extra amino groups in the IP-R based membranes [22]. The different rejections against $MgCl_2$ in Figures 5

and 6 thus could be attributed to the different surface functional groups in the IP or IP-R based membranes.

To confirm the above hypothesis, 1% 2-ethylhexanoyl chloride in hexane was used to eliminate secondary amino groups in the barrier layer of the IP-R based membrane. The NF results for the IP-R based membrane prepared by using 0.1 (w/v) % TMC (in hexane) and 1% PIP (in water) before and after the treatment (reaction time was 1 min) are shown in Figure 7. After the treatment (i.e., secondary amino groups reacted with 2-ethylhexanoyl chloride) the surface water contact angle of the IP-R membrane changed from 16.6^{o} to 55.8^{o}. However, neither the $MgCl_2$ rejection nor the flux was changed by the treatment. Figure 8 represents the results of the streaming potential test for the IP-R based membrane, whose preparation conditions are shown in the figure caption. The positive potential at low pH value was due to unreacted secondary amino groups and negative potential at high pH value was due to carboxylic groups. Therefore, the extra secondary amino groups on the IP-R based membrane surface could mean that the amino groups were comparatively more than carboxylic groups. The isoelectric point of the membrane was 5.5, where the pH values of the feed solutions (2000 ppm $MgCl_2$ and 2000 ppm $MgSO_4$) were in the range of 6.0 and 6.6. The surface zeta potential of the chosen IP-R based membrane under the given test conditions was negative instead of positive. The above results thus implied that surface functional groups or surface charge of the IP-R based membranes probably had little or no effect on the high rejection capability toward $MgCl_2$.

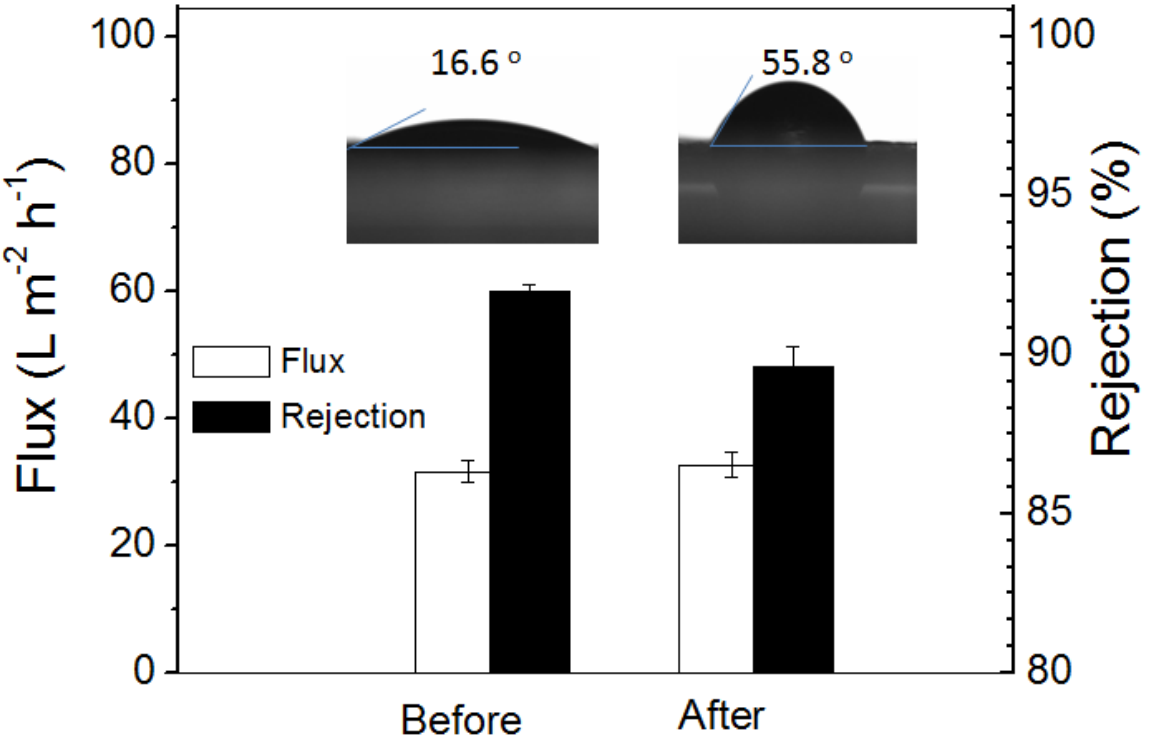

Figure 4.7 Water contact angles and filtration performance of IP-R based membrane before and after surface modification with 1% 2-ethylhexanoyl chloride in hexane. The membranes were prepared on the CN/PAN/PET scaffold under 1-min reaction between 0.1% TMC in hexane and 1% PIP in water. The test conditions were as follows: 2000 ppm $MgCl_2$ feed solution, 4.8 bar applied pressure and temperature of 25 ^{o}C.

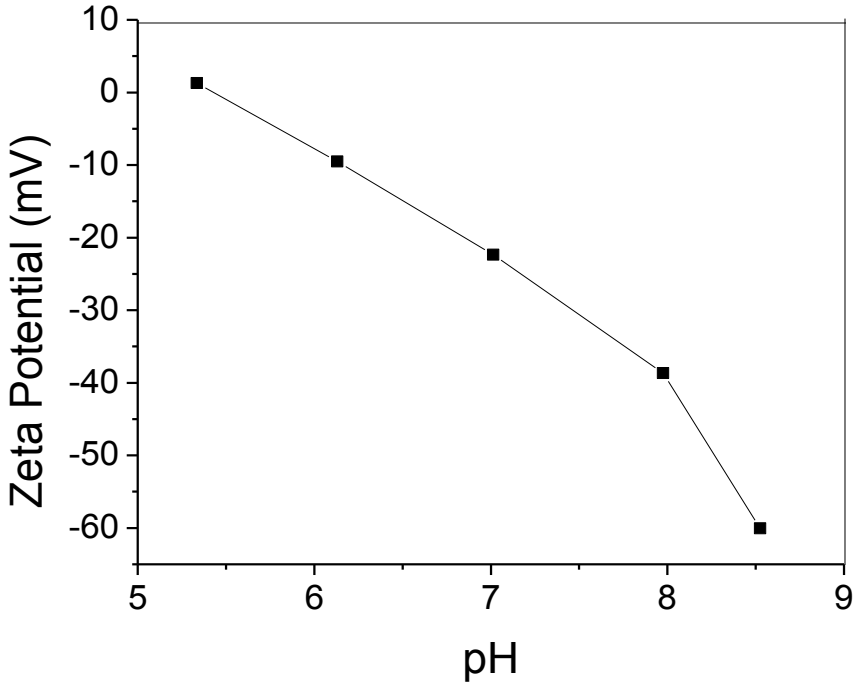

Figure 4.8 Zeta potential of IP-R based membrane as a function of the pH value. The membrane was prepared on the CN/PAN/PET scaffold under 1-min reaction between 0.1% TMC in hexane and 1% PIP in water without any further surface modification.

4.3.3.2 Pore size of NF membranes

Aside from the Donnan ion repulsion effect, pore size can also be a factor to affect the ion selectivity of NF membranes [32]. The pore size distributions of the chosen membranes (IP- and IP-R) were obtained by using aqueous solutions containing different uncharged solutes [25], where the results are shown in Figure 4.9 and Figure 4.10, respectively. It was found that the average pore size became smaller with increasing PIP concentration because both degree of cross-linking and thickness of the barrier layer increased with increasing monomer concentration [23]. By comparison, the IP-R based membranes always exhibited smaller average pore sizes and narrower pores size distributions than IP based membranes prepared under the same PIP concentration. However, such a difference became smaller with increasing PIP concentration. In

Figures 4.5(b) and 4.6(b), the difference between the $MgCl_2$ rejections with respect to the PIP concentration exhibited a similar trend. Thus, we conclude that the factor of pore size might be the only reason to explain the higher rejection against $MgCl_2$ by the IP-R based membrane.

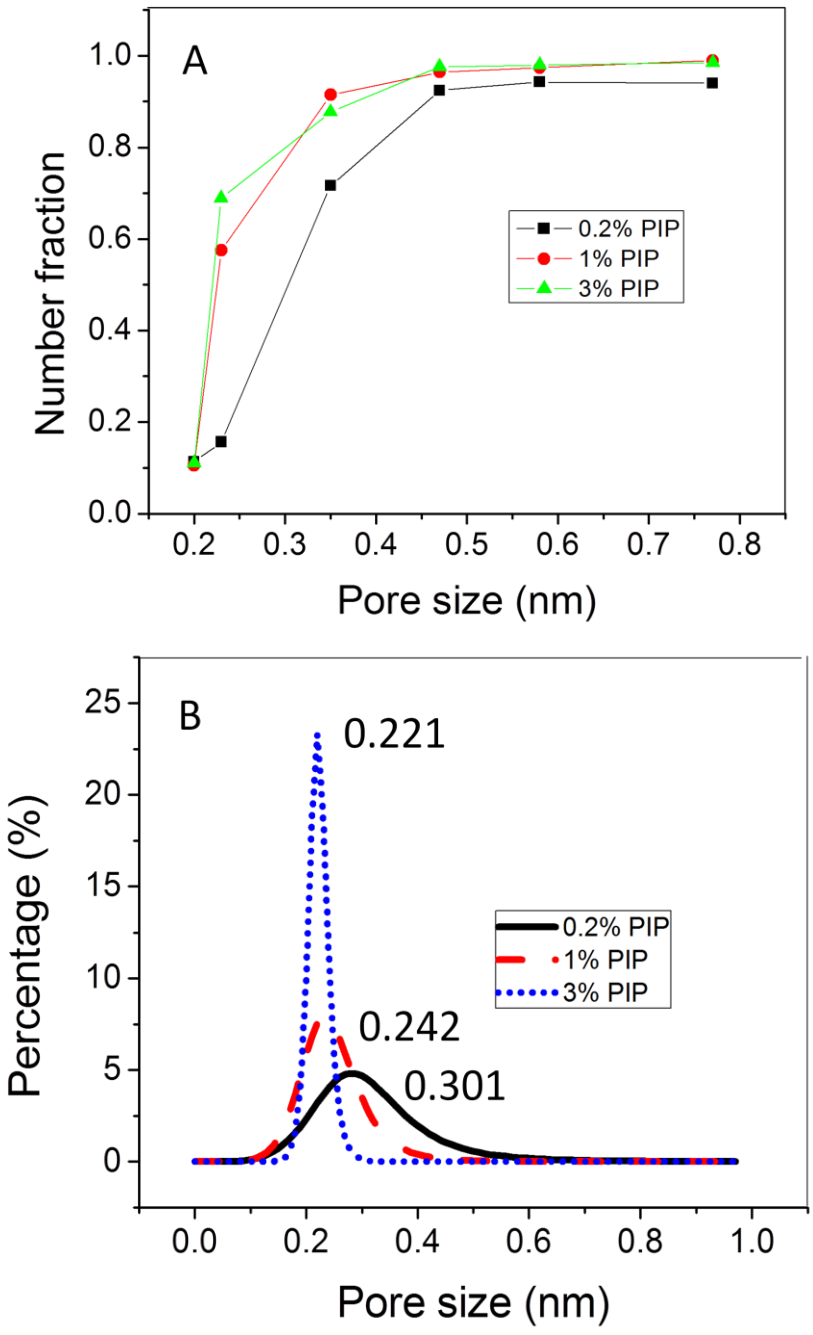

Figure 4.9 Pore size (radius of the pore) distribution of IP based membranes prepared by different PIP concentrations: (a) cumulative pore size distribution curves and (b) curves of pore size distribution. The membranes were prepared on the CN/PAN/PET scaffold under 1-min reaction between 0.1% TMC in hexane and different concentrations of PIP in water without any further surface modification.

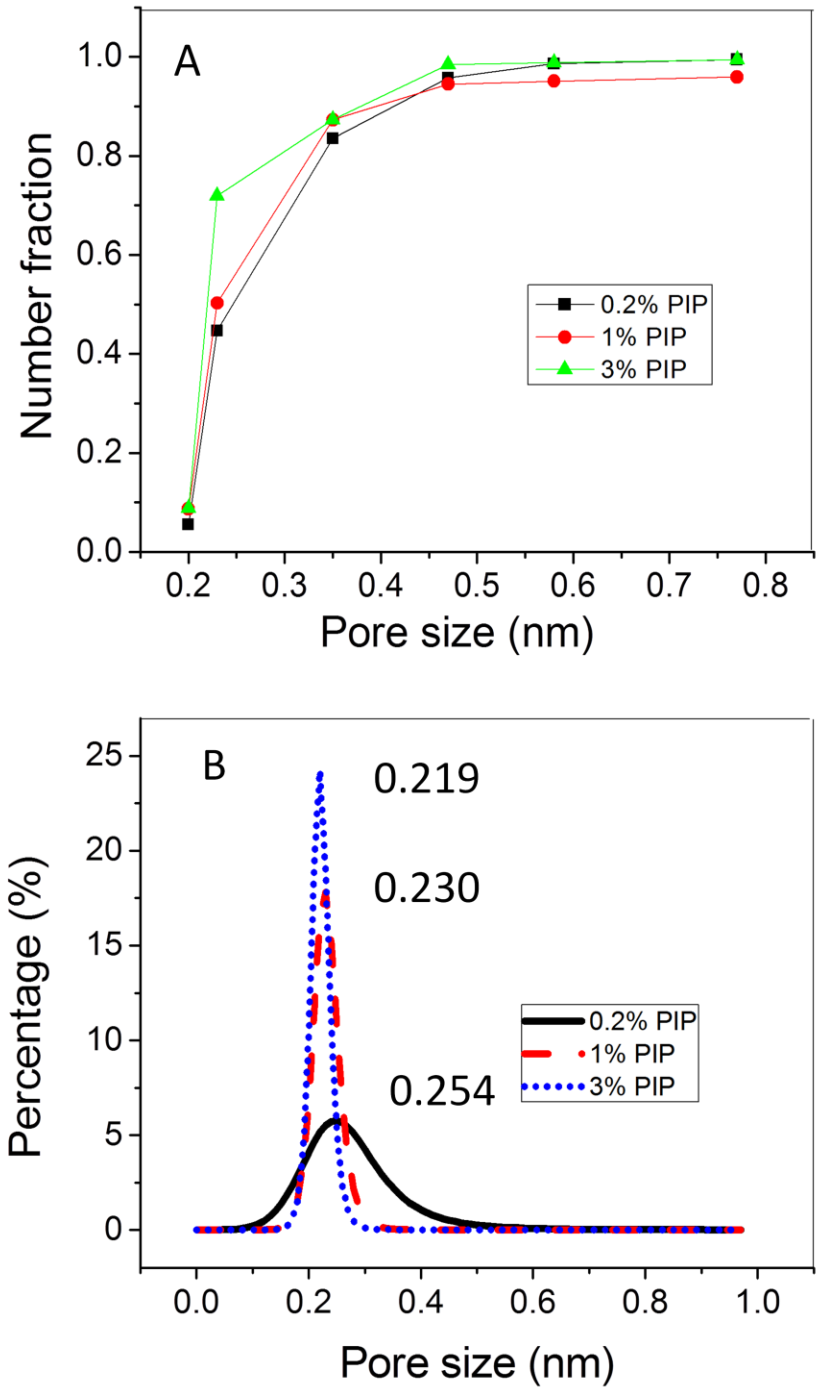

Figure 4.10 Pore size (radius of the pore) distributions IP-R based membranes prepared by different PIP concentrations: (a) cumulative pore size distribution curves and (b) curves of pore size distribution. The membranes were prepared on the CN/PAN/PET scaffold under 1-min reaction between 0.1% TMC in hexane and different concentrations of PIP in water without any further surface modification.

4.3.4 Effect of CN/PAN/PET substrate on the formation of the barrier layer

In an ideal reaction condition, in the absence of gravity, and under the same reaction time and monomer concentrations, the pore size distribution and the salt rejection in the barrier layer of either IP based or RIP based membrane should be the same. However, the results clearly showed deviation from this expectation, especially at lower aqueous monomer concentrations. This deviation could be attributed to the effect of the substrate, which had not been taken into consideration. Clearly, the different barrier layer structure, as a result of the CN/PAN/PET scaffold, is an important factor leading to the different performance of IP and IP-R based membranes.

The effect of the CN/PAN/PET substrate on the formation of barrier layer in different membrane was studied as follows. In preparation of IP based membranes, the substrate was first impregnated by an aqueous solution and then air dried before the introduction of organic phase. In this case, the reacting interface, although immersed within the substrate, was near the CN layer surface due to the hydrophilic nature of the scaffold. As a result, the formation the composite barrier layer was relatively above the CN/PAN/PET substrate, which was clearly seen in the TEM cross-section image (Figure 4.11(a)). In contrast, during the preparation of IP-R membranes, the substrate was first impregnated by organic solution and then air dried to assure the solution surface fall within the CN/PAN/PET substrate surface before the introduction of aqueous solution. Because of the faster evaporation rate of the organic phase, the reacting interface became immersed further down within the CN/PAN/PET substrate, which was consistent with the TEM observation in Figure 4.11(b).

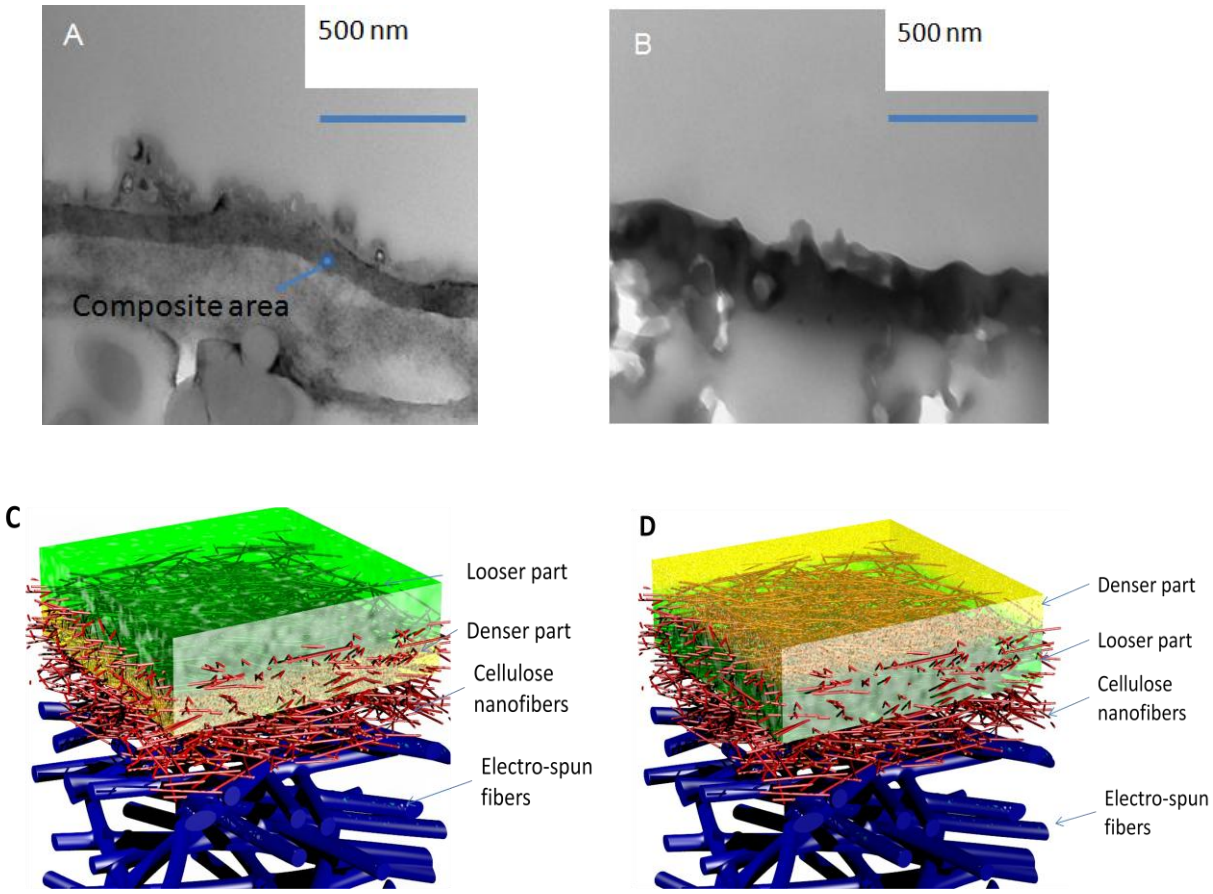

PET non-woven layer at the bottom is not shown

Figure 4.11 TEM cross-section images of (a) IP based membrane and (b) IP-R based membrane on CN/PAN/PET, where their corresponding schematics are shown in (c) and (d), respectively. In (a), the composite are can be identified with reasonable assurance, while in B, the composite area becomes more closely mingled with not only the cellulose layer below but also the polymer layer on top.

In addition of the scaffold effect, there was another mechanism that could also introduce heterogeneity in the barrier layer. That is, during interfacial polymerization, the denser part of the barrier layer was always formed at the interface first, while the looser part grew subsequently through diffusion of the monomers from the aqueous phase to the organic phase [23]. Due to the

combined effects of such a mechanism and the scaffold effect, a very different heterogeneous structure in the barrier layer could be created between the IP and IP-R based membranes. Based on experimental results, the schematics of the different barrier layer topology in the IP versus IP-R based membranes are illustrated in Figures 4.11(c) and 4.11(d), respectively. In the schematics, the formation of the denser part of the barrier layer in the IP membrane was deeply immersed in the CN substrate, while the denser part of the barrier layer in the IP-R based membrane was near the top of the CN substrate. Selectivity (or average pore size) of the NF membranes was determined by the non-immersed portion of the barrier layer. Hence, the effective pore sizes of the composite barrier layer in the IP based membrane tended to be larger than those in the IP-R based membrane.

The proposed model can also explain the effect of CN substrate on the permeability of IP or IP-R based membranes. Although the composite structure of polyamide and CN in the barrier layer could improve permeability through the formation of directed water channels between the composite interface [19], the growth of the polyamide layer towards the surface of CN substrate (i.e. towards the organic phase) would form a relatively loose part of the barrier layer for IP based membranes, which porosity was difficult to control by changing the cross-linking conditions (e.g. with increasing concentration of aqueous monomers). In contrast, the loose part of the polyamide layer would grow into the CN substrate, where the effective thickness of the dense part of the barrier layer (without the incorporation of CN) could remain the same for IP-R based membranes. The porosity of this portion of the barrier layer would be strongly dependent on the cross-linking conditions, which was consistent with the experimental results. It was interesting to note that the IP-R based membrane generally yielded better filtration performance than IP based membranes. For example, in Figure 4.5 and Figure 4.6, the flux performance of IP-

R based membranes ($MgSO_4$ solution: 41.7, $MgCl_2$ solution: 29.0 L m^{-2} h^{-1}) was definitely higher than IP based membranes ($MgSO_4$ solution: 31.7 L m^{-2} h^{-1}, $MgCl_2$ solution: 23.6 L m^{-2} h^{-1}) at the highest PIP concentration (3%), while the maintaining the same rejection.

As the dense part of the barrier layer (without CN) in the IP-R based membrane contained an excess amount of secondary amino groups, post-treatment with 1% TMC in hexane for 1 min would lead to further cross-linking reaction. Indeed, this was verified in TMC modified IP-R based membranes, where the NaCl rejection was improved from 74% to 91% (Figure 4.12). Clearly, the further cross-linked IP-R membrane would be a good candidate as low pressure RO membranes. For IP based membranes, the NaCl rejection was not enhanced by TMC post-treatment because the excess secondary amino groups were imbedded in the CN substrate, where the permeability of the barrier layer was mainly through the interface through nanofibers and polymer matrix.

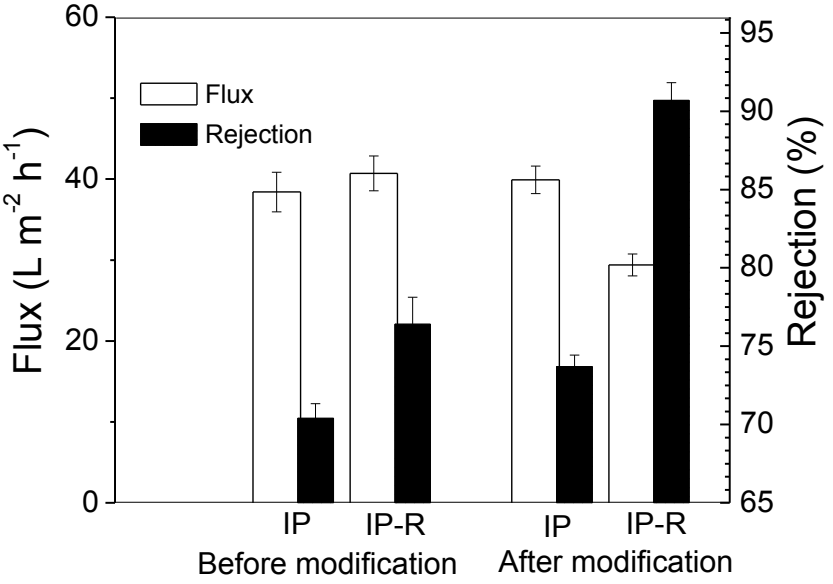

Figure 4.12 Nanofiltration performance of membranes prepared by IP and IP-R methods before and after surface the modification with 1% TMC in hexane. The membranes were prepared on the CN/PAN/PET scaffold under 1-min reaction between 0.1% TMC in hexane and 3% PIP in water. The test conditions were as follows: 500 ppm NaCl feed solution, 6.9 bar applied pressure and temperature of 25 ^{o}C.

4.4 Conclusions

NF membranes prepared by IP and IP-R methods (i.e., interfacial polymerization with different arrangement of the aqueous and organic phases) on a nanofibrous substrate, which was a 3-layered thin-film nanofibrous composite (TFNC) membrane, were studied. It was found that IP-R based membranes (interfacial polymerization with the aqueous phase above the organic phase) possessed smaller pore size than IP based membrane under the same reaction conditions because the dense part of the barrier layer of the former was formed on top of the nanofibrous substrate. In contrast the dense part of the barrier layer was immersed within the nanofibrous substrate of IP based membranes, which permeability was mainly controlled by the direct water-channels formed between the interface of nanofibers and polyamide. It was found that the IP-R based membranes generally possessed better NF performance (i.e., higher flux and higher rejection) than IP based membranes. The post treatment of using TMC to react with excess secondary amino groups of IP-R based membranes provided an effective way to increase the cross-linking density of the barrier layer, resulting in smaller pore size and RO performance. It is thought this RO performance can be further improved with the optimization of reaction time, monomer concentration and improved coating method.

References

[1] M. Liu, S. Yu, M. Qi, Q. Pan, C. Gao, Impact of manufacture technique on seawater desalination performance of thin-film composite polyamide-urethane reverse osmosis membranes and their spiral wound elements, Journal of Membrane Science, 348 (2010) 268-276.

[2] R.F. Service, Desalination Freshens Up, Science, 313 (2006) 1088-1090.

[3] P. Robert J, Composite reverse osmosis and nanofiltration membranes, Journal of Membrane Science, 83 (1993) 81-150.

[4] C.K. Kim, J.H. Kim, I.J. Roh, J.J. Kim, The changes of membrane performance with polyamide molecular structure in the reverse osmosis process, Journal of Membrane Science, 165 (2000) 189-199.

[5] Y. Mansourpanah, S.S. Madaeni, A. Rahimpour, Fabrication and development of interfacial polymerized thin-film composite nanofiltration membrane using different surfactants in organic phase; study of morphology and performance, Journal of Membrane Science, 343 (2009) 219-228.

[6] L. Yung, H. Ma, X. Wang, K. Yoon, R. Wang, B.S. Hsiao, B. Chu, Fabrication of thin-film nanofibrous composite membranes by interfacial polymerization using ionic liquids as additives, Journal of Membrane Science, 365 (2010) 52-58.

[7] M.L. Lind, A.K. Ghosh, A. Jawor, X. Huang, W. Hou, Y. Yang, E.M.V. Hoek, Influence of Zeolite Crystal Size on Zeolite-Polyamide Thin Film Nanocomposite Membranes, Langmuir, 25 (2009) 10139-10145.

[8] M. Hirose, H. Ito, Y. Kamiyama, Effect of skin layer surface structures on the flux behaviour of RO membranes, Journal of Membrane Science, 121 (1996) 209-215.

[9] C. Kong, T. Shintani, T. Kamada, V. Freger, T. Tsuru, Co-solvent-mediated synthesis of thin polyamide membranes, Journal of Membrane Science, 384 (2011) 10-16.

[10] Y. Jin, Z. Su, Effects of polymerization conditions on hydrophilic groups in aromatic polyamide thin films, Journal of Membrane Science, 330 (2009) 175-179.

[11] A.K. Ghosh, B.-H. Jeong, X. Huang, E.M.V. Hoek, Impacts of reaction and curing conditions on polyamide composite reverse osmosis membrane properties, Journal of Membrane Science, 311 (2008) 34-45.

[12] A.K. Ghosh, E.M.V. Hoek, Impacts of support membrane structure and chemistry on polyamide–polysulfone interfacial composite membranes, Journal of Membrane Science, 336 (2009) 140-148.

[13] H. Ma, C. Burger, B.S. Hsiao, B. Chu, Highly Permeable Polymer Membranes Containing Directed Channels for Water Purification, ACS Macro Letters, 1 (2012) 723-726.

[14] M.A. Shannon, P.W. Bohn, M. Elimelech, J.G. Georgiadis, B.J. Marinas, A.M. Mayes, Science and technology for water purification in the coming decades, Nature, 452 (2008) 301-310.

[15] M. Zhou, P.R. Nemade, X. Lu, X. Zeng, E.S. Hatakeyama, R.D. Noble, D.L. Gin, New Type of Membrane Material for Water Desalination Based on a Cross-Linked Bicontinuous Cubic Lyotropic Liquid Crystal Assembly, Journal of the American Chemical Society, 129 (2007) 9574-9575.

[16] B. Chu, B.S. Hsiao, The role of polymers in breakthrough technologies for water purification, Journal of Polymer Science Part B: Polymer Physics, 47 (2009) 2431-2435.

[17] K. Yoon, B.S. Hsiao, B. Chu, High flux nanofiltration membranes based on interfacially polymerized polyamide barrier layer on polyacrylonitrile nanofibrous scaffolds, Journal of Membrane Science, 326 (2009) 484-492.

[18] H. Ma, C. Burger, B.S. Hsiao, B. Chu, Ultrafine Polysaccharide Nanofibrous Membranes for Water Purification, Biomacromolecules, 12 (2011) 970-976.

[19] X. Wang, D. Fang, B.S. Hsiao, B. Chu, Nano-Filtration Membranes based on Thin-Film Nano-Composites To be submitted, (2013).

[20] S. Kaur, S. Sundarrajan, R. Gopal, S. Ramakrishna, Formation and characterization of polyamide composite electrospun nanofibrous membranes for salt separation, Journal of Applied Polymer Science, 124 (2012) E205-E215.

[21] V. Freger, Kinetics of Film Formation by Interfacial Polycondensation, Langmuir, 21 (2005) 1884-1894.

[22] C.C. Wamser, M.I. Gilbert, Detection of surface functional group asymmetry in interfacially-polymerized films by contact angle titrations, Langmuir, 8 (1992) 1608-1614.

[23] R. Oizerovich-Honig, V. Raim, S. Srebnik, Simulation of Thin Film Membranes Formed by Interfacial Polymerization, Langmuir, 26 (2009) 299-306.

[24] B. Chu, B.S. Hsiao, D. Fang, Apparatus and methods for electrospinning polymeric fibers and membranes, in, The Research Foundation of State University of New York, USA . 2002, pp. 55 pp.

[25] J.A. Otero, O. Mazarrasa, J. Villasante, V. Silva, P. Prádanos, J.I. Calvo, A. Hernández, Three independent ways to obtain information on pore size distributions of nanofiltration membranes, Journal of Membrane Science, 309 (2008) 17-27.

[26] R. Wang, Y. Liu, B. Li, B.S. Hsiao, B. Chu, Electrospun nanofibrous membranes for high flux microfiltration, Journal of Membrane Science, 392–393 (2012) 167-174.

[27] X. Song, Z. Liu, D.D. Sun, Nano gives the answer: breaking the bottleneck of internal concentration polarization with a nanofiber composite forward osmosis membrane for a high water production rate, Adv Mater, 23 (2011) 3256-3260.

[28] V. Yangali-Quintanilla, A. Verliefde, T.U. Kim, A. Sadmani, M. Kennedy, G. Amy, Artificial neural network models based on QSAR for predicting rejection of neutral organic compounds by polyamide nanofiltration and reverse osmosis membranes, Journal of Membrane Science, 342 (2009) 251-262.

[29] M. Mulder, Basic principles of membrane technology, in, Kluwer Academic, Dordrecht ; Boston, 1996, pp. 235.

[30] B. Tansel, J. Sager, T. Rector, J. Garland, R.F. Strayer, L. Levine, M. Roberts, M. Hummerick, J. Bauer, Significance of hydrated radius and hydration shells on ionic permeability during nanofiltration in dead end and cross flow modes, Separation and Purification Technology, 51 (2006) 40-47.

[31] R. Malaisamy, M.L. Bruening, High-Flux Nanofiltration Membranes Prepared by Adsorption of Multilayer Polyelectrolyte Membranes on Polymeric Supports, Langmuir, 21 (2005) 10587-10592.

[32] W. Richard Bowen, A. Wahab Mohammad, Diafiltration by nanofiltration: Prediction and optimization, AIChE Journal, 44 (1998) 1799-1812.

Chapter 5 Thin-film Nanofibrous Composite (TFNC) Membranes for Reverse Osmosis

The thin-film nanofibrous composite (TFNC) substrate was also used to fabricate high-flux reverse osmosis (RO) membranes. The chosen TFNC substrate consisted of a three-layered structure: poly (ethylene terephthalate) non-woven cloth, electrospun polyacrylonitrile (PAN) mid-layer scaffold and ultrafine cellulose nanofibers top layer (~ 150 nm thick). A dense barrier layer was further prepared through interfacial polymerization of m-phenylenediamine and trimesoyl chloride around the CN layer. The resulting membrane was strong enough to sustain a hydraulic pressure up to 800 psi compatible with practical operations. A comonomer (piperazine) and an additive (1-octyl-3-methylimidazolium chloride) were used to improve the membrane flux for the treatment of brackish water. To further enhance the membrane performance, a spray coating technology was introduced to control the loading amount of the aqueous solution on the substrate surface, thus the barrier layer thickness. Based on the above approaches, the membrane with the best performance exhibited 96.5% of rejection ratio against NaCl and a flux of 28.6 L/m^2 h at 100 psi. Compared with a commercial RO membrane, XLE (Filmtec, DOW), which had a rejection of 94.7% and a flux of 45.7 L/m^2 h under the same test condition, the TFNC RO membrane still had a space to get improved. The inclusion of the cellulose nanofiber layer provided a much smoother surface than the electrospun scaffold with it, leaving more room to optimize the barrier layer for practical applications.

5.1 Introduction

Reverse osmosis (RO) is an energy efficient separation technology that is widely used for desalination of seawater and brackish water. The RO separation process requires high pressure (100-1000 psi) [1] to overcome the osmosis pressure from the salt solution allowing pure water to pass through the semi-permeable membranes. The current state-of-the-art RO membrane has a thin film nanocomposite (TFC) structure [2], which contains a thin and dense polymer barrier layer on top of a porous polymeric substrate. Materials for the dense top barrier layer are typically crosslinked polyamides prepared through interfacial polymerization, where this layer determines the final performance of salt retention and energy consumption. The conventional substrate in the TFC membrane is a 'sponge-like' polymer layer deposited on the polyester non-woven cloth through the phase inversion method. The major functions of this substrate are to provide mechanical strength and integrity to support a thin dense barrier layer allowing the flow of permeate solution.

The polyamide barrier layer is prepared at the interface of two immiscible aqueous and organic phases, which contain multifunctional amine and acyl chloride, respectively. In the past few decades, many monomers have been tested [1, 3-9], where m-phenylenediamine and trimesoyl chloride have been widely considered as the most common ingredients to fabricate high performance RO membranes. Additives have also been incorporated in the polyamide layer to further improve its RO performance. For example, nanoparticles, such as zeolites [10-12], silver nanoparticles [13], silica nanoparticles [14] and titanium dioxide (TiO_2) nanoparticles [15] have been embedded into the polyamide layer to enhance either permeability or salt rejection. Small organic molecules, such as acetone [16], isopropyl alcohol [17, 18], phenol [18] and n-propanol [17] have also been added into the aqueous phase to improve the permeability with

essentially little additional rejection loss. In addition, small molecules, such as an anionic surfactant [19, 20], ionic liquid [21] and slats formed by organic acid and amine [7, 22] have been used to adjust the membrane permeability. There are clearly varying tradeoffs between permeability and salt rejection when different additive is incorporated in the barrier layer, and the effects can be further influenced by the membrane fabrication process [23]. Often, for each new membrane fabrication scheme, it is necessary to optimize the filtration performances through formulation adjustment and operational procedures.

Although the polymer substrate seem to have no direct impact on the RO performance, recent studies imply that the morphology of the substrate actually plays an important role in the fabrication of the barrier layer. For example, a series of polyethersulfone (PES) substrates with varying pore sizes and surface hydrophilicity have been prepared by the Hoek group and the interfacial polymerization was carried out to prepare barrier layers on these substrates. It was found that the substrate having larger pore sizes and more hydrophilic surface could lead to a highly permeable RO membrane by forming a comparatively thin barrier layer [24]. In recent studies, a new porous substrate format containing a nonwoven nanofibrous scaffold, has been used to replace the conventional porous membrane format by the phase-inversion method in fabrication of NF/RO membranes. This new substrate can be fabricated by depositing polymer nanofibers (with diameters of 100 – 200 nm) on the non-woven microfibrous cloth through the electrospinning technology [25], and the resulting structure is termed thin-film nanofibrous composite (TFNC). The pore size distribution of the electrospun nanofibrous layer is typically in the microfiltration (MF) range, which was much larger than the conventional porous layer obtained by the phase inversion method (the pore size distribution is typically in the ultrafiltration (UF) range). Based on the above two-layered fibrous structure, interfacial

polymerization has been used directly to produce NF membranes, where the TFNC format was found to lead to higher permeability than the thin-film composite (TFC) format with comparable salt selectivity [21, 26, 27]. The relationships between the NF performance of such TFNC membranes and the morphology of the nanofibrous substrate have been studied by Ramakrishna's group. They found that diameters of electrospun nanofibers could be tuned in the range of 50 – 500 nm by varying the concentration of polymer solution used in the electrospinning process. When the fiber diameter was decreased, the substrate pore size became smaller. The TFNC membrane using the substrate with smaller fiber diameters tended to yield higher salt rejection at the expense of permeability [28].

Ultrafine cellulose nanofibers (CNs) are the new fibrous material recently introduced for water purification. With 'diameters' of only about 5 nm, CNs could be deposited onto an electrospun scaffold and formed an ultra-thin top layer (with thicknesses ~ 100 nm), where the three-layered structure is ideal for high flux UF application. For example our previous studies showed that this new UF membrane exhibited about 10-fold higher permeability than commercial UF membranes with the same rejection (99.5%A) on oil/water emulsion [29]. When this three-layered structure was used as a substrate to produce TFNC NF membranes, the NF membranes possessed higher permeability than membranes based on other substrates, including the two-layered fibrous structure. Perhaps this is because the ultrafine nanofibers can be combined with the polyamide and form a nanocomposite barrier layer containing a "channel structure" to facilitate the water transport capability [30, 31]. Moreover, the barrier layer thickness can be further controlled through machine coating on the smooth surface provided by the CNs layer. Permeability of the best performing TFNC NF membrane was found to be 100% higher than that from the commercial NF membranes without sacrificing the salt rejection [30].

In this chapter, the newly developed CN-based TFNC UF membrane was used as a support for fabricating TFNC RO membranes. Due to its nanofibrous structure and smoother surface, the performance of the resulting TFNC RO membrane should be better than the one based on the composite scaffold without the CN layer. To check this assumption, interfacial polymerization was conducted on the surface of both fibrous substrates, i.e., with and without CNs on the electrospun scaffold, and the performance of the resulting RO membranes was compared. Scanning electron microscopy was used to study the effects of fibrous substrates on the surface morphology. A large range of hydraulic pressures (100 psi – 800 psi) was used to evaluate the mechanical strength and integrity of the RO membrane. To target the use of the TFNC RO membrane for the treatment of low concentration brackish water (500 ppm NaCl), comonomers and inner additives were incorporate in the aqueous phase during interfacial polymerization to create a higher content of free volume in the barrier layer, where their concentrations were also optimized. Finally, a new additive, 1-octyl-3-methylimidazolium chloride (an ionic liquid) was also tested in interfacial polymerization and its effects were compared with other typical RO additives to obtain a significant improvement on flux at a slight cost of rejection. The flux of the TFNC RO membranes was further improved by loading the aqueous solution through spray coating, where the process reduced the barrier layer thickness. The coating condition was optimized to get RO membranes having a flux as high as possible and a rejection of above 95% on the CN UF membrane and performances of the spray-coated RO membranes on the two different fibrous substrates were further compared.

5.2 Experimental

5.2.1 Materials and reagents

Polyacrylonitrile (PAN) (Mw = 150,000, Polysciences, Inc.) was dissolved in dimethylformamide (DMF) for electrospinning, where PAN nanofibers were deposited onto the (ethylene terephthalate) (PET) non-woven cloth (Junyaku Co., Ltd., Japan). Wood pulps (Biofloc 96, Thembec Tartas factory, France) were treated by the following oxidation scheme to prepare cellulose nanofibers (CN) [29]. The scheme involved the use of chemicals including 2,2,6,6-tetramethyl-1-piperidinyloxy (TEMPO) from Acros Organics, sodium bromide (NaBr), and 10-15% sodium hypochlorite (NaClO) solution and sodium Hydroxide (NaOH), all from Fisher Scientific Company The RO barrier layer was synthesized by means of interfacial polymerization between two immiscible aqueous and organic phases. The aqueous phase was prepared by dissolving m-phenylenediamine (MPD) in de-ionized (DI) water. In addition, piperazine (PIP) was used as aqueous comonomer, and Triethylamine (TEA), 1-octyl-3-methylimidazolium chloride (OMIC), camphor-10-sulfonic acid (CSA), isopropyl alcohol (IA) and o-aminobenzoic acid (*o*-ABA), sodium lauryl sulfate (SLS) were used as aqueous additives to improve the membrane permeability. The organic phase was prepared by dissolving trimesoyl chloride (TMC) in hexane. The resulting RO membranes were tested using 500 ppm sodium chloride (NaCl) solution. Except mentioned otherwise, all above chemicals were purchased from Sigma-Aldrich and used without further purification.

5.2.2 Preparation of PAN electrospun layer

PAN was dissolved in DMF for two days at 60 ^{o}C to obtain a homogenous 10 wt% solution. The PAN solution was electrospun at 20 KV on the PET non-woven cloth using a custom-built multiple-jet machine. The chosen flow rate in each jet was 20 µl/min and the distance between jets and PET support was 7 cm. The product will be referred to as PAN/PET.

5.2.3 Fabrication of the CN layer

CN suspension was prepared following the protocol reported by Hongyang Ma et al. [29]. The concentration of the CN suspension was measured by the total organic carbon (TOC) analysis. In this step, the PAN/PET substrate was first saturated by HCl aqueous solution (pH = 2). A rubber roller was used to squeeze the substrate and to remove extra HCl solution on its surface. 0.1% CN suspension was introduced onto the wet PAN/PET substrate and coated by using a draw-down machine (Gardco DP-8301). The wet coating thickness was controlled to be around 200 μm. The coated membrane was then dried in 90 ^{o}C oven. The resulting substrate will be referred to as CN/PAN/PET.

5.2.4 Preparation of polyamide barrier layer by interfacial polymerization

The aqueous phase was prepared by dissolving MPD in deionized (DI) water. The solution concentration was varied from 1 wt% to 4 wt%. PIP (0 – 2 wt%) was added as comonomer in the aqueous phase to improve the membrane permeability. Other additives, such as TEA, OMIC, CSA, IA, *o*-ABA, SLS, were also incorporated in the aqueous phase with concentrations of 0-2 wt% to further improve membrane permeability. At the same concentration in the aqueous solution, capabilities of the additives to enhance permeability were compared. The most effective additive was applied for the later spray coating. 0.1 g TMC was dissolved into 100 ml hexane to obtain the organic phase. Both PAN/PET and CN/PAN/PET substrates were used to prepare RO membranes.

The interfacial polymerization was carried out in a glassware with a flat bottom (19 cm × 12 cm). A piece of the substrate (8 cm × 8 cm) was soaked and saturated by the aqueous phase and

then squeezed by a rubber roller to remove the extra solution on the substrate surface. The impregnated substrate was fixed in the glassware with four edges sealed by adhesive tapes (with thickness of ~ 60 μm). ~50 ml organic solution was introduced onto the top of the substrate gently. After 10 seconds, the organic solution was drained out and the membrane was cured in 80 ^{o}C oven for 10 min. The resulting RO membranes based on PAN/PET and CN/PAN/PET substrates were referred to as PA/PAN and PA/CN, respectively.

5.2.5 Membrane performance test

A custom-built cross-flow NF system with active filtration area of 42 cm^2 was used to characterize the membrane performance. Since the commercial membrane XLE was used as a reference, the filtration test of all the membranes in our experiment followed the test conditions provided by Filmtec, DOW (http://www.rosystems.com/pdf/Filmtec-Membranes/filmtecliterature.pdf). 500 ppm NaCl was used as the feed aqueous solution, which was circulated through the system at a flow rate of 0.1 gallon per minute (GPM) under pressure from 100 to 800 psi. Circulation was carried out for three hours to stabilize the membrane performance before testing. The solution temperature was controlled at 25±2 ^{o}C by using a recirculating chiller (Thermoflex 1400). The permeate solution was collected every 10 minutes and weighed by using a top loading balance (Cole-Parmer Symmetry ECII-800). The solution conductivity was monitored by a conductivity meter (Oakton CON 110). The salt rejection (R) was calculated by Equation 3.3.

Water permeability (*A* value) and salt permeability (*B* value) are the two important coefficients to evaluate the membrane performance and they do not vary with test conditions.

The following equations were derived from the solution-diffusion model [33] to calculate *A* and *B* values:

$$A = \frac{J_w}{(\Delta P - \Delta \pi)} \quad (5.1)$$

$$B = \frac{(1-R) \bullet A \bullet (\Delta P - \Delta \pi)}{R} \quad (5.2)$$

where $\mathbf{J_w}$ is water (solvent) flux, $\mathbf{\Delta P}$ is hydraulic pressure added on the membrane sample, $\mathbf{\Delta \pi}$ is osmosis pressure across the membrane. *A* value is measured with pure water as feed solution. In this condition, $\Delta \pi = 0$.

5.2.6 Scanning electron microscopy (SEM) measurements

The morphology of the sample was characterized by SEM (LEO 1550) using Schottky field emission gun and Robinson backscatter detector. Cross-sectioned SEM samples were prepared by fracturing water-wetted membranes in liquid nitrogen. All specimens received a one-minute gold coating.

5.2.7 Preparation of RO membrane through spray coating

The aqueous solution for interfacial polymerization was sprayed onto the substrate using an air atomizing and siphon-fed nozzle (XASR, BETE Fog Nozzle Inc.) having a round spray pattern. The standard set-up of the spray system is shown in Figure 5.1. The aqueous solution was siphoned into the nozzle from the solution tank and atomized by high air pressures (0.7 - 4.0 bar). The air delivery was controlled by a shut-off valve and filtrated by an air filter. At the downstream of the filter, an air regulator and a control valve were used to adjust the air pressure and flow rate, respectively. The RO substrate was mounted on a flat steel plate by adhesive tapes

and settled under the nozzle horizontally. The spray direction was perpendicular to the substrate surface. The operating conditions are given in Table 5.1. We found that the spray angle (A), liquid flow rate and volume medium diameter (VMD) all depended on the air pressure. Once the air pressure was fixed to be 2.8 bar through the regulator, the corresponding factor values were given by the nozzle provided in the literature, which was given in the caption of Figure 5.1. At pressure of 2.8 bar, 30 cm has been suggested to be the maximum pattern distance (D) and a value (28 cm) close to the maximum distance was selected to obtain a large spray coverage in this study. After the loading of aqueous solution through spraying, an organic solution of 0.1 % (w/v) TMC in hexane was manually introduced onto the top of the spray-coated membrane to achieve interfacial polymerization. After 10 seconds, the organic solution was drained out and the membrane was cured in an 80 ^{o}C oven for 10 min. Performance of the membrane was adjusted by varying the spraying time.

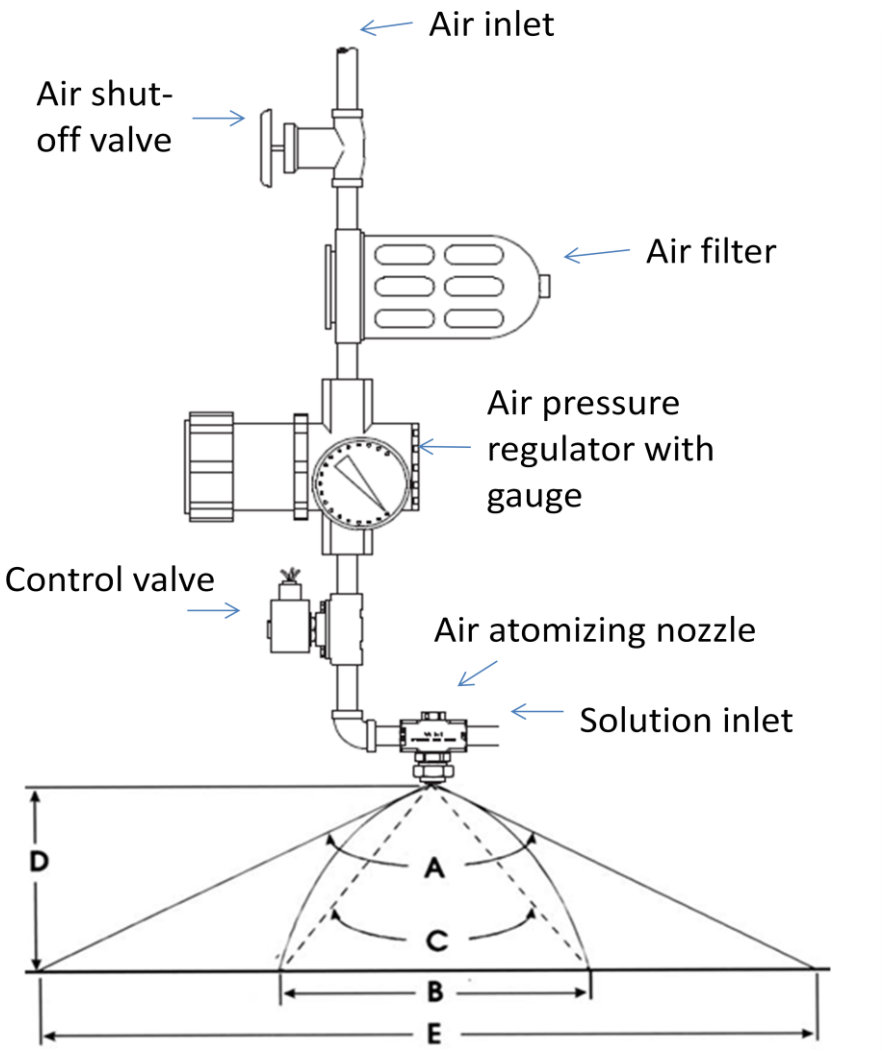

Figure 5.1 Standard set-up of XASR siphon system (copied from the file "Troubles shooting BETE XA nozzles" and "BETE engineering information" at http://www.bete.com/literature/index.html). A is the spray angle measured close to the orifice. B is the actual coverage at a specified distance (D) from the nozzle. C is the angle calculated from B and D. E is the theoretical coverage calculated from A and D.

Table 5.1 Operating conditions in spray coating

Pressure	D	A**	B*	Liquid flow rate**	VMD**
2.8 bar	28 cm	18^{o}	7.5 cm	0.03 L/min	15 μm

VMD is volume median diameter, which means half of the total liquid volume is made up of droplets with diameters larger than the median value and the other half with diameters smaller.
*The data were obtained by measuring the diameter of the round pattern on the substrate after 1 min spray treatment.
** The data were obtained from the file "BETE engineering information" at http://www.bete.com/literature/index.html

5.3 Results and discussion

5.3.1 Morphology of PAN/PET and CN/PAN/PET

TFNC RO membranes were prepared by conducting interfacial polymerization on the surface of different nanofibrous support. Morphologies of the two different supports, PAN/PET and CN/PAN/PET are shown in Figure 5.2 and their properties are given in Table 5.2. PAN/PET was fabricated using electrospun nanofibers with diameters of ~ 250 nm, which layer had a large average pore size (0.65±0.1 μm). As shown in Figure 5.2 (C) and (D), CN/PAN/PET was also used, where this support was prepared by depositing an thin layer (thickness ~ 100 nm) of CNs on PAN/PET to narrow down the pore size of the surface. It is known that CNs had fiber diameters of ~ 5 nm and significant hydrophilicity. Although the CN/PAN/PET support exhibited a pure water flux of around two orders of magnitude lower than the PAN/PET support (Table 5.2), the former's permeability was found to be superior to those of conventional sponge-like UF membranes due to the nanofibrous structure [29]. It has been shown that the NF membrane based on PAN/PET exhibited notable advantages over those based on conventional

UF membranes because of its large surface porosity, which allowed liquid flow to pass through the top barrier layer along a comparatively short pathway [26]. Performance of NF nanofibrous membranes were further improved by CN/PAN/PET because the structure of directed water channels was further incorporated through the combination of CNs and polyamide [31]. It was interesting to note that in Table 5.2, the average surface roughness (R_a) of CN/PAN/PET was only 41.6 nm, which was notably smoother than PAN/PET (with R_a of 8.93×10^2 nm). The smoother surface provided more opportunity to obtain thinner barrier layer and higher membrane permeability through the coating process [30]. Recently, some studies on the RO membranes using electrospun fibers as supports indicated that these membranes had better permeability than those based on the phase-inversed substrates [27, 32]. When the PAN/PET support was replaced by CN/PAN/PET, the performances of RO membranes should be further improved, which is discussed next.

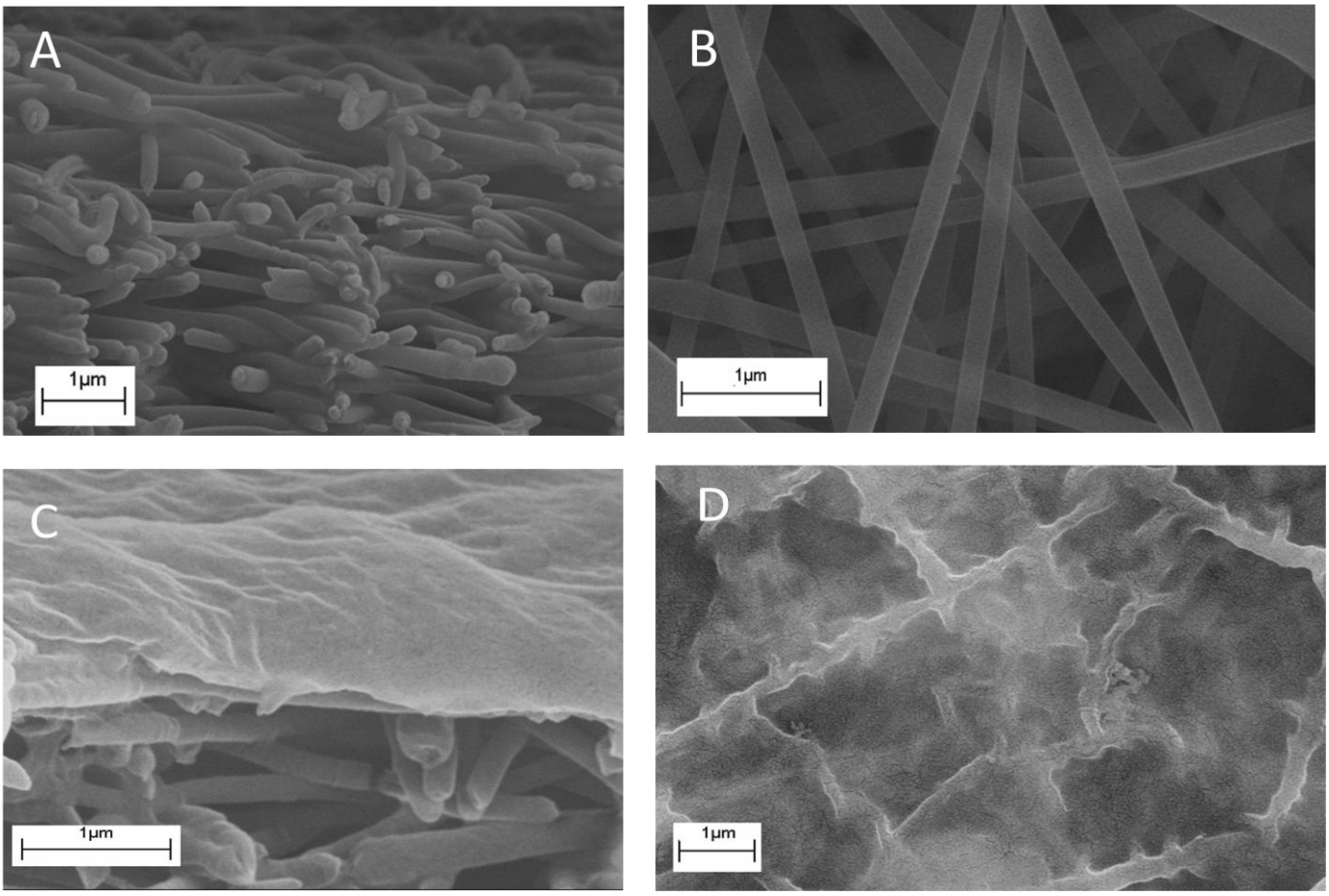

Figure 5.2 SEM cross-section images of (A) PAN/PET and (C) CN/PAN/PET, and SEM top-view images of (B) PAN/PET and (D) CN/PAN/PET. The bottom layer, PET non-woven cloth was not included.

Table 5.2 Properties of different nanofibrous substrates

	Pore size /MWCO	**Pure water flux L/(m^2•h•bar)**	**Surface roughness**		
			R_a (nm)	**R_q (nm)**	**R_{max} (nm)**
PAN/PET	0.65±0.1 μm[a]	3.67×10^4 [c]	8.93×10^2	1.18×10^3	1.19×10^4
CN/PAN/PET	5000 K Da [b]	238 [d]	41.6	56	5.07×10^2

[a] The pore size was measured in a capillary flow porometer (CFP-1500A from PMI porous material, Inc). Wet air flow rate was measured by rinsing the sample with Galwick wetting fluid.
[b] The molecular weight cut off (MWCO) was measured with series of 1000 ppm dextran standard solutions. Each solution was driven through the membrane sample by compressed air (3.4 bar). Molecular weights of dextran vary in the range of 200 K – 5000 K. Concentrations of both feed and permeate were monitored by TOC.
[c] Pure water was driven through the membrane in a dead-end cell by gravity (0.157 bar). The permeate water was collected in 1 min and weighed on a top loading balance.
Pure water flux was measured in a dead-end cell (Amicon 8050) under 2.1 bar provided by compressed air. The permeate water was collected in 1 min and weighted on top loading balance.

5.3.2 RO membranes based on PAN/PET and CN/PAN/PET

The effects of concentration of MPD on the membrane rejection and flux were investigated by using different nanofibrous substrates. In these tests, the concentration of TMC in hexane was fixed at 0.1% (w/v). As shown in Figure 5.3, both flux and rejection were found to be not so sensitive to the variation of MPD concentration. When the MPD concentration was increased from 1 wt% to 4 wt%, rejections of both PA/CN and PA/PAN only had a slight increase (~ 1%) and their fluxes had a modest decrease (~ 15%). It should be noted that the rejection of PA/CN was always higher than that of PA/PAN. One possible reason for this observation was revealed by examining the SEM cross-section images of the RO membranes (Figure 5.4). It was seen that on PAN/PET, a dense layer with great ridge-valley structures was formed along the electrospun fibers. The thickness of the barrier layer had a relatively non-uniform distribution. According to the diffusion mechanism [33], the thinner areas contributed to the low rejection in PA/PAN. In Figure 5.4 (B), the PA/CN had a comparatively uniform thickness distribution due to the smoother CN layer. There was no clear boundary between PA and CN, implying a good interpenetration between the two layers. Our previous study on TFNC NF membranes indicated that the combination of CNs and polyamide led to a channel structure at the interface that can improve the membrane permeability [30]. In the case of RO, this improvement was not

significant probably because of the use of a denser RO barrier layer. However, when compared with PAN/PET, CN/PAN/PET had a smoother surface, thereby making it possible to retain a higher rejection when the membrane permeability was improved. For PA/CN, when the MPD concentration was above 2 wt%, the membrane had no more increase in rejection but a steep decrease in flux. Therefore, PA/CN prepared by 2 wt% MPD and 0.1% (w/v) TMC was used for subsequent optimizations.

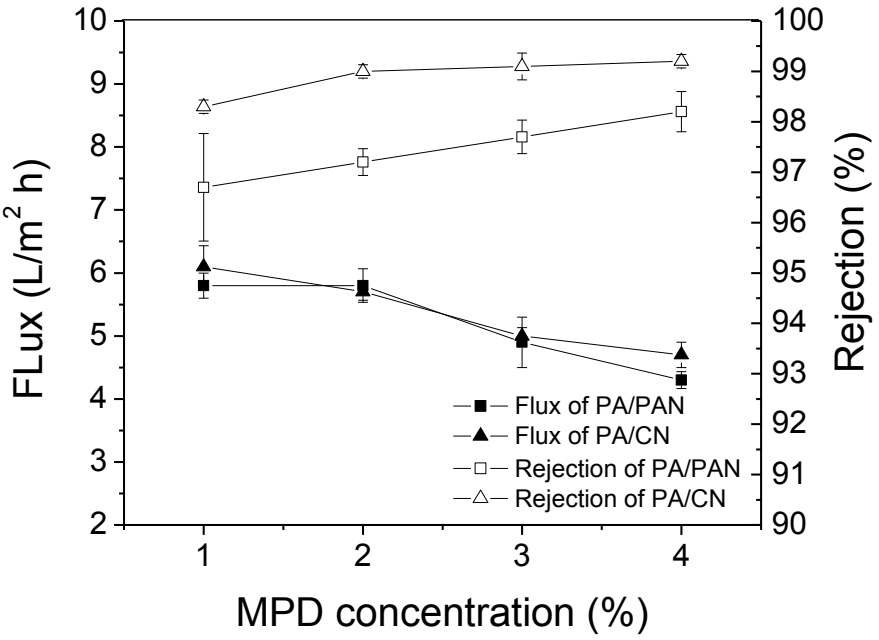

Figure 5.3 Flux and rejection in PA/PAN and PA/CN vary with MPD concentration in aqueous solution. The organic solution was 0.1% (w/v) in hexane. The test conditions were as follows: 500 ppm NaCl as feed solution, 100 psi applied pressure and temperature at 25 ^{o}C.

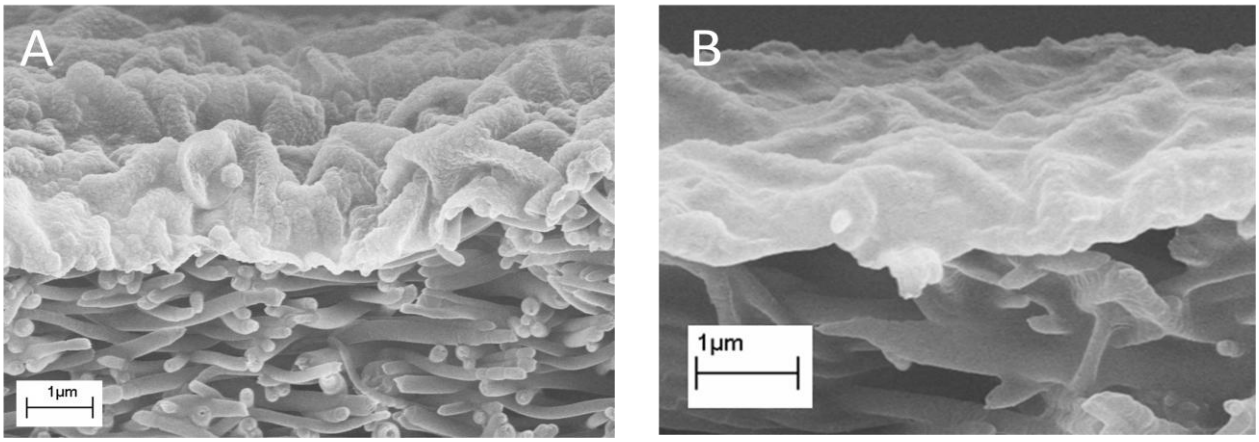

Figure 5.4 SEM cross-section images of RO membranes based on (A) PAN/PET and (B) CN/PAN/PET. The RO membrane was prepared through 10s interfacial polymerization of 2 wt% MPD in water and 0.1% (w/v) in hexane.

High-flux NF nanofibrous membranes based on CN/PAN/PET were developed successfully in our previous study [30, 34]. The potential hurdle to use this support to develop the RO membranes could be its mechanical strength. This is because the typical operating pressure of the NF membrane is usually lower than 100 psi, while the RO pressure can be varied from 100 psi to 800 psi depending on the salt concentration of the feed solution [1]. Brackish water with salt concentrations of 500 - 2000 ppm can be treated under lower pressures (100 -225 psi) as the high pressure treatment (800 – 1000 psi) is usually for seawater with salt concentrations of ~ 30,000 ppm. To verify the potential of CN/PAN/PET for RO applications, higher pressures were applied to PA/CN. The results are shown in Figure 5.5. A high salt rejection ratio (above 99%) was kept when the pressure was as high as 800 psi, which demonstrated PAN/CN was strong enough to treat both brackish water and seawater. Changes of flux against pressure followed a nearly linear relationship because the RO flux is driven by the pressure gradient according to Fick's law [33].

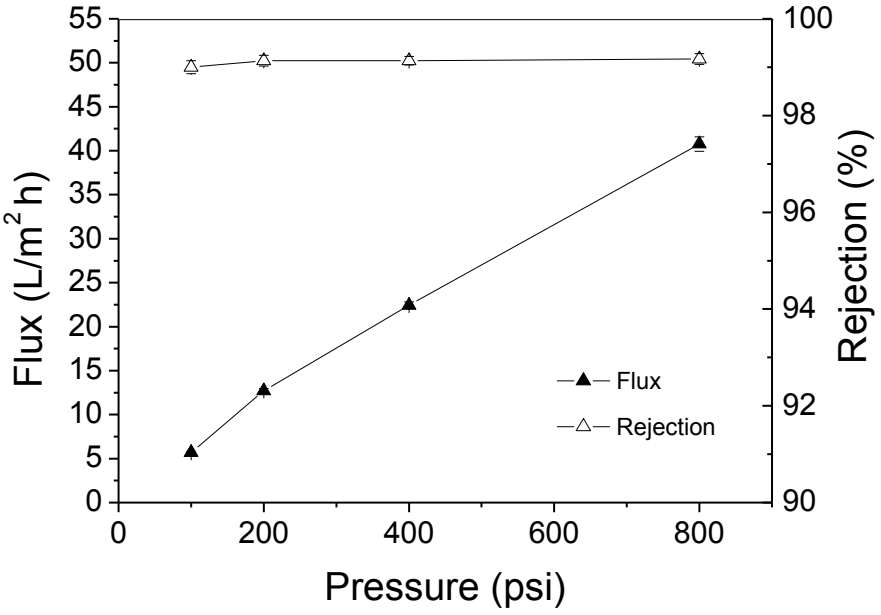

Figure 5.5 Performances of PA/PAN under various hydraulic pressures (0~800 psi). PA/PAN was prepared from 2 wt% MPD in water and 0.1% (v/w) in hexane. The test conditions were as follows: 500 ppm NaCl as feed solution, 100 psi applied pressure and temperature at 25 ^{o}C.

5.3.3 Membrane flux improved by PIP

The research focus in this chapter is to develop a high-flux RO membrane for the treatment of brackish water. A commercial RO membrane, XLE (Filmtec, DOW) was selected to work as the reference. XLE has usually been used to treat 500 ppm NaCl solution under 100 psi. Tested in our custom-built cross flow system, XLE had water permeability of 0.47 $\pm$ 0.04 L/(m^2 h psi) and rejection of 94.7 $\pm$ 0.4 %. Comparing with the reference, PA/CN prepared by 2 wt% MPD and 0.1% (w/v) TMC, our membrane had a rejection of 99.0 % and a water permeability of 6.1 $\times$ 10^{-2} L/(m^2 h psi). To obtain a RO membrane with performances comparable to XLE, co-monomers and additives were introduced into PA/CN to balance its rejection and permeability.

In our previous study, the NF membrane based on CN/PAN/PET prepared by PIP and TMC exhibited the permeability above 0.5 L/(m^2 h psi) and around 70% rejection on NaCl [34]. PIP

was mixed with 2 wt% MPD in the aqueous phase to work as a comonomer and its effect on membrane performances was plotted in Figure 5.6. When the PIP concentration was varied from 0 – 2 wt%, the membrane flux was almost tripled at a slight cost of rejection (~ 4%). As the PIP changed from 0 to 1 wt%, the flux had a quick increase. After 1 wt%, the increase became modest. Therefore, PA/CN based on the two PIP concentrations, 0.5 wt% and 1 wt% were selected for further optimization.

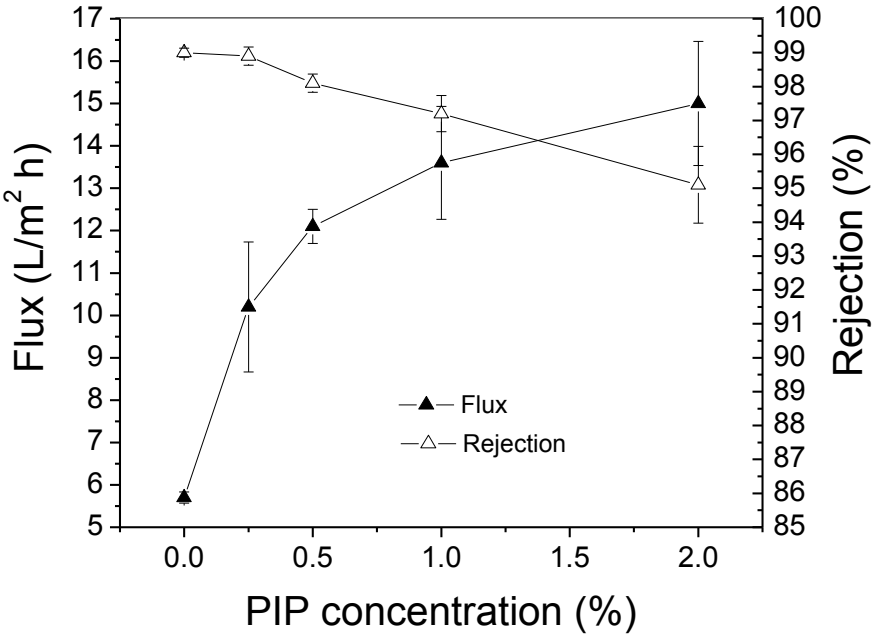

Figure 5.6 Flux and rejection in PA/CN varied with PIP concentration in aqueous solution. MPD in the aqueous solution was fixed at 2 wt%. The organic solution was 0.1% (w/v) in hexane. The membrane was tested under 100 psi at 25 ^{o}C with 500 ppm NaCl as feed solution.

5.3.4 Membrane flux improved by additives

1-octyl-3-methylimidazolium chloride (OMIC) is an ionic liquid, which was used to improve the permeability of TFNC NF membranes in our previous study [21]. Working as the surfactant, OMIC tends to aggregate at the interface during interfacial polymerization and stays in the formed barrier layer to introduce more free volumes. The effect of OMIC on RO membranes

were investigated and plotted in Figure 5.7. The only difference between Recipe A and Recipe B used for the membrane fabrication were their PIP concentrations. The Recipe A based PA/CN membranes had comparatively denser structures and were not sensitive to the addition of OMIC. As the OMIC concentration was increased from 0 to 2 wt%, only ~ 25% improvement was obtained in flux with a fixed salt rejection. The flux of Recipe B based PA/CN membranes was improved ~ 80%. A definite increase in flux was observed with 1 wt% OMIC and a large cost of salt rejection was introduced with further increase in OMIC concentration.

There are several typical additives used for the fabrication of RO membranes, such as organic salts, surfactants and small organic molecules. Although the membrane permeability can be all enhanced by these additives, the related mechanisms can be different. The organic salts, which are usually prepared by organic acid and triethylamine, are believed to protect the microporous skin layer of the support layer from annealing during curing [22]. Recently, a more effective organic salt, o-ABA/TEA was reported to form hydrophilic pathways in the barrier layer due to its reactive amine groups [35]. The role of surfactants in interfacial polymerization is to improve the absorption of aqueous solution in the substrate [1] and to introduce more free volumes in the barrier layer [21]. Small organic molecules can improve membrane permeability by modest swelling of the polyamide barrier layer [18].

For the aqueous solution containing 2 wt% MPD and 1 wt% PIP, the effects of different additives on membrane performance are compared in Table 5.3. When the additive concentration was fixed to 1 wt%, IPA led to the highest flux but at a large expense of salt rejection. To balance the tradeoff between flux and rejection, 0.3 wt% IPA was adapted to prepare a membrane with a comparable rejection to those membranes containing other additives. It is noted that OMIC possesses more advantages to enhance flux than other additives.

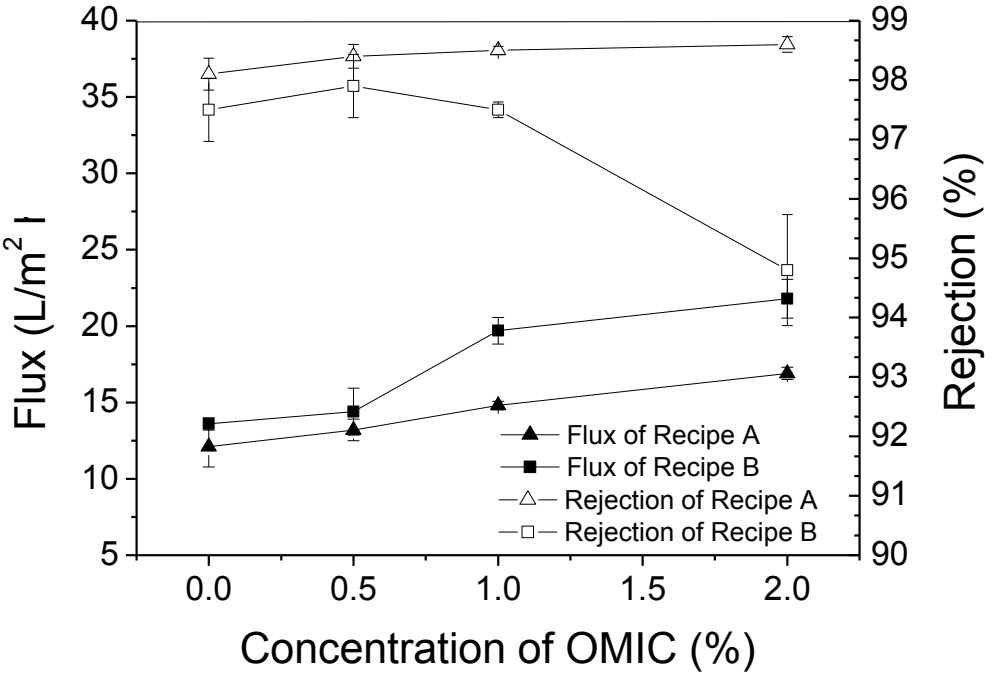

Figure 5.7 Flux and rejection in PA/CN varied with OMIC concentration. The organic solution used for reaction was 0.1% (w/v) in hexane. Recipe A: 2 wt% MPD, 0.5 wt% PIP and OMIC in aqueous solution. Recipe B: 2 wt% MPD, 1 wt% PIP and OMIC in aqueous solution. The test conditions were as follows: 500 ppm feed solution, 100 psi applied pressure and temperature at 25 ^{o}C.

Table 5.3 Effects of additives on RO membrane performances

Additive	**Concentration (%)**	**Flux (L/m^2 h)**	**Rejection (%)**
OMIC	1	19.7 ± 0.9	97.5 ± 0.4
IPA	1	33.4 ± 1.3	88.6 ± 2.3
IPA	0.3	16.2 ± 0.6	97.4 ± 0.5
CSA/TEA	1	15.7 ± 1.0	97.3 ± 0.3
o-ABA/TEA	1	12 ± 0.9	97.9 ± 0.3

5.3. 5 Membrane flux improved by spray coating

The flux of PA/CN was further enhanced via the loading of aqueous solution onto the substrate by using spray coating. The coating condition and related factors are given in Table 5.1 and the experimental result is shown in Figure 5.8. With the flow rate of the aqueous solution being fixed at 0.03 L/min, the time for the spray treatment was proportional to the amount of loading of the solution. Interfacial polymerization has been regarded as a "self-limiting" reaction because a dense polymer layer is formed quickly at the interface to retard further reaction between monomers from the two phases. Monomers present in the two phases are more than enough for the intended reaction. Through machine coating, the amount of solution introduced for interfacial polymerization can be controlled systematically. When the solution amount is controlled to be small enough, monomers in the solution will play the role of a "limiting reagent" to limit the barrier layer thickness. Figure 5.8 indicates that the flux was significantly improved by decreasing the time of spray treatment. At 60 s, the membrane exhibited flux and rejection values (18.5 L/m^2 h, 98.0 %) comparable to the ones prepare manually (19.6 L/m^2 h, 97.5%). From 60 s to 10 s, a modest change of rejection (~ 4%) was observed and further decrease of spray time led to a substantial decrease in rejection (~10%). As rejection of the reference RO membrane (XLE) was 94.7%, the spray time (30 s) leading to a comparable rejection was used to prepare a higher-flux PA/CN membrane.

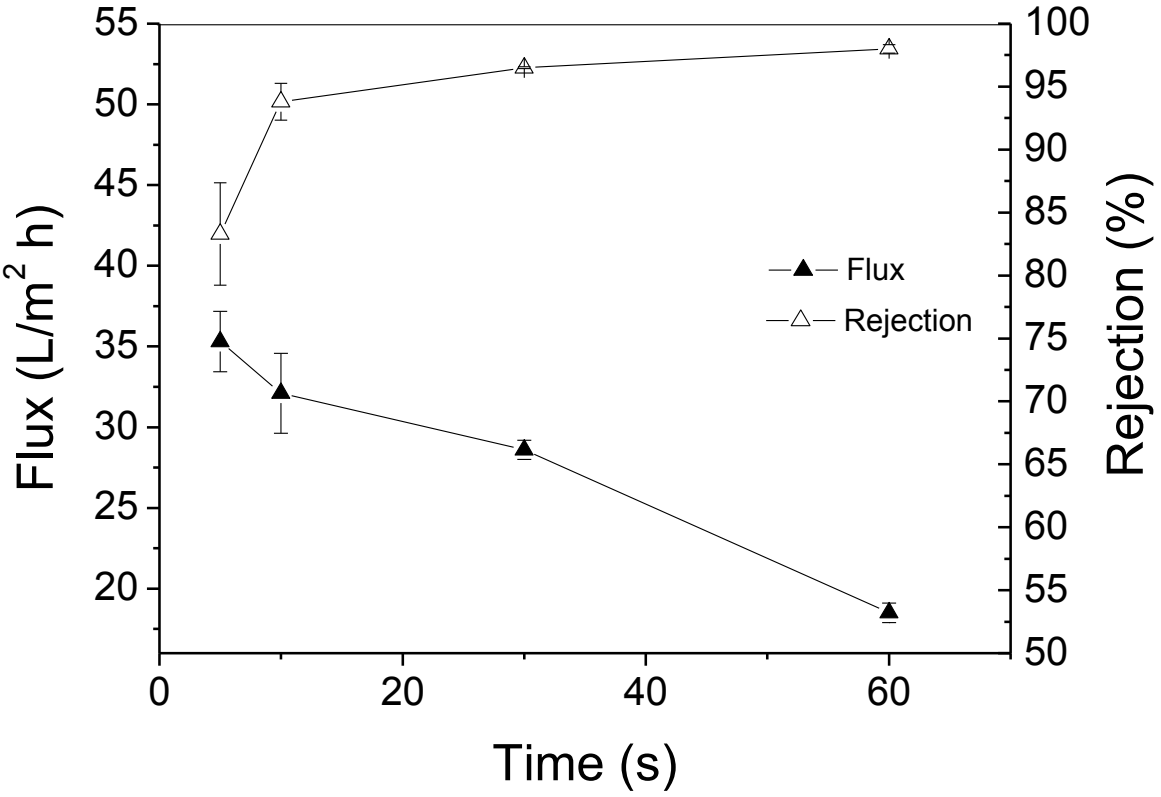

Figure 5.8 Flux and rejection in PA/CN varied by the time of spray treatment. The aqueous solution for spray was 2% MPD, 1%PIP and 1% OMIC in water. The organic solution used for reaction was 0.1% (w/v) in hexane. The test conditions were as follows: 500 ppm feed solution, 100 psi applied pressure and temperature at 25 ^{o}C.

The performance of PA/CN and PA/PAN prepared through manual coating and spray coating is compared in Figure 5.9. With manual coating, PA/CN had slightly higher rejection and flux than PA/PAN. A significant improvement in flux was obtained in both PA/CN and PA/PAN via the spray coating approach. For PA/CN, the expense on the improvement was only ~1% rejection. However, for PA/PAN, a substantial loss in rejection (~ 10%) was observed. The aqueous solution was atomized into small droplets having sizes in the micron scale and randomly loaded onto the substrate in the actual coverage area. A decrease in the spray time tended to enhance the less uniform dispersion of the aqueous solution onto the substrate surface, resulting

in less uniform dispersion of the barrier layer thickness after interfacial polymerization. Large surface roughness of PAN/PET decreased the uniformity, which contributed to a substantial decrease in rejection.

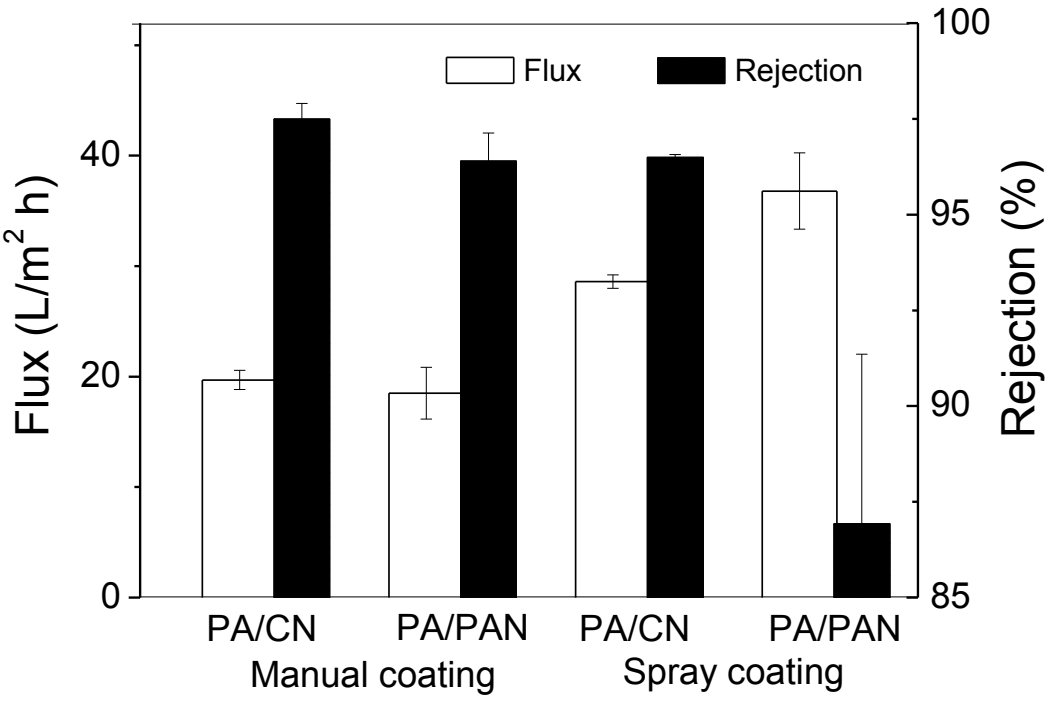

Figure 5.9 Flux and rejection of PA/CN and PA/PAN prepared through manual coating and spray coating respectively. The aqueous solution was 2 wt% MPD, 1 wt% PIP and 1 wt% OMIC in water. The organic solution used for reaction was 0.1% (w/v) in hexane. The time of spray treatment was fixed at 30 s. The test conditions were as follows: 500 ppm feed solution, 100 psi applied pressure and temperature at 25 ^{o}C.

5.4 Conclusions

TFNC RO membrane was successfully prepared based on the three-layered fibrous structure contacting a top CN layer in combination of interfacial polymerization to produce a nanocomposite surface. Comparing with PAN/PET, CN/PAN/PET led to a uniform RO barrier layer and slightly higher salt rejection due to its smoother surface. CN/PAN/PET exhibited

excellent mechanical strength to meet typical RO operation requirements for the treatment of either brackish water or seawater. To develop a high flux RO membrane for brackish water treatment, additives were applied to improve the membrane efficiency and OMIC was shown to be more effective than IPA, CSA/TEA and *o*-ABA/TEA. To formulate the conditions, aqueous solutions having different concentrations of MPD, PIP and OMIC were manually coated on the CN/PAN scaffold to react with 0.1 % (w/v) in hexane. The results showed that 2 wt% MPD, 1 wt% PIP and 1 wt% OMIC led to the membrane with the highest flux, where its rejection could remain at above 95%. The loading amount of the aqueous solution could be controlled by spray coating to further improve the membrane flux. For PA/CN spray coated for 30s, it had a flux of 28.6 L/m^2 h and a rejection of 96.5%. Comparing with the manual coating, 50% improvement on the flux was obtained by the spray treatment at a slight expense of salt rejection (~ 1%). When the same spray treatment was conducted on PAN/PET, the resulting membrane had a flux of 36.8 L/m^2 h and a rejection of 86.9%. A substantial loss of salt rejection (~ 10%) was observed due to its large surface roughness.

References

[1] P. Robert J, Composite reverse osmosis and nanofiltration membranes, Journal of Membrane Science, 83 (1993) 81-150.

[2] G.-R. Xu, J.-N. Wang, C.-J. Li, Strategies for improving the performance of the polyamide thin film composite (PA-TFC) reverse osmosis (RO) membranes: Surface modifications and nanoparticles incorporations, Desalination, 328 (2013) 83-100.

[3] C. Kim, J. Kim, I. Roh, J. Kim, The changes of membrane performance with polyamide molecular structure in the reverse osmosis process, Journal of Membrane Science, 165 (2000) 189-199.

[4] N. Saha, S. Joshi, Performance evaluation of thin film composite polyamide nanofiltration membrane with variation in monomer type, Journal of Membrane Science, 342 (2009) 60-69.

[5] H. Wang, L. Li, X. Zhang, S. Zhang, Polyamide thin-film composite membranes prepared from a novel triamine 3,5-diamino-N-(4-aminophenyl)-benzamide monomer and m-phenylenediamine, Journal of Membrane Science, 353 (2010) 78-84.

[6] J.E. Cadotte, Interfacially synthesized reverse osmosis membrane, US Patent 4,277,344 1981.

[7] J.E. Tomaschke, I.E. Ary, Interfacially synthesized reverse osmosis membranes and processes for preparing the same, US Patent 5,254,261 1993.

[8] J.-J. Kim, C.-K. Kim, S.-Y. Kwak, Composite reverse osmosis membrane having active layer of aromatic polyester or copolymer of aromatic polyester and aromatic polyamide, US Patent 5,593,588 1997.

[9] M. Schreckenberg, R. Dhein, R. Lange, W. Waldenrath, Polyether-polycarbonates for dialysis membranes, US Patent 4,563,516 1986.

[10] B.-H. Jeong, E. Hoek, Y. Yan, A. Subramani, X. Huang, G. Hurwitz, A.K. Ghosh, A. Jawor, Interfacial polymerization of thin film nanocomposites: A new concept for reverse osmosis membranes, Journal of Membrane Science, 294 (2007) 1-7.

[11] M.L. Lind, A.K. Ghosh, A. Jawor, X. Huang, W. Hou, Y. Yang, E.M.V. Hoek, Influence of Zeolite Crystal Size on Zeolite-Polyamide Thin Film Nanocomposite Membranes, Langmuir, 25 (2009) 10139-10145.

[12] M.L. Lind, B.-H. Jeong, A. Subramani, X. Huang, E. Hoek, Effect of mobile cation on zeolite-polyamide thin film nanocomposite membranes, Journal of Materials Research, 24 (2009) 1624-1631.

[13] S.Y. Lee, H.J. Kim, R. Patel, S.J. Im, J.H. Kim, B.R. Min, Silver nanoparticles immobilized on thin film composite polyamide membrane: characterization, nanofiltration, antifouling properties, Polymers for Advanced Technologies, 18 (2007) 562-568.

[14] G.L. Jadav, P.S. Singh, Synthesis of novel silica-polyamide nanocomposite membrane with enhanced properties, Journal of Membrane Science, 328 (2009) 257-267.

[15] H.S. Lee, S.J. Im, J.H. Kim, H.J. Kim, J.P. Kim, B.R. Min, Polyamide thin-film nanofiltration membranes containing TiO_2 nanoparticles, Desalination, 219 (2008) 48-56.

[16] C. Kong, M. Kanezashi, T. Yamomoto, T. Shintani, T. Tsuru, Controlled synthesis of high performance polyamide membrane with thin dense layer for water desalination, Journal of Membrane Science, 362 (2010) 76-80.

[17] J. Jegal, S.G. Min, K.H. Lee, Factors affecting the interfacial polymerization of polyamide active layers for the formation of polyamide composite membranes, Journal of Applied Polymer Science, 86 (2002) 2781-2787.

[18] S. Qiu, L. Wu, L. Zhang, H. Chen, C. Gao, Preparation of reverse osmosis composite membrane with high flux by interfacial polymerization of MPD and TMC, Journal of Applied Polymer Science, 112 (2009) 2066-2072.

[19] Y. Mansourpanah, S.S. Madaeni, A. Rahimpour, Fabrication and development of interfacial polymerized thin-film composite nanofiltration membrane using different surfactants in organic phase; study of morphology and performance, Journal of Membrane Science, 343 (2009) 219-228.

[20] H. Hachisuka, K. Ikeda, Composite reverse osmosis membrane having a separation layer with polyvinyl alcohol coating and method of reverse osmotic treatment of water using the same, US Patent 6,177,011 2001.

[21] L. Yung, H. Ma, X. Wang, K. Yoon, R. Wang, B.S. Hsiao, B. Chu, Fabrication of thin-film nanofibrous composite membranes by interfacial polymerization using ionic liquids as additives, Journal of Membrane Science, 365 (2010) 52-58.

[22] A.K. Ghosh, B.-H. Jeong, X. Huang, E.M.V. Hoek, Impacts of reaction and curing conditions on polyamide composite reverse osmosis membrane properties, Journal of Membrane Science, 311 (2008) 34-45.

[23] M.A. Kuehne, R.Q. Song, N.N. Li, R.J. Petersen, Flux enhancement in TFC RO membranes, Environmental progress, 20 (2001) 23-26.

[24] A.K. Ghosh, E.M.V. Hoek, Impacts of support membrane structure and chemistry on polyamide–polysulfone interfacial composite membranes, Journal of Membrane Science, 336 (2009) 140-148.

[25] R. Wang, Y. Liu, B. Li, B.S. Hsiao, B. Chu, Electrospun nanofibrous membranes for high flux microfiltration, Journal of Membrane Science, 392–393 (2012) 167-174.

[26] K. Yoon, B.S. Hsiao, B. Chu, High flux nanofiltration membranes based on interfacially polymerized polyamide barrier layer on polyacrylonitrile nanofibrous scaffolds, Journal of Membrane Science, 326 (2009) 484-492.

[27] X. Song, Z. Liu, D.D. Sun, Nano gives the answer: breaking the bottleneck of internal concentration polarization with a nanofiber composite forward osmosis membrane for a high water production rate, Adv Mater, 23 (2011) 3256-3260.

[28] S. Kaur, S. Sundarrajan, D. Rana, T. Matsuura, S. Ramakrishna, Influence of electrospun fiber size on the separation efficiency of thin film nanofiltration composite membrane, Journal of Membrane Science, 392–393 (2012) 101-111.

[29] H. Ma, C. Burger, B.S. Hsiao, B. Chu, Ultrafine Polysaccharide Nanofibrous Membranes for Water Purification, Biomacromolecules, 12 (2011) 970-976.

[30] Xiao Wang, Dufei Fang, Benjamin Hsiao, Benjamin Chu, Nano-Filtration Membranes based on Thin-Film Nano-Composites To be submitted, (2013).

[31] H. Ma, C. Burger, B.S. Hsiao, B. Chu, Highly Permeable Polymer Membranes Containing Directed Channels for Water Purification, ACS Macro Letters, 1 (2012) 723-726.

[32] N.-N. Bui, M.L. Lind, E.M.V. Hoek, J.R. McCutcheon, Electrospun nanofiber supported thin film composite membranes for engineered osmosis, Journal of Membrane Science, 385–386 (2011) 10-19.

[33] M.E. Williams, A review of reverse osmosis theory, EET Corporation and Williams Engineering Services Company, Inc, (2003).

[34] Xiao Wang, Zhe Wang, Rui Yang, Ran Wang, Hongyang Ma, Benjamin S. Hsiao and Benjamin Chu, Nanofiltration Membranes Prepared by Interfacial Polymerization on Thin-Film Nanofibrous Composite Scaffold, polymer, in press.

[35] L. Zhao, P.C.-Y. Chang, W. Ho, High-flux reverse osmosis membranes incorporated with hydrophilic additives for brackish water desalination, Desalination, (2012).

Chapter 6 Summary

NF and RO are two important water treatment processes to provide clean water for our daily life and/or industrial applications. Large amount of energy is usually needed to create high pressure for these treatments, which significantly increase the cost of these processes (from plant construction to routine operations and maintenance). The improvement over the NF/RO efficiency can directly save the energy consumption (e.g., lower hydraulic pressure) and reduce the operational cost. As separation membranes are the most critical component of any NF/RO units, we have investigated new and innovative ways to improve the membrane performance through new materials design and preparation.

The most popular membrane format is known as “thin-film nanocomposite (TFC)”, which has an ultrathin polymer barrier layer supported by a porous substrate. Recent development of TFC was reviewed in Chapter 1. Although some advanced materials, such as carbon nanotubes, Aquaporin proteins and liquid crystal, have been adopted to improve the performance further, there still exists a substantial gap in the utilization of new materials to achieve large-scale production with breakthrough working performances when compared with existing commercial membranes. To provide a highly efficient NF/RO membrane, a new porous support, fabricated by nanofibers, has been used to replace the conventional sponge-like supports in this study This nanofibrous support allows the liquid flow to pass through the barrier layer faster due to its larger surface porosity and formation of new water pathways (directed water channels) at the interface between ultrathin nanofibers and the polymer matrix forming the barrier layer.

The efficiency of NF/RO membranes was further improved by using better controlled machine coating technology (i.e., slot die), instead of manual coating. The slot-die coating process was developed to quantitatively control the wet coating thickness and to achieve a very thin coating layer. Chapter 2 discussed the design of the slot-die system based on the unique characteristics of nanofibrous support. Due to the short width of our slot die, a uniform flow distribution could be obtained directly with a T-shape internal manifold, where no compensation on the pressure drop was needed with the adoption of a coat hanger manifold. The coating liquid could be driven by a syringe pump and the coating windows were plotted through coating experiments to shown the stable working conditions.

Interfacial polymerization was used to prepare the barrier layer of NF membranes using three different supports, i.e. the conventional sponge-like substrate, the electrospun scaffold and the substrate with cellulose nanofibers on top of the electrospun scaffold. For membranes prepared by manual coating, high efficiency membranes were obtained on both the electrospun scaffold and the electrospun scaffold with a cellulose nanofiber layer on top. The cellulose nanofiber based NF membrane showed better permeability. The slot-die coating process was applied to limit the growth of the polymer layer through the control of wet coating thickness of the organic solution during interfacial polymerization. Successful coatings could be achieved on the conventional substrate and fibrous substrates with cellulose nanofiber coatings because of their smoother surfaces. In addition to the thickness control, other membrane properties, i.e., pore size distribution and surface charge density not found to be affected by the slot-die coating process. Therefore, the coating process could definitively improve the membrane permeability at a relatively smaller cost of the membrane selectivity.

The effect of the cellulose nanofibrous substrate on NF membrane performances was presented in Chapter 4. Interfacial polymerization was carried out with the positions of the two phases reversed, i.e. the aqueous phase on top of the organic phase. The purpose of this design was to obtain high membrane permeability with more composite region of the polymer matrix and the cellulose nanofibrous substrate because the polyamide layer tends to grow in the organic phase. No significant improvement on membrane permeability was observed but the membrane average pore size was decreased through the modified process. In the modified process, the dense part of the barrier layer was left on top without any combination with the cellulose fibrous substrate.

Preliminary work on the preparation of reverse osmosis (RO) membranes with cellulose nanofibers was introduced in Chapter 5. Comparing with the electrospun scaffold, the cellulose nanofiber based membrane had a higher rejection, perhaps because of the smoother surface of the cellulose substrate. The membranes were tested under a high hydraulic pressure to show that the mechanical strength could withstand operations related to RO. Different additives were introduced and their effects on membrane permeability were compared. It was found that the ionic liquid could lead to better membrane performance than other conventional additives. Spray coating was also used to load aqueous solution on the substrate for interfacial polymerization. Within a range of the amount of loading for the aqueous solution, the RO membrane permeability could be improved at a relatively small cost of salt rejection.

Bibliography

Bui, N. N.; Lind, M. L.; Hoek, E. M. V.; McCutcheon, J. R. Journal of Membrane Science 2011, 385–386, 10-19.

Cadotte, J. E.; US Patent 4277344, 1981.

Carvalho, M. S.; Kheshgi, H. S. AIChE Journal 2000, 46, 1907-1917.

Chang, H. M.; Chang, Y. R.; Lin, C. F.; Liu, T. J. Polymer Engineering & Science 2007, 47, 1927-1936.

Chang, Y.R.; Lin, C.F.; Liu, T.J. Polymer Engineering & Science 2009, 49, 1158-1167.

Childress, A. E.; Elimelech, M. Environmental Science & Technology 2000, 34, 3710-3716.

Childress, A. E.; Elimelech, M. Journal of Membrane Science 1996, 119, 253-268.

Chu, B.; Hsiao, B. S. Journal of Polymer Science Part B: Polymer Physics 2009, 47, 2431-2435.

Chu, B.; Hsiao, B. S.; Fang, D.; The Research Foundation of State University of New York, USA . 2002, p 55.

Du, R.; Zhao, J. Journal of Membrane Science 2004, 239, 183-188.

Du, R.; Zhao, J. Journal of Membrane Science 2004, 239, 183-188.

El-Hashani, A.; Toutianoush, A.; Tieke, B. Journal of Membrane Science 2008, 318, 65-70.

Fane, A. Progress in filtration and separation 1986, 4, 101-179.

Freger, V. Environmental Science & Technology 2004, 38, 3168-3175.

Freger, V. Langmuir 2005, 21, 1884-1894.

Ghosh, A. K.; Hoek, E. M. V. Journal of Membrane Science 2009, 336, 140-148.

Ghosh, A. K.; Jeong, B.-H.; Huang, X.; Hoek, E. M. V. Journal of Membrane Science 2008, 311, 34-45.

Gozálvez-Zafrilla, J. M.; Gómez-Martínez, B.; Santafé-Moros, A. Computer Aided Chemical Engineering 2005, 20, 457-462.

Gutoff, E. B. The Journal of imaging science and technology 1993, 37, 615-627.

Gutoff, E. B. The Journal of imaging science and technology 1994, 38, 584-593.

Hachisuka, H.; Ikeda, K.; US Patent 6177011, 2001.

Hilal, N.; Al-Zoubi, H.; Darwish, N.; Mohamma, A.; Abu Arabi, M. Desalination 2004, 170, 281-308.

Hinds, B. J.; Chopra, N.; Rantell, T.; Andrews, R.; Gavalas, V.; Bachas, L. G. Science 2004, 303, 62-65.

Hirose, M.; Ito, H.; Kamiyama, Y. Journal of Membrane Science 1996, 121, 209-215.

Holt, J. K.; Park, H. G.; Wang, Y.; Stadermann, M.; Artyukhin, A. B.; Grigoropoulos, C. P.; Noy, A.; Bakajin, O. Science 2006, 312, 1034-1037.

Homayoonfal, M.; Akbari, A.; Mehrnia, M. R. Desalination 2010, 263, 217-225.

Jadav, G. L.; Singh, P. S. Journal of Membrane Science 2009, 328, 257-267.

Jegal, J.; Min, S. G.; Lee, K. H. Journal of Applied Polymer Science 2002, 86, 2781-2787.

Jeong, B.-H.; Hoek, E.; Yan, Y.; Subramani, A.; Huang, X.; Hurwitz, G.; Ghosh, A. K.; Jawor, A. Journal of Membrane Science 2007, 294, 1-7.

Jin, W.; Toutianoush, A.; Tieke, B. Langmuir 2003, 19, 2550-2553.

Jin, Y.; Su, Z. Journal of Membrane Science 2009, 330, 175-179.

Kaur, S.; Sundarrajan, S.; Gopal, R.; Ramakrishna, S. Journal of Applied Polymer Science 2012, 124, 205-215.

Kaur, S.; Sundarrajan, S.; Rana, D.; Matsuura, T.; Ramakrishna, S. Journal of Membrane Science 2012, 392–393, 101-111.

Kim, C. K.; Kim, J. H.; Roh, I. J.; Kim, J. J. Journal of Membrane Science 2000, 165, 189-199.

Kim, C.; Kim, J.; Roh, I.; Kim, J. Journal of Membrane Science 2000, 165, 189-199.

Kim, J.J.; Kim, C.-K.; Kwak, S.-Y.; US Patent 5593588, 1997.

Kong, C.; Kanezashi, M.; Yamomoto, T.; Shintani, T.; Tsuru, T. Journal of Membrane Science 2010, 362, 76-80.

Kong, C.; Shintani, T.; Kamada, T.; Freger, V.; Tsuru, T. Journal of Membrane Science 2011, 384, 10-16.

Kuehne, M. A.; Song, R. Q.; Li, N. N.; Petersen, R. J. Environmental progress 2001, 20, 23-26.

Kumar, M.; Grzelakowski, M.; Zilles, J.; Clark, M.; Meier, W. Proceedings of the National Academy of Sciences 2007, 104, 20719-20724.

Lee, H. S.; Im, S. J.; Kim, J. H.; Kim, H. J.; Kim, J. P.; Min, B. R. Desalination 2008, 219, 48-56.

Lee, K. P.; Arnot, T. C.; Mattia, D. Journal of Membrane Science 2011, 370, 1-22.

Lee, S. Y.; Kim, H. J.; Patel, R.; Im, S. J.; Kim, J. H.; Min, B. R. Polymers for Advanced Technologies 2007, 18, 562-568.

Lianchao, L.; Baoguo, W.; Huimin, T.; Tianlu, C.; Jiping, X. Journal of Membrane Science 2006, 269, 84-93.

Lianchao, L.; Baoguo, W.; Huimin, T.; Tianlu, C.; Jiping, X. Journal of Membrane Science 2006, 269, 84-93.

Lim, H. S.; Park, S. H.; Koo, S. H.; Kwark, Y.-J.; Thomas, E. L.; Jeong, Y.; Cho, J. H. Langmuir 2010, 26, 19159-19162.

Lin, C. F.; Hill Wong, D. S.; Liu, T.-J.; Wu, P.-Y. Advances in Polymer Technology 2010, 29, 31-44.

Lind, M. L.; Eumine Suk, D.; Nguyen, T.-V.; Hoek, E. M. Environmental Science & Technology 2010, 44, 8230-8235.

Lind, M. L.; Ghosh, A. K.; Jawor, A.; Huang, X.; Hou, W.; Yang, Y.; Hoek, E. M. Langmuir 2009, 25, 10139-10145.

Lind, M. L.; Ghosh, A. K.; Jawor, A.; Huang, X.; Hou, W.; Yang, Y.; Hoek, E. M. V. Langmuir 2009, 25, 10139-10145.

Lind, M. L.; Jeong, B. H.; Subramani, A.; Huang, X.; Hoek, E. Journal of Materials Research 2009, 24, 1624-1631.

Lippert, H. G. Coatings Technology Handbook 1991, 1559-1564.

Liu, M.; Yu, S.; Qi, M.; Pan, Q.; Gao, C. Journal of Membrane Science 2010, 348, 268-276.

Lu, Y.; Suzuki, T.; Zhang, W.; Moore, J. S.; Mariñas, B. J. Chemistry of Materials 2007, 19, 3194-3204.

Ma, H.; Burger, C.; Hsiao, B. S.; Chu, B. ACS Macro Letters 2012, 1, 723-726.

Ma, H.; Burger, C.; Hsiao, B. S.; Chu, B. Biomacromolecules 2011, 13, 180-186.

Ma, H.; Burger, C.; Hsiao, B. S.; Chu, B. Biomacromolecules 2011, 12, 970-976.

Ma, H.; Burger, C.; Hsiao, B. S.; Chu, B. Biomacromolecules 2011, 12, 970-976.

Ma, H.; Hsiao, B. S.; Chu, B. ACS Macro Letters 2011, 1, 213-216.

Malaisamy, R.; Bruening, M. L. Langmuir 2005, 21, 10587-10592.

Mansourpanah, Y.; Madaeni, S. S.; Rahimpour, A. Journal of Membrane Science 2009, 343, 219-228.

Mansourpanah, Y.; Madaeni, S.; Rahimpour, A. Separation and Purification Technology 2009, 69, 234-242.

McCloskey, B. D.; Park, H. B.; Ju, H.; Rowe, B. W.; Miller, D. J.; Chun, B. J.; Kin, K.; Freeman, B. D. Polymer 2010, 51, 3472-3485.

Meihong, L.; Sanchuan, Y.; Yong, Z.; Congjie, G. Journal of Membrane Science 2008, 310, 289-295.

Miao, J.; Chen, G.; Li, L.; Dong, S. Separation Science and Technology 2007, 42, 3085-3099.

Moon, R. J.; Martini, A.; Nairn, J.; Simonsen, J.; Youngblood, J. Chemical Society Reviews 2011, 40, 3941-3994.

Mulder, M.; Kluwer Academic: Dordrecht ; Boston, 1996, p 235.

Mulder, M.; Kluwer Academic: Dordrecht ; Boston, 1996, p 287.

Oizerovich-Honig, R.; Raim, V.; Srebnik, S. Langmuir 2009, 26, 299-306.

Otero, J. A.; Mazarrasa, O.; Villasante, J.; Silva, V.; Prádanos, P.; Calvo, J. I.; Hernández, A. Journal of Membrane Science 2008, 309, 17-27.

Qiu, S.; Wu, L.; Zhang, L.; Chen, H.; Gao, C. Journal of Applied Polymer Science 2009, 112, 2066-2072.

Richard Bowen, W.; Wahab Mohammad, A. AIChE Journal 1998, 44, 1799-1812.

Robert J, P. Journal of Membrane Science 1993, 83, 81-150.

Saha, N.; Joshi, S. Journal of Membrane Science 2009, 342, 60-69.

Schreckenberg, M.; Dhein, R.; Lange, R.; Waldenrath, W.; US Patent 4563516, 1986.

Service, R. F. Science 2006, 313, 1088-1090.

Shannon, M. A.; Bohn, P. W.; Elimelech, M.; Georgiadis, J. G.; Marinas, B. J.; Mayes, A. M. Nature 2008, 452, 301-310.

Song, X.; Liu, Z.; Sun, D. D. Adv Mater 2011, 23, 3256-3260.

Tadmor, Z.; Gogos, C. G. Principles of polymer processing; Wiley. com, 2006.

Tang, B.; Huo, Z.; Wu, P. Journal of Membrane Science 2008, 320, 198-205.

Tansel, B.; Sager, J.; Rector, T.; Garland, J.; Strayer, R. F.; Levine, L.; Roberts, M.; Hummerick, M.; Bauer, J. Separation and Purification Technology 2006, 51, 40-47.

Tiraferri, A.; Elimelech, M. Journal of Membrane Science 2012, 389, 499-508.

Tomaschke, J. E.; Ary, I. E.; US Patent 5254261, 1993.

Van der Bruggen, B. European Polymer Journal 2009, 45, 1873-1882.

Wamser, C. C.; Gilbert, M. I. Langmuir 1992, 8, 1608-1614.

Wang, H.; Li, L.; Zhang, X.; Zhang, S. Journal of Membrane Science 2010, 353, 78-84.

Wang, R.; Guan, S.; Sato, A.; Wang, X.; Wang, Z.; Yang, R.; Hsiao, B. S.; Chu, B. Journal of Membrane Science 2013, 446, 376-382.

Wang, R.; Liu, Y.; Li, B.; Hsiao, B. S.; Chu, B. Journal of Membrane Science 2012, 392–393, 167-174.

Weinstein, S. J.; Ruschak, K. J. AIChE Journal 1996, 42, 2401-2414.

Williams, M. E. EET Corporation and Williams Engineering Services Company, Inc 2003.

Wang, X.; Fang, D.; Hsiao, S. B.; Chu, B. To be submitted 2013.

Wang, X.; Yeh, T.; Wang, Z.; Yang, R.; Wang, R.; Ma, H.; Hsiao, S. B; Chu, B. Polymer, in press.

Xu, G. R.; Wang, J. N.; Li, C. J. Desalination 2013, 328, 83-100.

Yangali-Quintanilla, V.; Verliefde, A.; Kim, T. U.; Sadmani, A.; Kennedy, M.; Amy, G. Journal of Membrane Science 2009, 342, 251-262.

Yoon, K.; Hsiao, B. S.; Chu, B. Journal of Membrane Science 2009, 326, 484-492.

Youn, S. I.; Kim, S. Y.; Shin, D. M.; Lee, J. S.; Jung, H. W.; Hyun, J. C. Korea-Australia Rheology Journal 2006, 18, 209-215.

Yung, L.; Ma, H.; Wang, X.; Yoon, K.; Wang, R.; Hsiao, B. S.; Chu, B. Journal of Membrane Science 2010, 365, 52-58.

Zhao, L.; Chang, P. C.-Y.; Ho, W. Desalination 2012.

Zhou, M.; Nemade, P. R.; Lu, X.; Zeng, X.; Hatakeyama, E. S.; Noble, R. D.; Gin, D. L.

Journal of the American Chemical Society 2007, 129, 9574-9575.

Zhou, M.j.; Kidd, T. J.; Noble, R. D.; Gin, D. L. Advanced Materials 2005, 17, 1850-1853.